# DEPARTMENT OF LIFE SCIENCES

RÚBEN FILIPE MADEIRA DOURADO BSc in Cell and Molecular Biology

VALIDATION OF ARMS-HRMA
FOR KRAS MUTATIONS IN TUMOR AND
PLASMA SAMPLES FROM PANCREATIC
CANCER PATIENTS

MASTER IN MOLECULAR GENETICS AND BIOMEDICINE NOVA University Lisbon September, 2024





## DEPARTMENT OF LIFE SCIENCES

# VALIDATION OF ARMS-HRMA FOR KRAS MUTATIONS IN TUMOR AND PLASMA SAMPLES FROM PANCREATIC CANCER PATIENTS

#### **RÚBEN FILIPE MADEIRA DOURADO**

BSc in Cell and Molecular Biology

Advisers: Prof. Doctor Pedro Miguel Ribeiro Viana Baptista

Full Professor, NOVA School of Science and Technology, NOVA University Lisbon

Prof. Doctor Maria Alexandra Núncio de Carvalho Ramos Fernandes Associate Professor, NOVA School of Science and Technology, NOVA University Lisbon

#### **Examination Committee:**

Chair: Doctor Ana Rita Fialho Grosso

Associate Professor, NOVA School of Science and Technology,

NOVA University Lisbon

Rapporteurs: Doctor Vasco Temudo e Melo Cabral Barreto

Associate Professor, NOVA School of Science and Technology,

**NOVA University Lisbon** 

Adviser: Doctor Pedro Miguel Ribeiro Viana Baptista

Full Professor, NOVA School of Science and Technology,

**NOVA University Lisbon** 

Validation of ARMS-HRMA for <i>KRAS</i> mutations in tumor and plasma samples from pancreatic cancer patients
Copyright © Rúben Filipe Madeira Dourado, NOVA School of Science and Technology, NOVA University Lisbon.
The NOVA School of Science and Technology and the NOVA University Lisbon have the right, perpetual and without geographical boundaries, to file and publish this dissertation through printed copies reproduced on paper or on digital form, or by any other means known or that may be invented, and to disseminate through scientific repositories and admit its copying and distribution for non-commercial, educational or research purposes, as long as credit is given to the author and editor.

#### **A**CKNOWLEDGMENTS

I would like to thank FCT - Fundação para a Ciência e a Tecnologia, who funded this work, I.P., DOI:10.54499/UIDP/04378/2020 and DOI:10.54499/UIDB/04378/2020 of UCIBIO and LA/P/0140/2020 of i4HB.

I would like to thank my advisors, Prof. Doctor Pedro Viana Baptista and Prof. Doctor Alexandra R. Fernandes for allowing me to work on my master's thesis on their laboratory and for trusting me with such an important project. Thank you for the great advice that allowed me to grow not only as a student but as a person as well, and for always being available to answer any questions I had.

Thank you to everyone from the Nanomedicine and Human Genetics and Cancer Therapeutics laboratories for always being so nice and eager to help and for the great advice. A special thanks to PhD student André Luz for teaching me, for always available to help and specially for being so patient with me (and sorry for the frostbitten hands).

This journey would have not been the same without my three dear lab mates Lara, Edvânia and Vanessa. Thank you so much for the good laughs, great gossip and most importantly for your continuous support. And thank you to the amazing group of friends who I shared amazing dinners with, for being such amazing people. I wish you all a life of great success.

A special thanks to my parents and sister, for always working hard to make sure I could succeed in my academic life. I hope I can return the investment. And thank you to all my old friends and to David, for your continuous support throughout these 2 years.

#### **A**BSTRACT

Pancreatic cancer (PC) has proved to be a difficult disease to diagnose and treat. The lack of symptoms in the early stages of the disease results in late diagnosis, and the only curative option is the complete resection of the tumor, which in 80% of patients it is not possible. Kirsten rat sarcoma viral oncogene homologue (*KRAS*) mutations play a critical role in the carcinogenesis process and chemoresistant nature of PC, being present in around 90% of pancreatic ductal adenocarcinomas (PDAC) – the most common form of PC.

The molecular characterization of PDAC could prove useful in aiding treatment strategy, as new *KRAS* targeted therapies have been developed. Liquid biopsies provide a biological fluid to obtain real time information on the tumor's molecular profile by accessing circulating tumor DNA (ctDNA). However, the low % of ctDNA requires the development of better, high sensitivity molecular detection tools.

In this work, the coupling of the Amplification Refractory Mutation System (ARMS) and High-Resolution Melting Analysis (HRMA) methodologies - ARMS-HRMA - was further validated to detect codon 12 and codon 13 *KRAS* mutations (G12D, G12V, G12R, G12C and G13D) in tumor and plasma samples. In a cohort of 97 pancreatic cancer patients, ARMS-HRMA was successfully performed in 93 tumor samples, where 72 out of 93 tested positive for *KRAS* mutations (77%). Out of the 72 positive cases, 35 were G12D (49%), 22 were G12V (31%), 10 were G12R (14%), 1 were G12C (1%), 1 were G13D (1%), 2 were positive for both G12D and G12V (3%) and 1 was positive for both G12C and G12D (1%). Sanger Sequencing (SS), the current gold standard for mutation analysis, only detected *KRAS* mutations in 52 out of 97 tumor samples (54%). ARMS-HRMA detected every *KRAS* mutation described by SS, while showing improved sensitivity and maintaining specificity. 20 out of 65 plasma samples (31%) presented the same *KRAS* mutation as their corresponding tumor samples when analyzed by ARMS-HRMA. As a simple, rapid and cheap technique, ARMS-HRMA is a promising tool for the management of PDAC, not only by allowing the molecular characterization of pancreatic tumors, but also by improving disease monitoring through the detection of *KRAS* mutations in ctDNA.

#### **RESUMO**

O cancro do pâncreas (CP) é uma doença difícil de diagnosticar e tratar. A ausência de sintomas nas fases iniciais da doença resulta num diagnóstico tardio, e a única opção curativa é a ressecção completa do tumor, o que em 80% dos doentes não é possível. Mutações no gene *Kirsten rat sarcoma viral oncogene homologue* (*KRAS*) desempenham um papel crítico no processo de carcinogénese e na natureza quimiorresistente do CP, estando presentes em cerca de 90% dos adenocarcinomas ductais pancreáticos (ACDP) - a forma mais comum de CP.

A caracterização molecular de ACDP pode ser útil a escolher a estratégia de tratamento, visto que novas terapias direcionadas a KRAS foram desenvolvidas. As biópsias líquidas fornecem fluidos biológicos onde é possível obter informação em tempo real sobre o perfil molecular do tumor, ao analisar DNA tumoral circulante (ctDNA). No entanto, a baixa % de ctDNA requer o desenvolvimento de melhores ferramentas de deteção molecular de alta sensibilidade.

Neste trabalho, o acoplamento das metodologias Amplification Refractory Mutation System (ARMS) e High-Resolution Melting Analysis (HRMA) - ARMS-HRMA - foi validado para detetar mutações no gene KRAS nos codões 12 e 13 (G12D, G12V, G12R, G12C e G13D) em amostras de tumor e de plasma. Numa coorte de 97 doentes com CP, ARMS-HRMA foi realizado com sucesso em 93 amostras de tumores, onde 72 (77%) apresentaram mutações no gene KRAS. Destas 72 amostras, a mutação G12D foi detetada em 35 (49%), G12V em 22 (31%), G12R em 10 (14%), G12C numa (1%), G13D numa (1%), G12D e G12V em 2 (3%) e 1 uma testou positivo para G12C e G12D (1%). A Sequenciação de Sanger (SS), a atual técnica de referência para análise de mutações, detetou apenas mutações no gene KRAS em 52 das 97 amostras de tumores (54%). ARMS-HRMA detetou todas as mutações no KRAS descritas pela SS, monstrando melhor sensibilidade e manutendo a especificidade. Vinte das 65 amostras de plasma (31%) apresentaram a mesma mutação que as amostras de tumor correspondentes quando analisadas por ARMS-HRMA. Por ser uma técnica simples, rápida e barata, a ARMS-HRMA é uma ferramenta promissora para a gestão de ADCP, não só por permitir a caracterização molecular de tumores do pâncreas, mas também por melhorar a monitorização da doença através da deteção de mutações no KRAS em ctDNA.

Palavas chave: ACDP; KRAS; biópsia líquida; ctDNA; ARMS; HRMA

## **C**ONTENTS

1. Introduction	1
1.1. Pancreatic cancer	1
1.2. General processes of tumorigenesis	3
1.3. Carcinogenesis of pancreatic ductal adenocarcinomas (PDAC)	4
1.4. The KRAS protein	7
1.4.1. Normal function of the KRAS protein	7
1.4.2. Disruption of normal KRAS function	8
1.4.2.2. KRAS mutations across different cancers	9
1.4.2.3. KRAS mutations in PDAC	10
1.5. Personalized medicine	11
1.5.1. Personalized medicine in cancer treatment	11
1.5.2. PDAC diagnosis and monitoring	12
1.5.2.1. Solid biopsies	12
1.5.2.2. Liquid biopsies (LB)	13
1.6. Molecular techniques for cancer diagnostics	16
1.6.1. Molecular techniques routinely used in clinical practice	16
1.6.2. Molecular techniques that are not routinely used in a clinical setting	20
1.7. Aim of this work	26
2. Materials and methods	28
2.1. Biological Materials	28
2.2. Control samples (cell lines)	29
2.3. Cell culture	30
2.4. DNA extraction	30
2.5. Amplification of <i>KRAS</i> exon 2	31
2.7. Gel Electrophoresis	32
2.8. Direct sequencing	33
2.9. ARMS-HRMA	33
2.9.1. Statistical analysis of ARMS-HRMA results	35
2.9.2. Data presentation	35

3. RESULTS AND DISCUSSION	37
3.1. Cohort characterization	37
3.2. DNA Extraction of tumor and plasma samples	37
3.3. KRAS amplification by PCR and Gel electrophoresis	38
3.4. SS results	40
3.5. Mutation scoring using ARMS-HRMA	41
3.5.1. ARMS-HRMA on tumor samples	44
3.5.1.1. G12D mutation analysis in tumor samples	44
3.5.1.2. G12V mutation analysis in tumor samples	47
3.5.1.3. G12R mutation analysis in tumor samples	50
3.5.1.4. G12C mutation analysis in tumor samples	52
3.5.1.5 G13D mutation analysis in tumor samples	54
3.5.1.6. ARMS-HRMA tumor samples - summary	56
3.5.2. ARMS-HRMA on plasma samples	58
3.5.2.1. G12D mutation analysis in plasma samples	60
3.5.2.2. G12V mutation analysis in plasma samples	63
3.5.2.3. G12R mutation analysis in plasma samples	65
3.5.2.4. G12C mutation analysis in plasma samples	68
3.5.2.5. G13D mutation analysis in plasma samples	69
3.5.2.6. ARMS-HRMA on plasma samples - summary	70
3.6. Comparison between ARMS-HRMA and other molecular techniques	72
3.7. Influence of experimental replicates on mutation scoring	76
4. CONCLUSIONS AND FUTURE PROSPECTS	78
5.BIBLIOGRAPHY	83
6. APPENDIX	93

## LIST OF FIGURES

Figure 1.1: Incidence and mortality from different types of cancer in Portugal in 2022. 2
Figure 1.2: Model of the PDAC carcinogenesis process6
Figure 1.3: Simplified representation of the KRAS signaling pathway
Figure 1.4: Proportion of different KRAS mutations across different types of cancer9
Figure 1.5: Origin of ctDNA15
Figure 1.6: qPCR17
Figure 1.7: Schematic representation of the modern SS methodology18
Figure 1.8: ARMS principle19
Figure 1.9: Schematization of the HRMA principle22
Figure 3.1: Gel Electrophoresis of PCR products39
Figure 3.2: Gel Electrophoresis of plasma samples amplification products39
<b>Figure 3.3:</b> Representative images of the region under study extracted from chromatograms of 5 different tumor samples
Figure 3.4: Schematization of a typical ARMS-HRMA derivative plot and formula used to normalize fluorescence
<b>Figure 3.5:</b> ARMS-HRMA results used in G12D mutation scoring of tumor samples 115T 119T and 141T <b>4</b> 5
Figure 3.6: G12D scoring based on the normalized melting peak intensity of ARMS-HRMA47
<b>Figure 3.7:</b> ARMS-HRMA results used in G12V mutation scoring of tumor samples 142T 143T and 150T48
Figure 3.8: G12V scoring based on the normalized melting peak intensity of ARMS-HRMA49
Figure 3.9: ARMS-HRMA results used in G12R mutation scoring of tumor samples 1417 and 149T51
Figure 3.10: G12R scoring based on the normalized melting peak intensity of ARMS-HRMA52
Figure 3.11: ARMS-HRMA results used in G12C mutation scoring of tumor samples 109T and 65T53

Figure 3.12: ARMS-HRMA results used in G13D mutation scoring of tumor samples 127T and 129T55
Figure 3.13: Melting curves of different concentrations of the G13D positive control HCT116 and wild-type control HT-29
Figure 3.14: ARMS-HRMA results used in G12D mutation scoring of plasma samples 31P1 and 31P261
Figure 3.15: G12D scoring based on the normalized melting peak intensity of ARMS-HRMA62
Figure 3.16: ARMS-HRMA results used in G12V mutation scoring of plasma samples 140P1 and 143P164
Figure 3.17: G12V scoring based on the normalized melting peak intensity of ARMS-HRMA65
Figure 3.18: ARMS-HRMA results used in G12R mutation scoring of plasma samples 28P1, 28P2 and 110P166
Figure 3.19: G12R scoring based on the normalized melting peak intensity of ARMS-HRMA
Figure 3.20: ARMS-HRMA results used in G12C mutation scoring of plasma sample 65P1.
Figure 3.21: ARMS-HRMA results used in G13D mutation scoring of plasma sample 127P269
Figure 3.22: Sankey chart diagram of the ARMS-HRMA results of tumor and plasma samples71
Figure 3.23: Sankey chart diagram of SS and HRMA results of all tumor samples73
Figure 3.24: Sankey chart diagram of SS, ARMS-HRMA and ddPCR results for tumor samples
Figure 3.25: Sankey chart diagram comparing only the mutated tumor samples with concordant results by SS, ARMS-HRMA and ddPCR and plasma samples ARMS-HRMA results
Figure 3.26: Effect of using only the first assay in the tumor scoring process76

### LIST OF TABLES

<b>Table 1.1:</b> Comparison of different molecular techniques for mutation analysis (advantages, disadvantages, limit of detection, routine use in clinics and references24
Table 2.1: Characterization of the different cell lines used in this study29
Table 2.2: Primers used for the amplification of the exon 2 of KRAS31
Table 2.3: PCR Reaction Mixture used to amplify exon 2 of KRAS32
Table 2.4: PCR Program used for the amplification of exon 2 of the KRAS gene32
Table 2.5: Primers used in ARMS-HRMA34
Table 2.6: Reaction mixture used in ARMS-HRMA
Table 2.7: ARMS-HRMA program used34
Table 3.1: SS results of all tumor samples used in this study41
Table 3.2: Summary of G12D mutations found in tumor samples analyzed by ARMS-HRMA46
Table 3.3: Summary of G12V mutations found in tumor samples analyzed by ARMS-HRMA
Table 3.4: Summary of G12R mutations found in tumor samples analyzed by ARMS-         HRMA
Table 3.5: Summary of G13D mutations found in tumor samples analyzed by ARMS-         HRMA55
Table 3.7: Summary of G12D mutations found in plasma samples analyzed by ARMS-         HRMA62
Table 3.8: Summary of G12V mutations found in plasma samples analyzed by ARMS-         HRMA64
Table 3.9: Summary of G12R mutations found in plasma samples analyzed by ARMS-         HRMA
Table 3.11: Comparison between tumor sample SS and ARMS-HRMA results72

#### **ACRONYMS**

ADM Acinar-to-ductal metaplasia

ARMS Amplification refractory mutation system

CAT 19-9 Carbohydrate antigen 19-9
CAF Cancer associated fibroblast

cfDNA Circulating-free DNA

CTA Computed tomography angiography

ctDNAcirculating tumor DNAddPCRDroplet digital PCR

dNTP Deoxynucleotide TriphosphateEGFR Epidermal growth factor receptorEMT Epithelial-Mesenchymal Transition

**EUS** Endoscopic ultrasound

EUS-FNA Endoscopic Ultrasonography-Guided Fine-Needle Aspiration
EUS-FNB Endoscopic Ultrasonography-Guided Fine-Needle Biopsy

GAP GTPase-activating protein

**gDNA** Genomic DNA

**GEF** Guanine nucleotide exchange factor

**HRMA** High Resolution Melting

**KRAS** Kirsten rat sarcoma viral oncogene homologue

LB Liquid Biopsies

MRI Magnetic resonance imaging
NGS Next generation sequencing

PanIN Pancreatic intraepithelial neoplasia

PC Pancreatic cancer

PCR Polymerase chain reaction

PDAC Pancreatic ductal adenocarcinoma

qPCR Quantitative PCRSS Sanger Sequencing

**TAM** Tumor-associated macrophage

TS Targeted sequencing

#### 1. Introduction

Even with today's knowledge and technology, cancer was still responsible for the death of an estimated 10 million people worldwide in 2020 according to the World Health Organization<sup>1</sup>. To reduce cancer burden, it is necessary to continuously invest in the development of better screening and diagnosis tools<sup>2</sup> and in more efficient, personalized and affordable treatment options<sup>3</sup>.

#### 1.1. Pancreatic cancer

Pancreatic cancer (PC) has been in the spotlight for having a concerningly low 5-year survival rate, consistently being amongst the poorest in terms of prognosis<sup>1</sup>. In the USA, the 5-year survival rate of PC was around 9% for patients diagnosed between 2007 and 2011<sup>4</sup>. While not among the more common cancers such as colorectal, breast, lung, and prostate cancers, in Portugal PC was responsible for 2086 deaths in 2022 alone, while 2158 people were diagnosed with the disease, according to the Global Cancer Observatory (Figure 1.1). The similarity between the number of new cases and deaths highlights the concerning mortality of this cancer. Unfortunately, this high mortality rate seems to be on the rise over the last 40 years<sup>5</sup>, mostly due to the low efficacy of the current treatment strategies and the late-stage diagnosis of the disease.

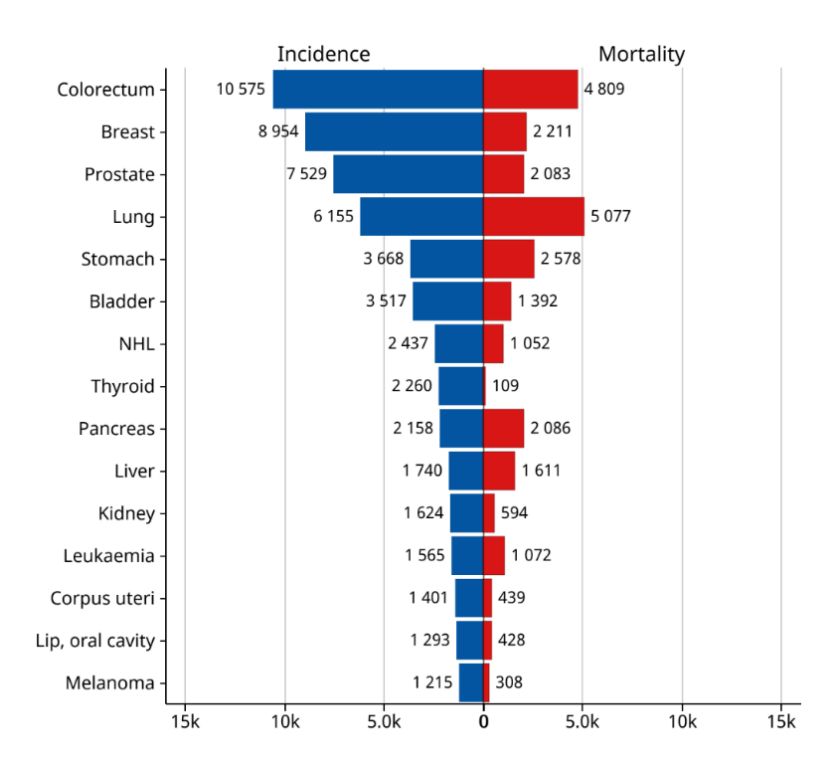


Figure 1.1: Incidence and mortality from different types of cancer in Portugal in 2022. Although pancreatic cancer ranked 9th in number of new cases in 2022, it ranked 5th in number of deaths. Colorectal cancer for example has 4.9 times the incidence of pancreatic cancer while only having 2.3 times the mortality. Data from Global Cancer Observatory: Cancer Today<sup>6(p1)</sup>.

There are two main factors that contribute to the extremely high mortality rate of PC: our inability to detect the disease early enough to begin treatment and the ineffectiveness of the available treatment options<sup>7</sup>.

The silent nature of the disease heavily contributes to its late diagnosis. Most patients experience very few if any, symptoms<sup>7</sup> until the cancer is at a very advanced local stage or often at a metastatic stage, where the chances of a possible recovery drop significantly<sup>8</sup>. When those symptoms are present, they are mostly non-specific, leading to non-specific complaints such as bloating, back pain, nausea, or a change in stool consistency, delaying the search for a possible neoplasia<sup>7</sup>. Without major symptoms, PC screening is only done if other family members also have a PC and/or if the patient is carrying a germline mutation associated with a higher risk of PC, such as breast cancer susceptibility genes (*BRCA1* and *BRCA2*) and cyclin-dependent kinase inhibitor 2A (*CDKN2A*) mutations<sup>7</sup>.

As of today, the only curative option is the complete resection of the tumor<sup>7</sup>. Unfortunately, this is not an option for most of the patients (around 80%) as their tumors are already

in a locally advanced stage or in a metastatic stage, where resections are no longer viable<sup>7</sup>. The impact of resectability as a prognosis parameter is highly relevant, as the 5-year survival rate from patients diagnosed in 2011 is 17.4% in surgically resected patients, while non-resected patients presented a rate of 0.9%<sup>8</sup>. Furthermore, patients with resected tumors still have a high rate of disease recurrence, as up to 71% of patients even with a negative margin resection (R0), may relapse.<sup>4</sup>

In most of PC cases, chemotherapy is used as an adjuvant therapy in a post-operative setting for patients with resectable tumors to increase disease-free survival, or as neo-adjuvant therapy to reduce the tumor size in patients with a locally advanced tumor to make it resectable<sup>7,9</sup>.

#### 1.2. General processes of tumorigenesis

In a state of homeostasis, our cells rely on highly regulated molecular mechanisms to perform their respective functions and fulfill their role in contributing to the body's normal functioning. The general agreement is that cancer originates from a single somatic cell<sup>10</sup>, where the development of a malignant tumor is the result of a multistage process composed of tumor initiation, promotion, malignant conversion, and progression stages<sup>11</sup>.

The initial steps of tumorigenesis involve the acquisition of oncogenic mutations <sup>10</sup>. These mutations can be generated spontaneously during replication or by physical, chemical, and biological agents <sup>12</sup>. Although DNA lesions are very frequent, cells are equipped with several DNA repair mechanisms that are capable of repairing the different types of DNA damage to ensure genomic stability <sup>13</sup>. However, these mechanisms are not 100% guaranteed, and during an individual's life, multiple somatic mutations are continuously accumulated <sup>14</sup>. To circumvent this, cells are also equipped with other tumor-suppressive mechanisms that are able to arrest the cell cycle to detect and correct these errors, or as a last resort, induce cell death, to limit these aberrant cells from proliferating <sup>15</sup>. Still, some mutated cells manage to surpass these mechanisms and survive.

Precancerous cells originate from cells where the acquired mutations provide a clonal advantage, usually by occurring in critical genes involved in maintaining proliferation and/or in inactivating tumor-suppressive mechanisms<sup>10</sup>. Further environmental insults and DNA instability due to high proliferation rates induce the occurrence of additional mutations which can hinder other tumor-suppressive mechanisms, further pushing the cell into a cancerous phenotype with unchecked proliferation<sup>10</sup>. The emerging tumor is also in a constant cross-talk with

the surrounding cells, including fibroblasts and immune cells, creating an inflammatory, immunosuppressive tumor-promoting environment that supports its growth, evolves alongside it, and promotes further alterations<sup>16</sup>. Sites within the tissue where these precancerous cells are growing can be numerous and are described as precancerous lesions, which could stay as benign neoplasms or could evolve into malignant tumor<sup>10</sup>.

Even before they become malignant, cells in precancerous lesions already present a very altered morphology, function and structural organization. Eventually, these cells start to invade the surrounding tissue, becoming malignant which ultimately leads to their metastasization<sup>16</sup>. The disruption of the function of both the organ harboring the primary tumor and other organs colonized by metastases will affect the health of an individual and potentially might lead to death if untreated.

#### 1.3. Carcinogenesis of pancreatic ductal adenocarcinomas (PDAC)

PC originate from precursor lesions such as intraductal papillary mucinous neoplasms (IPMN), mucinous cystic pancreatic neoplasm (MCPN) and pancreatic intraepithelial neoplasia (PanIN)<sup>17</sup>. The most common form of PC is pancreatic ductal adenocarcinomas (PDAC). The most frequent and well-characterized PDAC-associated lesions are PanIN, defined as "microscopic, flat or papillary noninvasive epithelial neoplasms with differing amounts of mucin and grades of cytologic and architectural atypia"<sup>17</sup>. All these lesions have some potential to give rise to neoplasia and consequently are categorized into different levels based on the degree of dysplasia observed<sup>17</sup>. This categorization is relevant not only to the study of how a lesion evolves into a malignant tumor but also to assess the need for surgery when detecting one.

PDAC are malignancies of the exocrine pancreas. In the human pancreas more than 90% of cells are exocrine cells that are mainly composed of acinar cells<sup>18</sup>. Acinar cells are epithelial cells that produce digestive enzymes meant to be discharged in the duodenum alongside the pancreatic juices<sup>18</sup>. Because constant cell renewal is needed to maintain pancreatic homeostasis, acinar cells go through a process called acinar-to-ductal metaplasia (ADM). During ADM, acinar cells lose their exocrine-like characteristics to adopt ductal-like morphology while transiently acquiring a more proliferative progenitor-like phenotype<sup>18</sup>. This is a transient and reversible event that occurs in response to pancreatic tissue insults<sup>18</sup>. The plasticity associated with ADM, although essential for tissue homeostasis, can give rise to PanIN, the most common precursor lesion associated with PDAC. Indeed, persistent ADM can be associated with the combination of oncogenic mutations and continuous pancreatic insults. This can result

from pancreatitis or obesity, two risk factors for PDAC, due to processes such as chronic inflammation, metabolic dysfunction, and oxidative stress giving rise to previously acinar cells being locked in ductal state and eventually evolving into PanIN<sup>18</sup>.

Grade 1 PanIN, the initial stage of the lesion, is characterized by Kirsten rat sarcoma viral oncogene homolog (*KRAS*) proto-oncogene mutations, up-regulated epidermal growth factor receptor (EFGR) signaling and low levels of dysplasia<sup>9,19</sup>. *KRAS* mutations are found in 90% of PDAC, being closely associated with initiation events in this type of cancer<sup>19</sup>. Nevertheless, oncogenic *KRAS* mutations do not seem to be enough to progress the grade 1 lesions into PDAC, with the need of further genetic alterations and more severe inflammatory insults to do so<sup>19</sup>.

The transition to grade 2 PanIN is still accompanied by low levels of dysplasia of the precancerous cells and is characterized by the inactivation of *CDKN1A* and *CDKN2A*, which encode for two cyclin-dependent kinase inhibitors 1A and 2A, respectively, that act as tumor suppressors by being involved in cell cycle arrest<sup>19</sup>. At this point, the modulation of the immune system and the surrounding inflammatory microenvironment is promoting fibrogenesis and consequently the induction of a tumor-promoting, immunosuppressive environment that leads to lesion expansion. Still, the presence of Grade 2 PanIN is not predictive of PDAC<sup>19</sup>.

Grade 3 PanIN are characterized by mutations in tumor-suppressor genes such as tumor protein p53 (*TP53*), *BRCA1/BRCA2* and SMAD family member 4 (*SMAD4*) genes, and by high-grade dysplasia, often being referred to as carcinoma *in situ*. An intense desmoplastic reaction can be observed at this point associated with a cross-talk between different types of cancer-associated fibroblasts (CAFs), tumor-associated macrophages (TAM) and other immune system cells<sup>19</sup>. Unlike grade 1 and 2 PanIN, the presence of grade 3 PanIN is rarely seen without an association to PDAC, making the identification of these lesions essential for the early detection of PDAC<sup>19</sup>.

Moreover, before becoming malignant, the precancerous cells in these lesions can undergo a Epithelial-Mesenchymal Transition (EMT)<sup>20</sup>, where there is a transition of cells from an epithelial state to a mesenchymal state, which promotes mobility, and invasiveness and confer resistance to cell death<sup>21</sup>. Alongside EMT, there is also the loss of cell-cell adhesions and apicobasal polarity and the formation of invadopodia which further promotes the invasiveness and metastatic capacities of these cells<sup>21</sup>. The liver, peritoneum, and lung are the most common destinations for detached cancer cells to seed and colonize, originating metastases<sup>22</sup>. A representative model of these processes is depicted in Figure 1.2.

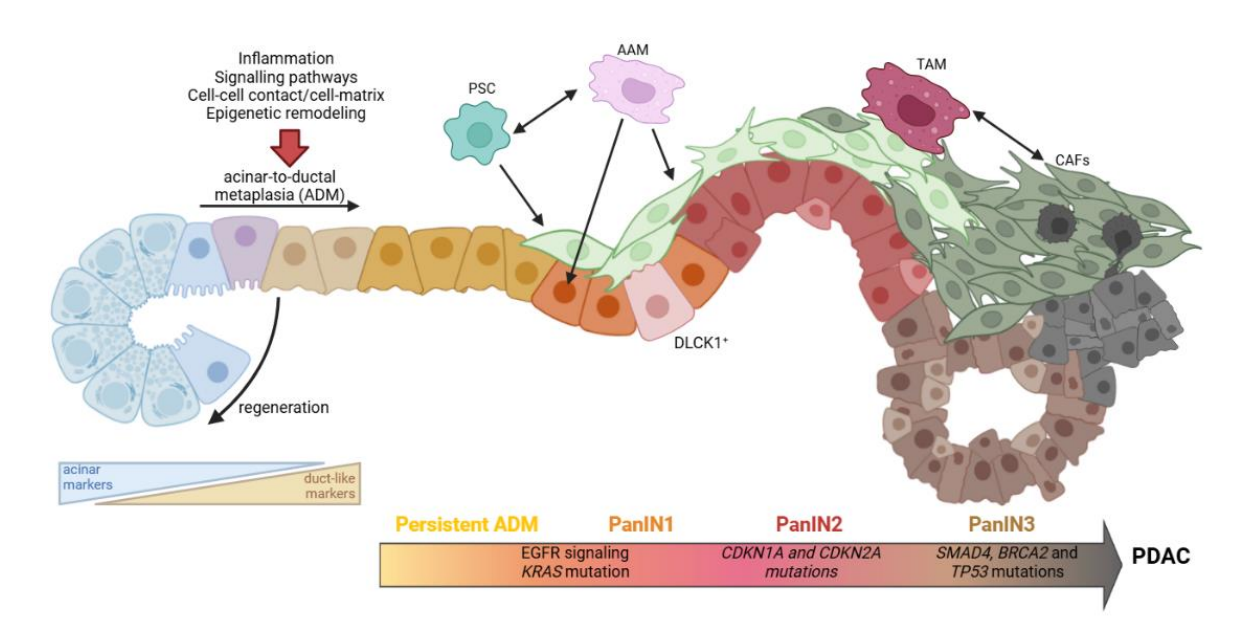


Figure 1.2: Model of the PDAC carcinogenesis process. Pancreatic tissue homeostasis requires the constant renovation of pancreatic cells, which is achieved by ADM. The induction of a persistent ADM state by chronic inflammation and the acquisition of *KRAS* mutations causes ADM cells to spend long periods in an undifferentiated state which can lead to the development of PanIN. Double cortin-like kinase 1 (DCLK1) -positive cells are characterized as a subpopulation of cells with cancer stem-cell properties. During the progression from PanIN1 to PanIN3 there is an increase in dysplasia and genetic instability alongside the accumulation of mutations in oncogenes and tumor suppressor genes. The interaction between pancreatic stellate cells (PSCs) and activated macrophages (AAM) is involved in the creation of a tumor-promoting and immunosuppressive microenvironment. Late stages of the lesion are characterized by the interaction of CAFs and TAM which exacerbate the desmoplastic. Eventually these lesions can become cancerous leading to PDAC. Adapted from Marstrand-Daucé et al.<sup>18</sup> and Storz et al.<sup>19</sup> Created in BioRender.com.

#### 1.4. The KRAS protein

#### 1.4.1. Normal function of the KRAS protein

As stated above, *KRAS* mutations are considered a hallmark of PDAC because of their role as an initiation event for the carcinogenesis process, being present in 90% of PDAC patients<sup>7,19,23</sup>.

The *KRAS* gene is located on the short arm of chromosome 12 that encodes a GTPase from the Ras family<sup>24</sup>. The KRAS protein is a G protein, a membrane-bound GTPase that acts as a binary switch<sup>25</sup>, controlling signal transduction from the interaction between external stimulus and membrane receptors to intracellular molecules<sup>25</sup>. When a stimulus such as the interaction of epidermal growth factor (EGF) and epidermal growth factor receptor (EGFR) occurs, guanine nucleotide exchange factor (GEFs) induces the switch from the KRAS-bound GDP to GTP which will then activate the KRAS protein. The now GTP-bound KRAS changes conformation, which allows it to bind and interact with downstream molecules and activate a variety of signaling cascades<sup>25</sup>. This switch can be turned off by the action of GAPs (GTPase-activating proteins) that induce the GTPase function of KRAS, which will result in the hydrolysis of the GTP into GDP, making the KRAS protein unable to interact with its downstream molecules and restoring its inactive state<sup>25</sup>.

Multiple stimuli can result in the activation of KRAS, such as growth factors like EGF, platelet-derived growth factor (PDGF) and fibroblast growth factors (FGFs), but also Ca<sup>2+</sup>, chemokines and receptor tyrosine kinases<sup>25</sup>. KRAS is involved in the activation of multiple signaling pathways (Figure 1.3) not only involved in cell proliferation, migration and differentiation through the activation of its canonical downstream target, the rapidly accelerated fibrosarcoma (RAF)- mitogen-activated protein kinase (MEK)- extracellular regulated protein kinases (ERK) pathway, but also of other pathways involved in the regulation of cell proliferation, metabolism, survival, protein synthesis and transcription through the activation of the Phosphoinositide 3-kinase (PI3K)- Protein kinase B (AKT)- mammalian target of rapamycin (mTOR) pathway<sup>25</sup>. Cell adhesion, migration and shape are also regulated by KRAS<sup>25</sup> through other pathways.

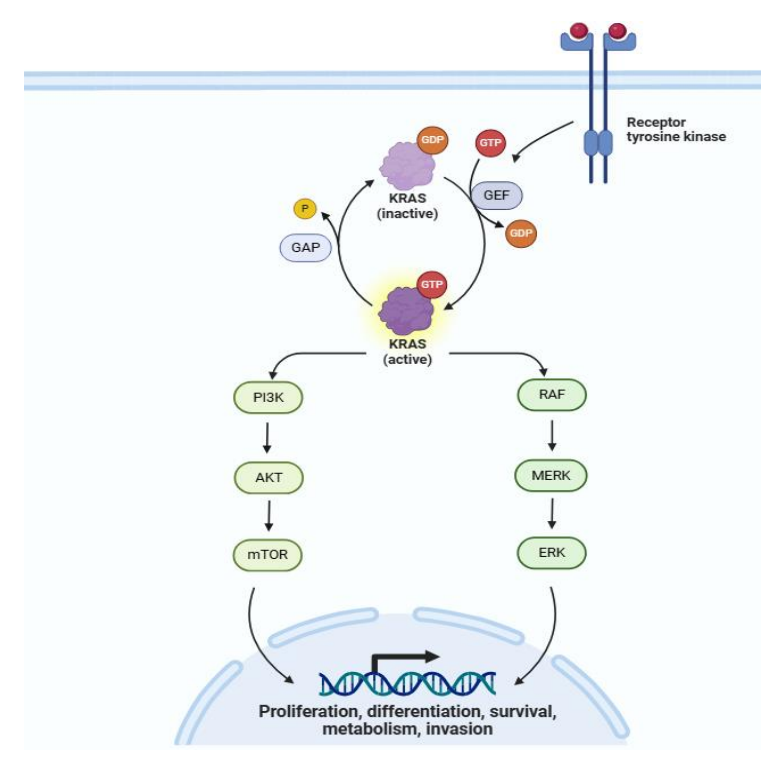


Figure 1.3: Simplified representation of the KRAS signaling pathway. A ligand interacts with its corresponding receptor, such as the interaction between EGF and EGFR. This causes the recruitment of a GEF molecule such as the Son of Sevenless (SOS) through the interaction with an adapter protein such as the growth factor receptor-bound protein 2 (GRB2). GEF activate the KRAS protein by inducing the substitution of GDP for GTP. The activated KRAS protein can then activate multiple signaling pathways such as RAF-MERK-ERK and PI3K-AKT-mTOR which are involved in regulating mechanisms such as proliferation, differentiation, survival, metabolism and invasion. Adapted from BioRender.com

#### 1.4.2. Disruption of normal KRAS function

When *KRAS* is mutated the KRAS protein stays in a permanent GTP-bound state<sup>23</sup> that leads to its constitutive activation and subsequently to the constant activation of the signaling pathways previously mentioned<sup>23</sup>. The disruption of the correct regulation of these pathways/mechanisms controlled by them will contribute to carcinogenesis-associated events like uncontrolled proliferation, inhibition of programmed cell death and migration<sup>23</sup>. *KRAS* mutations have been found to promote the interaction between epithelial cells, immune cells and fibroblasts which will contribute to the immunosuppressive fibroinflammatory microenvironment that hinders tumor elimination by antitumor drugs and/or immune cells, supporting its progression<sup>25</sup>.

#### 1.4.2.1. Targeting KRAS mutations

Many unsuccessful attempts at KRAS-targeted therapies have been made over the years due to its unique characteristics. The KRAS protein surface is described as being smooth, which hinders the development of inhibitory molecules that bind to surface grooves<sup>26</sup>. The affinity to GTP is also very high, which also hinders the development of GTP binding site blockers<sup>25</sup>. Additionally, common EGFR-targeted therapies used in cancer treatment are not effective in patients with a mutated *KRAS* gene, due to the constitutive activation of the KRAS protein, a downstream effector in the EGFR signaling pathway<sup>25</sup>.

#### 1.4.2.2. KRAS mutations across different cancers

*KRAS* is considered to be the most common oncogenic driver of human cancers<sup>25</sup> with several single base missense mutations described<sup>25</sup>. Mutation incidence differs significantly among different types of cancers. PDAC stands out by having the highest *KRAS* mutation incidence, of around 90%<sup>24</sup>, followed by colorectal cancer with an incidence of ~40%, and nonsmall cell lung cancer with an incidence of ~30%<sup>24</sup>. Lower incidences are observed in many other types of cancers such as cholangiocarcinoma with an incidence of ~9.5-18.2%, esophageal carcinomas with an incidence of ~4.5-9.1%, gastric adenocarcinomas with an incidence of ~9.8% and squamous cell carcinoma with an incidence of ~5%<sup>24</sup>. Mutation profile is also different among different types of cancers (Figure 1.4): G12C mutations are the most common in lung cancer (~40% of KRAS mutations) while only having an incidence of ~1% in PDAC<sup>24</sup>. G12V and G12D, the two most common KRAS mutations in PDAC are also well represented in colorectal and lung cancer, however, G13D mutation has an incidence of ~17% in colorectal cancer while having a <1% incidence in PDAC<sup>24</sup>.

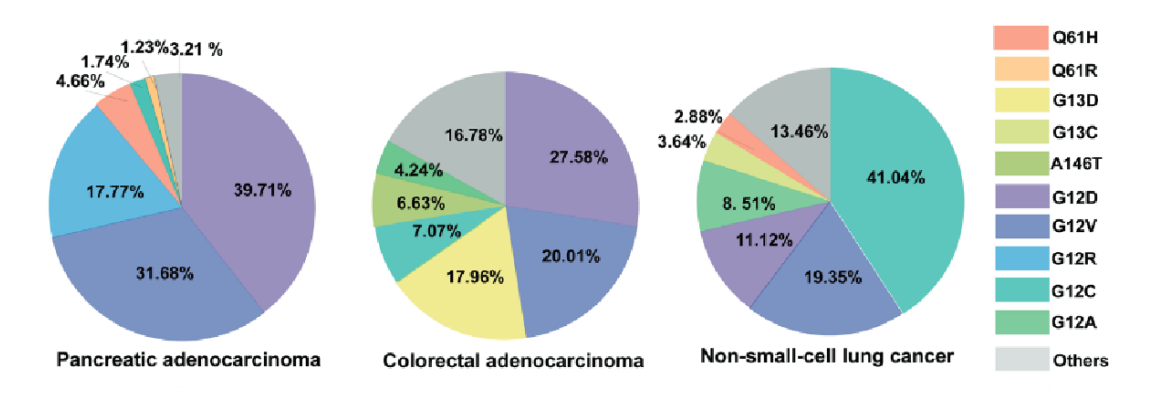


Figure 1.4: Proportion of different KRAS mutations across different types of cancer. Adapted from Huang et al.<sup>25</sup>

#### 1.4.2.3. KRAS mutations in PDAC

Most of the *KRAS* mutations that are found in PDAC patients are in codon 12, with G12D, G12V and G12R the most common<sup>24,25</sup>. Codon 13 and 61 mutations have also been described, but less frequently, and finally mutations in codon 146 have been described in rare cases<sup>,25</sup>. These different mutations can affect the biochemical properties of the KRAS protein in different ways<sup>27</sup>, being associated with different prognosis<sup>28</sup>, with the consensus that PDAC patients with wild-type KRAS have an overall better survival than the ones with mutant KRAS<sup>28</sup>.

#### Codon 12

Both codons 12 and 13 are located in the P-loop coding region, which binds the guanine nucleotides<sup>25</sup>, making G12 and G13 mutations in these codons result in conformation changes in the GTP-binding site which affects the intrinsic rate of GTP hydrolysis<sup>5</sup> and GAP binding<sup>28</sup>. G12D, the most common KRAS mutation associated with PDAC, is oftentimes associated with a worse prognosis<sup>28</sup> and is the target of a novel drug MRTX1133, a selective noncovalent inhibitor of KRAS<sup>29</sup>. AMG510 (or sotorasib) was the first drug to be approved by the FDA that directly targets mutated KRAS, being a non-covalent inhibitor of G12C, inducing a permanently inactive state of the KRAS G12C protein, inhibiting its interaction with its downstream effectors<sup>25</sup>. The discovery of this drug is associated with the observation that KRAS G12C seems to keep its intrinsic GTPase activity, allowing it to alternate between inactive and active states<sup>24</sup> and consequently allowing it to be locked into the inactive state. Inhibitors for other KRAS mutations, such as G12V and G12R, are also being developed with promising results<sup>25</sup>, most notably, the KRAS G12D inhibitor MRTX1133<sup>30</sup>.

#### Codon 13

Codon 13 mutations seem to be sensitive to hydrolysis mediated by the NF-1 GAP, contrasting with codon 12 and 61 mutations which seem to be insensitive<sup>24</sup>. In vivo studies point out that the KRAS G13D mutant organoids seem to be susceptible to EGFR inhibition<sup>31</sup>, going against the general notion that EGFR inhibitors do not have an effect in mutant KRAS cancers.

#### Codon 61

Codon 61 is located in the switch-II coding region, which allows the binding of not only KRAS effector proteins but also its regulators, GAP and GEF<sup>32</sup>. Mutations in this codon are rare, meaning that the disruption of this region might not be as impactful as the disruption of the P-loop. Q61 mutations seem to provide resistance to Src homology region 2 domain-containing phosphatase-2 (SHP2) inhibitors<sup>33</sup>, a potential therapeutic agent for mutant KRAS cancers.

#### 1.5. Personalized medicine

Personalized medicine is the tailoring of healthcare treatment based on the genetic, lifestyle and phenotypic information of an individual<sup>34</sup>. This medical model is continuously being integrated into the general medical practices as it assists medical doctors in making informed decisions on how to treat each patient, by providing information on the treatment efficacy, which dose should be used, the best time for its administration and the chances of causing an adverse reaction. This ultimately lead to higher success and survival rates, less wasted resources on ineffective treatments, and a lower risk of adverse reactions<sup>35</sup>.

#### 1.5.1. Personalized medicine in cancer treatment

The concept of personalized medicine is especially important in the oncology field since cancer is known to be a very heterogeneous disease<sup>36</sup>. Subsets of the same type of cancer can be associated with very different prognoses, which require different treatment strategies<sup>37</sup>. Inter-tumor heterogeneity (of the same type of cancer) can be attributed to different molecular profiles, due to different inherited susceptibility genes and/or acquired mutations<sup>37</sup>. Two examples of how PDAC heterogeneity can affect disease prognosis and treatment are provided: a study by Krasinskas et al.<sup>38</sup> showed that PDAC patients that presented *KRAS* mutant allelespecific imbalance (an increased dosage of the mutant allele over the wild-type one) were associated with were predominantly undifferentiated tumors, more likely to present at clinical stage IV, and were associated with shorter overall survival over PDAC patients who did not; in Barzi et al.<sup>39</sup> a case of a patient with PDAC who presented *ERBB2* (which encodes the HER2 protein) amplification, and *TP53* and *BRCA1* mutations in liquid biopsies was experiencing clinical improvement under anti-HER2 therapy is described. Once the patient started to experience disease progression again, he tested positive for *KRAS* G12R mutations and *ERBB2* was no longer detected.

The inhibition of specific molecular targets has improved clinical outcomes and is already part of standard care of many solid cancers such as breast, colorectal, lung and melanoma<sup>40</sup>. Even though cancer is a disease that benefits greatly from a personalized medicine approach, it also presents unique challenges to it such as intrinsic tumor heterogeneity (Intratumor), microenvironment complexity and evolving clonal dynamics<sup>40</sup>.

#### 1.5.2. PDAC diagnosis and monitoring

Considering the high mortality rate and, that, in the majority of PDAC cases, the disease is detected in advanced stages, an early diagnosis and proper classification of patients for successful therapeutic intervention is critical<sup>41</sup>. Initial detection of the tumor mass and monitoring of the disease after the beginning of treatment is usually done by imaging tools<sup>42</sup>, allowing the identification of pancreas lesions, masses and/or metastases, assess the resectability of the tumor and treatment response. Computed tomography angiography (CTA) with a dual-phase pancreatic protocol has a sensitivity of around 90%<sup>7</sup> and allows the identification of the hypodense appearance of pancreatic tumors when compared to the pancreatic parenchyma<sup>7</sup> and allows the visualization of the vascularization to assess staging and resectability<sup>7</sup>. Magnetic resonance imaging (MRI) alternatively can aid the assessment of the biliary tract and liver lesions<sup>7</sup>. Endoscopic ultrasound (EUS) can be used as an additional tool to identify the relationship between the tumor and the adjacent lymph nodes and vasculature<sup>7</sup>.

#### 1.5.2.1. Solid biopsies

Although the preliminary assessment of PDAC is done using imaging tools, confirmation of diagnosis, definitive staging and molecular subtyping is still done by solid tissue biopsy<sup>43</sup>. Moreover, pancreatic biopsies are also especially relevant in the presence of unresectable tumors, where chemotherapy will have a major role in the treatment strategy<sup>44</sup>.

Tissue biopsies collected for PDAC diagnostics are used for histochemical and immuno-histochemical characterization<sup>45</sup>, the gold standard for staging and assessment of PDAC molecular subtypes. Other techniques, such as flow cytometry<sup>46</sup> and genetic tests<sup>47</sup> can also be used to provide additional information, if necessary, and if there is enough material.

Tissue biopsies can be performed percutaneously or using either Endoscopic Ultrasonography-Guided Fine-Needle Aspiration (EUS-FNA) or Endoscopic Ultrasonography-Guided Fine-Needle Biopsy (EUS-FNB). EUS-FNA is described as a safe and well tolerated procedure, recommended for small lesions whose malignancy could not be assessed by the imaging tools<sup>48</sup>. Meta-analysis of EUS-FNA assisted diagnosis indicates that it is a very accurate diagnostic tool in diagnosing malignancy and identifying its etiology, with a sensitivity of over 85% and a specificity of over 96% in differentiating between benign and malignant lesions<sup>48</sup>. Nevertheless, EUS-FNA also has its drawbacks namely, in the presence of fibrosis and extensive necrotic regions, it has a reduced accuracy, can cause peritoneal dissemination and needle tract seeding at the puncture site on very rare cases<sup>49</sup>, does not preserve tissue architecture and is dependent on the skills of the operator. The EUS-FNB technique on the other side, retrieves higher-quality samples with a higher yield, which makes it more adequate for gene profiling,<sup>50</sup> while also preserving tissue architecture<sup>48</sup>, and allowing histological analyses.

The molecular profiling of PDAC is possible in samples obtained either from resection surgeries or from EUS-FNA and EUS-FNB<sup>51</sup>. Indeed, molecular profiling in PDAC has been gaining momentum and is now done as a routine assessment due to the high number of patients that harbor mutations in *KRAS*, a hallmark of PDAC, or in other crucial genes, associated with therapy resistance or with existent targeted therapy. Indeed, the emergence of mutant KRAS-targeted drugs drives the need for the detection and identification of mutations that provide valuable information on the prognosis and treatment strategy for these patients. Right now, there are not many *KRAS*-related actionable alterations since only the G12C mutation is currently targetable and it constitutes a very small fraction of *KRAS* mutations. The effects of molecular matched therapies on PDAC patient's overall survival are something that is being studied<sup>52</sup>. As new targeted drugs are developed, further studies on the effects of molecular matching therapies on patient survivability become increasingly more relevant.

#### 1.5.2.2. Liquid biopsies (LB)

Solid biopsies play a big role in confirming pancreatic cancer diagnosis, but they are still a very invasive procedure, which limits their use to monitor the disease especially after resection. Liquid biopsies (LB) on the other hand are a more easily obtainable, and a far less invasive option<sup>53</sup>. They can provide real time information on cancers through serial sample collections<sup>53</sup>, something that is not practical in solid tumors, since depending on tumor site it could require multiple surgeries and anesthesia with associated risks while also being significantly more uncomfortable for the patient. LB also allow the analysis of tumor components from multiple sites. Theoretically, they can serve as a temporal and spatial cancer monitoring approach<sup>53</sup>. In general LB analysis is cheaper and has a quicker turnaround time<sup>53</sup>.

LB allow the analysis of many different biomarkers, and the most commonly used is peripheral blood, but other body fluids such as urine, cerebrospinal fluid and saliva also have their uses<sup>53</sup>.

Carbohydrate antigen 19-9 (CA 19-9) levels in peripheral blood have been heavily studied as a PC biomarker<sup>54</sup>. CA 19-9 levels are more elevated in PC patients which could aid its diagnosis and high levels of CA 19-9 during treatment are associated with a worse prognosis, which could be used to monitor the disease<sup>48</sup>. However, this biomarker has shown to be not very reliable, since CA 19-9 can be elevated in other conditions, such as pancreatic inflammation and biliary infections or obstructions, which can lead to i) positives<sup>48</sup>. Also, individuals who are Lewis antigen negative have low or no production of CA 19-9 which leads to false negatives<sup>48,55</sup>. This means that investment in the research of other PDAC biomarkers is still needed to complement or substitute CA 19-9.

Circulating free DNA (cfDNA) is a portion of DNA that circulates freely in the blood-stream, and originates from cellular breakdown mechanisms such as necrosis, apoptosis and phagocytosis, and/or from the active secretion mechanisms<sup>56</sup>. circulating tumor DNA (ctDNA) is a type of cfDNA that has a tumor origin<sup>56</sup> (Figure 1.5). In people with cancer, around 1 to 2% of all cfDNA is ctDNA<sup>56</sup>. LB may allow to isolate not only ctDNA, but also the circulating tumor cells (CTCs), extracellular vesicles that may provide additional tumor-derived information and new biomarkers for early diagnosis<sup>53</sup>. Nevertheless, considering that molecular classification is now part of routine diagnosis, LB may allow the fast detection of *KRAS* mutations in peripheral blood of PDAC patients, a valuable tool for planning the most suitable therapeutic strategy and to monitor patient response.

Buscail et al.<sup>57</sup> analyzed a group of 24 studies that investigated the role of ctDNA in PDAC patients where most of the studies chose the detection of *KRAS* mutations as the evidence for mutated ctDNA. The authors state that this approach had limited value for the identification of earlier stages of the disease, suggesting that either these tumors do not shed enough cells to generate high amounts of ctDNA, or that the ctDNA is too degraded and its concentration too low for current techniques to detect it. Even with high sensitivity techniques such as digital PCR, concordance of *KRAS* mutations between tumor and ctDNA varied between from 25% to 75% where locally advanced and metastatic patients had a much higher concordance (70-80%) than patients with resectable tumors (30-68%). The presence of *KRAS* mutations in ctDNA was also correlated with a worse prognosis in 17 of those studies.

In another study, the correlation between *KRAS* mutations in ctDNA and PC staging reveal that combining the analysis of *KRAS* mutations in ctDNA and CA19-9 levels improved the performance of these biomarkers in predicting malignancy over the analysis of each individual parameters alone, providing an increase in the sensitivity of the test<sup>58</sup>.

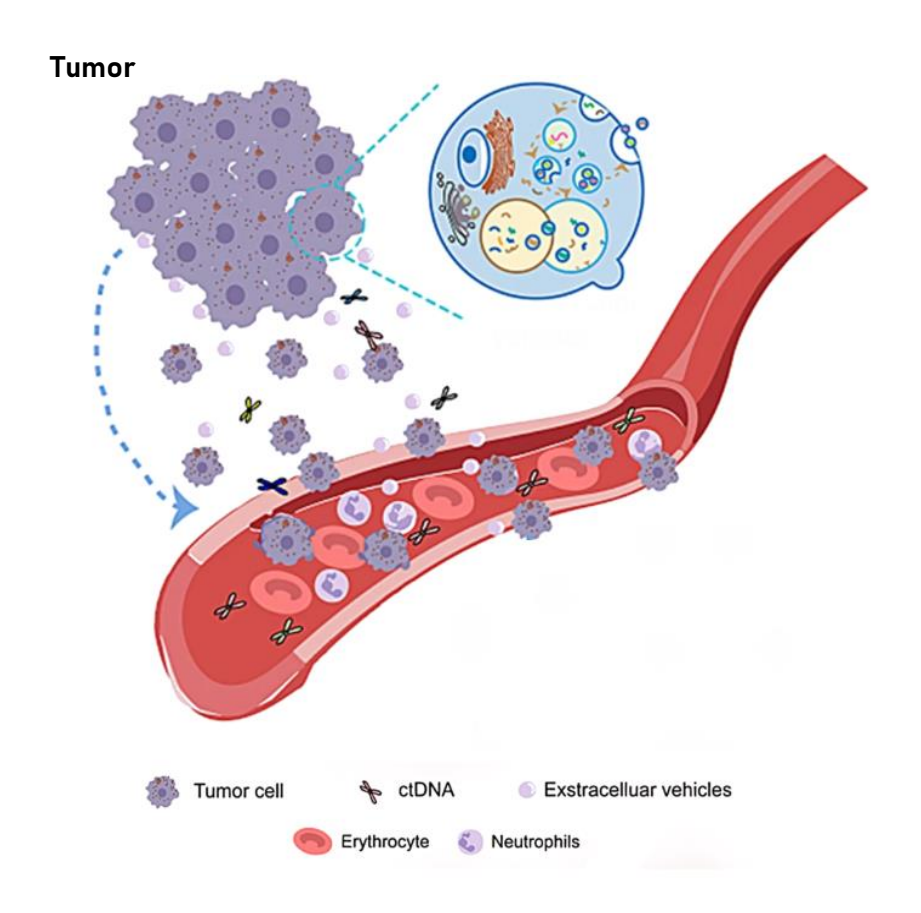


**Figure 1.5: Origin of ctDNA.** The release of cells, DNA and extracellular vesicles by the tumor allow the detection of mutated tumor DNA in the bloodstream. The collection of blood samples is a minimally invasive procedure and is already widely used so there is a growing interest in using this type of sample to obtain information on the tumor's genetic profile to aid cancer diagnosis and treatment. Adapted from Zhou et al.<sup>59</sup>

#### 1.6. Molecular techniques for cancer diagnostics

The discovery of relevant cancer biomarkers and their relevance for the diagnosis, prognosis and treatment of the disease is just as important as the development of tools that can detect and measure them with high specificity, sensitivity and accuracy. Many aspects must be taken into consideration when choosing the adequate technique, such as its higher specificity and sensitivity, lower cost and turnaround time. Currently, there are many techniques that can detect mutations in genes such as *KRAS*, where most of them are iterations of the PCR technique or use it as an initial step, such as sequencing techniques.

#### 1.6.1. Molecular techniques routinely used in clinical practice

In a clinical setting the techniques used for the molecular profiling of cancer patients are the ones that provide the more accurate results and are also economically viable to be performed on a large scale.

#### Polymerase Chain Reaction (PCR) and Quantitative PCR (qPCR)

Originally developed by Kary Mullis<sup>60</sup>, the Polymerase chain reaction (PCR) is a technique that can generate millions of copies of a DNA sequence from just one molecule, being extensively used in areas such as biosciences research, forensics and diagnostics. This technique allows the exponential amplification of a desired DNA sequence by submitting it through temperature cycles. The different temperatures in a PCR reaction, allow the sequential steps of DNA denaturation, annealing of the primers complementary to the desired region and a final sequence elongation to generate the specific product, which can then be visualized by subsequent analysis by agarose gel electrophoresis. The low high throughput and automation of analysis by agarose gel electrophoresis, and the development of fluorescent probes that can bind to DNA with high affinity, led to the development of new PCR equipment that allows to directly monitor amplification of PCR product by detection of fluorescence over time - real-time PCR or quantitative PCR (qPCR)<sup>61</sup>, resulting in the entire reaction and analysis happening in a closed tube. This can be done using a fluorescent dye whose fluorescence levels are proportional to the number of copies present in solution (Figure 1.6).

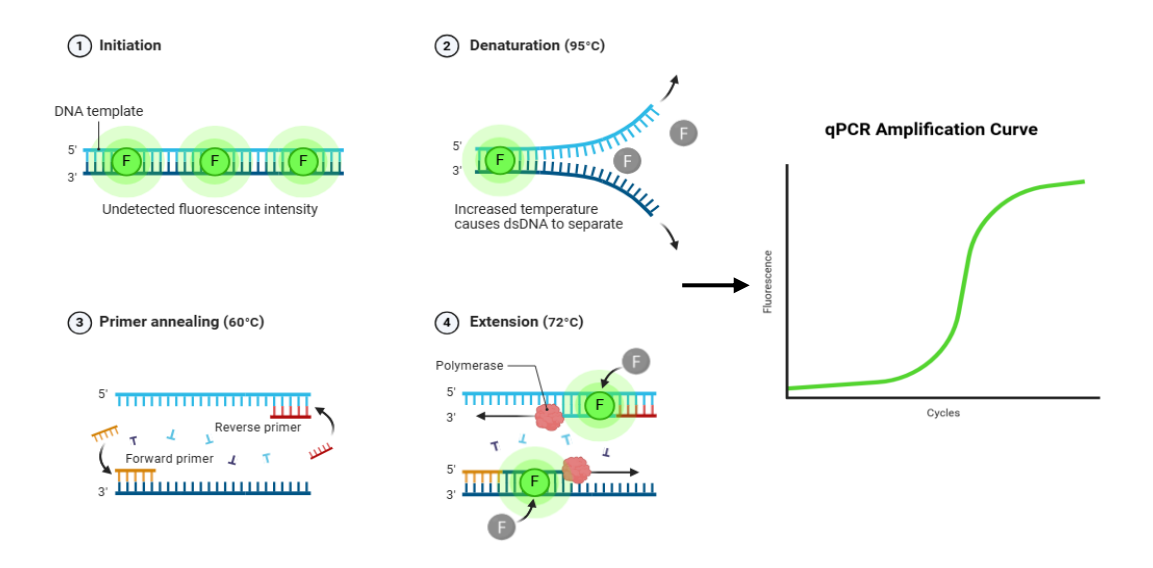


**Figure 1.6: qPCR.** In this technique, a fluorophore that emits a fluorescence signal when associated with dsDNA, allows to monitor the amplification of the target DNA over each cycle. As the number of copies of DNA target increase, the amount of dye associated with dsDNA increases and so does the fluorescence signal. Adapted from BioRender.com.

#### Sanger Sequencing (SS)

The Sanger Sequencing (SS) technique was first described in 1977 by Fred Sanger and his colleagues, where they used deoxynucleoside triphosphate analogues, dideoxynucleotides (ddNTPs), that were initially labeled with radioactive <sup>32</sup>P, and later with <sup>33</sup>P and <sup>35</sup>S, as chainterminating inhibitors of the DNA polymerase extension reaction<sup>62</sup>. The random incorporation of these analogues in the DNA sequence, resulted in DNA fragments of different sizes, which could then be analyzed by polyacrylamide gel electrophoresis (PAGE). After PAGE, the gel was dried, exposed in a darkroom to a large sheet X-ray film, and stored at -80 °C for a period. After X-ray film development, the DNA sequence was analyzed in a light box. Later on, due to the health problems generated by the exposure of lab personnel to radioisotopes, radioactive-labeled ddNTPs were replaced by fluorescent-labeled ddNTPs<sup>63</sup>, still in use as of today (Figure 1.7). This technique totally revolutionized the Molecular Genetics and Diagnostic fields, being widely adopted and the equipment's extensively improved to accelerate speed, accuracy and ease of the process. Due to its robustness, SS can still be considered the gold standard for sequencing of single genes, being widely used in scientific research and in the clinical setting to identify point mutations and polymorphisms<sup>64</sup>.

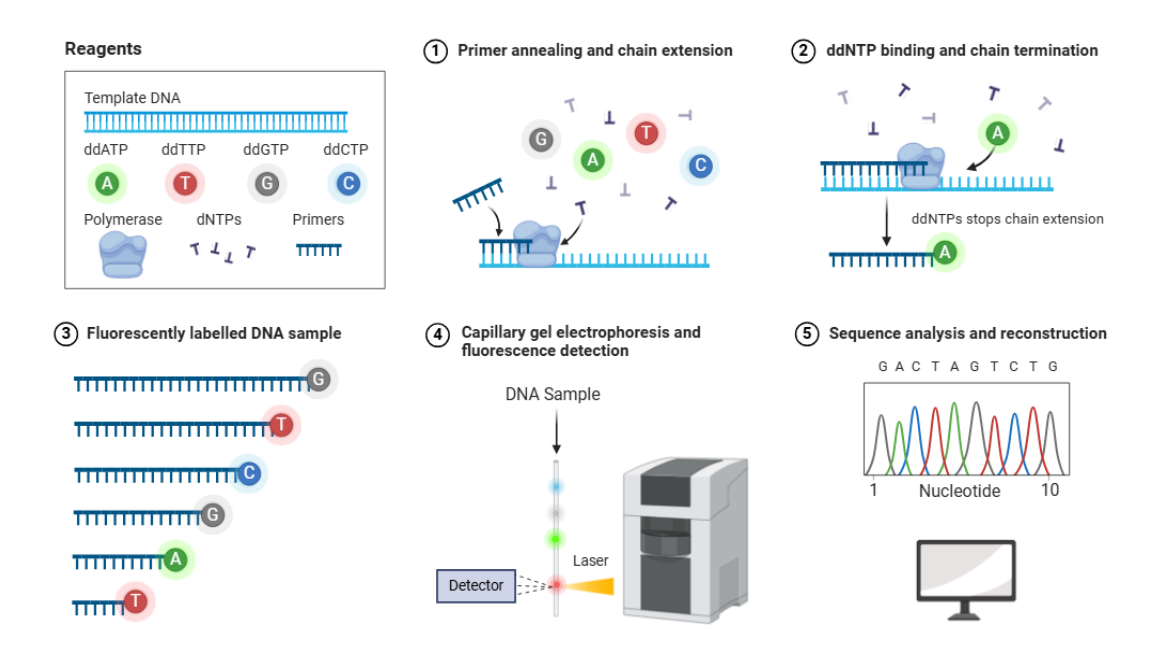


Figure 1.7: Schematic representation of the modern SS methodology. A mix of dNTPs and fluorescently labeled ddNTPs are used in the amplification reaction. When the fluorescently labeled ddNTPs are randomly incorporated, the chain can no longer be elongated by the polymerase (1 and 2). The different fluorescence signals associated with different size fragments (3) can then be detected and analyzed in a chromatogram (4 and 5). Retrieved from BioRender.com.

#### Amplification refractory mutation system (ARMS)

The amplification refractory mutation system (ARMS) is a technique developed by C. R. Newton and colleagues, being an adaptation of the classic PCR technique, that takes advantage of the fact that primers with a mismatched nucleotide bind less efficiently to the target DNA region<sup>65</sup>. This allows the identification of single nucleotide variants by using a mutation-specific primer that will have a mismatch with the wild-type sequence. To further reduce the possibility of amplification of the wild-type sequence, additional mismatched bases are added near the 3' end<sup>65</sup>. A PCR reaction using this primer will only amplify the target sequence in the presence of the mutation (Figure 1.8) while a second reaction using a wild-type matching primer will not amplify in the presence of the mutation. The PCR products can then be analyzed by observing the bands in an agarose gel, where the presence of a band in the lane with the mutation-specific primer reaction means the mutation is present in the analyzed locus, while a band in the lane with the wild-type-specific primer reaction means that the mutation is not present.

The presence of bands in both lanes means that the mutation is present in heterozygosity (Figure 1.8).

As with other molecular techniques, the need for high throughput, led to the development of variations of this methodology that used the same principle but with more all primers simultaneously in the same reaction, where an outer pair of wild-type matching primers is complemented with an inner mutation-specific primer, resulting in PCR products of different sizes depending on whether the inner primer is able to bind to the target sequence or even in a multiplex approach targeting different mutations in the same locus or different loci<sup>66</sup>. The results still need to be analyzed in an agarose gel electrophoresis to analyze the presence of multiple bands, corresponding to the wild-type alleles or the mutated alleles. The addition of another inner primer, wild-type specific, allows the detection of mutations in heterozygosity, as the resulting DNA fragments of mutated and wild-type sequences will be of different sizes. Since the mutation analysis is dependent on mutation-specific primers, the cost-effectiveness of the ARMS technique is considerably lower when analyzing multiple genes.

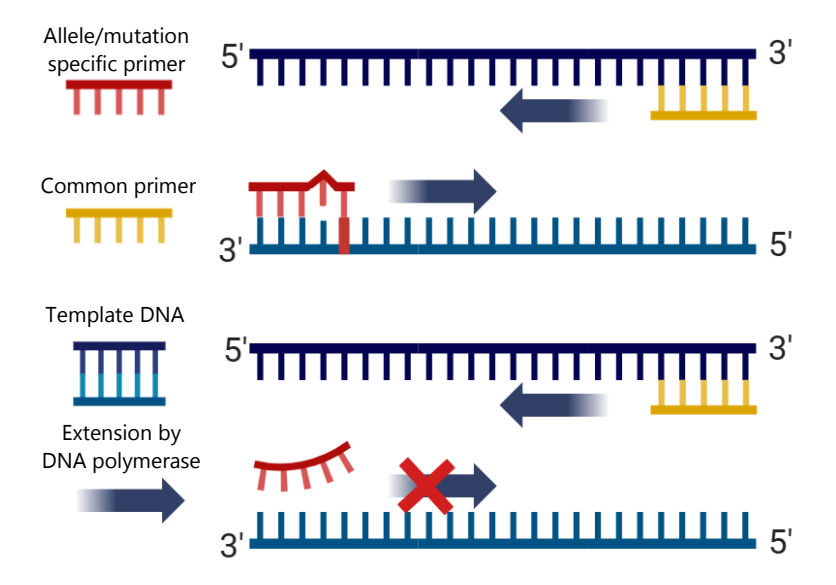


**Figure 1.8: ARMS principle.** One of the primers is designed to only bind to the template DNA when a specific mutation/allele is present, allowing extension by the DNA polymerase only in the presence of that mutation/allele, where only one base is mismatched. In the presence of the wild-type sequence, the mismatched bases significantly reduce the efficiency of the reaction. The amplification products can be visualized in an electrophoresis gel where the presence of a band means the amplification of the studied allele was successful. Created in BioRender.com.

## Droplet digital PCR (ddPCR)

Droplet digital PCR (ddPCR) is a version of qPCR where the sample is partitioned into thousands of nanoliter-sized droplets<sup>67</sup>, which can be obtained by the creation of a water-on-oil emulsion. Fluorescence is measured in each of these droplets to assess if the amplification was successful. Counting the number of droplets that are positive, i. e. that present fluorescence, allows the quantification of the target sequence<sup>68</sup>. Due to the nature of this technique, even miniscule amounts of the target sequence can be detected, as quantities as small as a single molecule can be amplified in a droplet. This makes ddPCR a powerful tool for the detection of genetic alterations, especially in the field of precision oncology, for allowing the detection of low-abundance molecular targets in various biological fluids such as the detection of ctDNA in blood. However, dPCR-based techniques still present some disadvantages such as incomplete amplifications due to small sample volumes, higher risk of sample contamination, limited use for large amplicons and limited multiplexing ability<sup>69</sup>.

Because of its high costs, the use of ddPCR is usually limited to laboratories specialized in cancer diagnostics and is yet to be a hallmark in all diagnostic laboratories.

## 1.6.2. Molecular techniques that are not routinely used in a clinical setting

Other molecular techniques can be used to detect gene mutations/polymorphisms in patient samples. These techniques can have many advantages such as very high sensitivities or the analysis of multiple genes at the same time, being widely used in a research context, but their use in the clinical practice is still limited, due to factors such as validation issues, cost, turnaround time or complexity.

### High Resolution Melting Analysis (HRMA)

HRMA is a technique that was described in 2003 by Wittwer and colleagues<sup>70</sup>, that is based on the high-resolution melting analysis of amplicons previously described by Gundry et al.<sup>71</sup> but without the need for labeled oligonucleotides. HRMA takes advantage of the presence of dyes that bind DNA, emitting fluorescence. These dyes bind efficiently to dsDNA which allows the monitoring the melting of DNA at different temperatures<sup>72</sup>. This technique requires the denaturation of PCR products followed by a rapid renaturation due to a sudden decrease in temperature. In homozygotic samples the DNA strands return to their normal state, forming homoduplexes, but if the sample is heterozygotic or if a mutation is present, the sudden

renaturation is going to originate heteroduplexes as well, due to the annealing of two different sequences. When the PCR products are submitted to a gradual temperature increase, they start to denature again. Because heteroduplexes have mismatched nucleotides their melting temperature is going to be lower than homoduplexes, since they are more unstable, and subsequently denature more easily. This difference in denaturation rates can be detected with the utilization of the previously mentioned fluorescent dyes. These dyes only present fluorescence when bound to dsDNA which means that it is possible to follow the denaturation process by measuring the fluorescence intensity. The presence of mutations and of different alleles can then be detected by analyzing the differences in the melting curve profiles (Figure 1.9). The analysis of the derivative plot of the generated melting curve is common as it allows the analysis of peaks associated with the melting temperatures of the different amplicons <sup>72</sup>.

HRMA is faster and cheaper than SS, but it cannot identify mutations per se, making it more suited for high throughput screening and requiring confirmation by other techniques on the positive cases which may hamper cost and translation to the clinics.

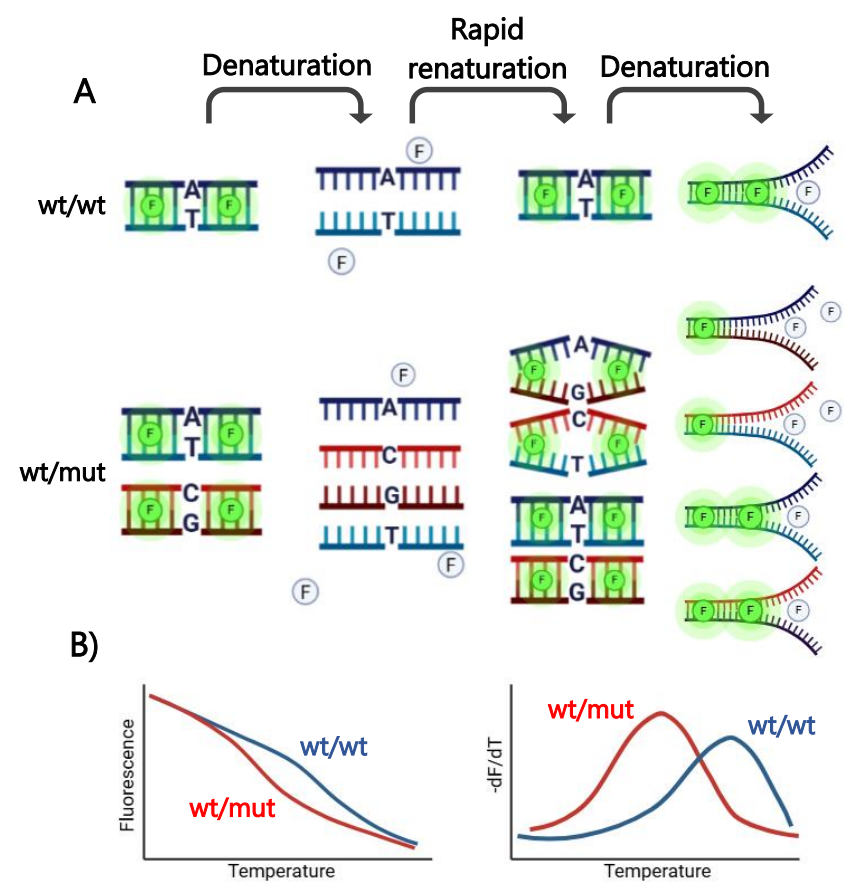


Figure 1.9: Schematization of the HRMA principle. A) After sample amplification, samples are denatured using high temperatures and renaturated using a sudden decrease in temperature. This rapid renaturation causes the formation of heteroduplexes with mismatches if the sample is heterozygotic or if a mutation is present. During the final denaturation step, heteroduplexes present lower melting temperatures due to the mismatches, causing a faster release of DNA-binding dyes. B) This results in a faster decrease in fluorescence that can be observed when comparing the melting curves of homozygotic and heterozygotic/mutated samples. Created in BioRender.com.

### **Next generation Sequencing (NGS)**

In the last few decades new sequencing technologies such as Illumina, 454 and Ion torrent have emerged, part of the next generation sequencing (NGS)<sup>64</sup>. NGS technologies use the massively parallel sequencing of single DNA molecules to dramatically increase sequencing data-output which allows the analysis of various lengths of DNA or RNA sequences or even whole genomes in relatively short periods<sup>73</sup>. In Illumina sequencing, adaptor-bound DNA fragments bind to a surface where a bridge amplification occurs. During the initial amplification,

several million dense clusters of double-stranded DNA are generated. In each sequencing cycle, a single labeled dNTP is added to the bound nucleic acid chains, terminating the polymerization temporarily. Since the dNTPs are fluorescently labelled, it is possible to detect which one was incorporated in each sequencing cycle<sup>74</sup>. In 454 sequencing adaptor-bound DNA fragments are amplified while bound to a bead. After amplification, each bead is placed in an individual well where DNA synthesis occurs. Only one of 4 fluorescently labeled dNTPs (A, T, C or G) is added each time, which allows the identification of where the incorporation occurred<sup>75</sup>. Ion torrent sequencing uses a similar approach as 454 sequencing but takes advantage of the fact that a proton is released as byproduct when a dNTP is incorporated. By adding one of the 4 dNTPs at a time, it is possible to detect if the pH changed and infer if and how many of the added dNTP were incorporated during DNA synthesis<sup>74</sup>.

The high costs, lack of standardized material for clinical application and the need for powerful bioinformatics tools and specialized personnel for both experimental and data analysis limit the use of NGS in diagnostic laboratories. However, targeted sequencing (TS), a specialized application of NGS, focuses on sequencing a smaller cluster of genes which requires less powerful bioinformatics tools and is associated with reduced costs and turnaround times while maintaining excellent coverage depth. This facilitates the implementation of NGS technologies in less specialized laboratories.

In Table 1.1 a comparison of the different molecular techniques used in research or clinical settings is depicted.

**Table 1.1:** Comparison of different molecular techniques for mutation analysis (advantages, disadvantages, limit of detection, routine use in clinics and references).

<sup>\*\*</sup>Whether these techniques are used routinely in clinical practice heavily depends on the economic context of the institution and country and the specialization of the laboratory

Technique	Advantages	Disadvantages	Limit of detection*	Routinely used in clinical practice?	References
SS	Allows the analysis of the entire region of interest	long turnaround time labor intensive high cost	10%-20%	Yes	76–78
ARMS	High sensitivity low run time high specificity	Can lead to false positives when mismatched primers allow amplification Only allows the detection of one mutation	1%	Yes	77,79
HRMA	Good for high- throughput screening not labor intensive	Low specificity need further tech- niques for mutation confirmation	5%-10%	No	77,78
ddPCR	Very high sensitivity	high cost	0.001%- 0.1%	No**	68,80
NGS/TS	Allows the analysis of entire regions of in- terest in single or multiple genes	Very High cost Not appropriate for analyzing a single gene (NGS)	2%-15%	NGS-No** TS-Yes	81,82

<sup>\*</sup>The lower proportion of mutant to wild-type DNA that the molecular technique can detect.

# 1.6.3. Choosing the right molecular technique for PDAC molecular diagnostics

Multiple techniques can be used to detect KRAS mutations. The gold standard until now has been the use of SS to analyze exon 2 of KRAS gene, allowing the detection of all mutations in codon 12 and 13 of KRAS protein, where the most frequent alterations associated with PDAC are described<sup>24,25</sup>. Considering the advantages/disadvantages of the above-described molecular techniques (Table 1.1), the cost of SS is not so high (as only one exon is analyzed per patient) but the turnaround time, the limit of detection and the labor-intensive nature of SS hampers its use in tumor samples. Indeed, up to 85% of a PDAC tumor can be constituted by stroma<sup>83</sup>, which along the tumor heterogeneity can mean that the percentage of cells that carry KRAS mutations in a tumor sample might be much lower than the limit of detection of SS, leading to false negative results. In fact, this has already been observed in studies that compared multiple techniques to detect KRAS mutations, where SS presented a high % of false negatives<sup>78</sup> when compared to ARMS or melting analysis-based techniques. The lower sensitivity of SS is even more prominent in LB, as the proportion of ctDNA in cancer patients can be as low as 0.1% of cfDNA<sup>84</sup>. This is corroborated by the work done in Beatriz et al.85 where the coupling of ARMS and HRMA presented a higher sensitivity than SS when analyzing both tumor and plasma samples of PDAC patients. NGS is not an appropriate option for testing a single gene like KRAS, since its major usefulness resides in testing large panels of multiple genes, but TS has in fact been implemented in clinical practice. NGS, and in this case, targeted resequencing seems to have a higher detection capability, being able to detect smaller proportions of mutated DNA. In fact it has been used successfully to detect KRAS mutations in plasma samples in research settings<sup>86</sup>. The use of targeted resequencing is, however, more expensive than SS, and this cost increases with the increase of number of loci under study.

The ARMS technique is also used to detect *KRAS* mutations, as it is an appropriate technique for the detection of single point mutations which dominate the PDAC mutational landscape. However, conventional ARMS, mostly used until now in the clinical practice, does not have the capability to detect all *KRAS* mutations at once, since the primers used in the ARMS are mutation specific, but it is still a cheap, fast and more sensitive option with a much lower limit of detection compared to SS. Nevertheless, there is also the possibility of false

positives, as mismatched primers still have a small capacity to allow amplification<sup>79</sup>. In the later years, multiplex ARMS entered the clinical practice with the validation of the Therascreen KRAS Mutation Detection kit (DxS Ltd, Manchester, United Kingdom), is an FDA-approved companion diagnostic (CDx) kit for the simultaneous detection of the 7 mutations in KRAS (G12A, G12D, G12R, G12C, G12S, G12V and G13D) in patient's tissue samples. Nevertheless, so far it has not been approved for PDAC tissue or plasma samples<sup>87(p2)</sup>. The limit of detection associated with ARMS, although lower than SS, could still the utilization of similar kits for LB.

The HRMA technique can be used as a high throughput option for *KRAS* mutation detection and even though its limit of detection is higher than ARMS, it is still lower than SS, while also being cheaper and not so labor intensive. These characteristics make this technique an attractive option when considering the integration of genomic testing in the PDAC treatment pipeline. However, as HRMA alone cannot discriminate the mutation present, its application as a stand-alone technique is limited. Since the objective is to not only assess the presence of certain mutations, but also to personalize the treatment approach based on the mutation present, using a technique that is able to do as a stand-alone, is of our best interest. A very sensitive technique capable of both detecting and identifying mutations such as ddPCR could be of great use, especially when analyzing plasma samples. Unfortunately, the characteristics that make this option attractive, namely its limit of detection, also it is much more expensive, which has been hindering its routine application in every clinical setting, being applied mostly in oncology labs.

#### 1.7. Aim of this work

Our inability to meaningfully reduce PDAC's burden in the last decades requires the investment in better diagnostic and monitoring tools. Therefore, this project was developed as a continuation of previous work by Oliveira et al.<sup>85</sup> which described a new methodology based on the combination of ARMS and HRMA to detect *KRAS* mutations in tumor and plasma samples. The validation of this methodology would provide an alternative to the current molecular techniques used in clinical settings to aid PDAC treatment.

The primary objective of this work was to increase the dataset, namely by using a larger cohort of tumor and plasma samples of PDAC patients (97) to obtain a more robust validation of the ARMS-HRMA technique for a future translation to a clinical setting. Indeed, the existence of simple, cheap and robust techniques that can detect *KRAS* ctDNA in LB may have a strong impact on early diagnostics and monitoring of PDAC patients. Moreover, taking into

consideration, the impact of the molecular classification of PDAC patients to choose the most suitable treatment strategy and existence of a drug for targeting G12C KRAS mutation (and soon to other KRAS codon 12 mutations), and the potential impact for personalized medicine of the presence of more than one *KRAS* mutations in PDAC patients, another objective of the present work, was to design, validate and detect three additional mutations in KRAS protein, G12R, G12C and G13D, in this new cohort of PDAC patients. SS was used as the gold standard technique for molecular analysis and comparison of results. At the end of this study, we hope to have validated the ARMS-HRMA technique for the detection of the 5 most frequent mutations in codons 12 and 13 of KRAS protein, namely, G12D, G12V, G12R, G12C, and G13D in 97 tumor and plasma samples of PDAC patients.

# 2. MATERIALS AND METHODS

#### Materials

- High Pure PCR Template Preparation Kit (Roche, Basel, Switzerland);
- Surgical blades (Nahita, Navarre, Spain);
- Needles (B. Braun, Lisbon, Portugal);
- Isopropanol (Merck, Darmstadt, Germany);
- DreamTag™ Buffer (10X) (Thermofisher, Waltham, Massachusetts, USA);
- dNTPs NZYMix (NzyTech, Lisbon, Portugal);
- DreamTag™ (NzyTech, Lisbon, Portugal);
- DEPC-treated water (Invitrogen by Thermofisher Scientific, Waltham, Massachusetts, USA);
- Agarose MB02703 (NzyTech, Lisbon, Portugal);
- Acetic acid (Merck, Darmstadt, Germany);
- EDTA (Chem Lab nv, Zedelgem, Belgium);
- Tris Base (Fisher BioReagents, Pittsburgh, Pennsylvania, USA);
- GelRed® Nucleic Acid Gel Stain (Biotium, Fremont, California, USA);
- GeneRuler DNA Ladder Mix SM0331 (Thermofisher Scientific, Waltham, Massachusetts, USA);
- Supreme NZYTaq II 2x Green Master Mix (NzyTech, Lisbon, Portugal);
- DMSO (Honeywell, North Carolina, USA);
- Primers for PCR and ARMS-HRMA (STABVIDA, Setubal, Portugal)

## 2.1. Biological Materials

In this work, patients with newly diagnosed and histologically proven PDAC treated at the referral center Hospital Beatriz Ângelo (Loures, Portugal) and Hospital da Luz (Lisbon, Portugal), between October 2017 and November 2022 were included. The study was conducted according to the guidelines of the Declaration of Helsinki and approved by the Ethics Committee of Hospital Beatriz Ângelo (1372/2015\_CMOEB 127 (approved on 31 December 2015)) and Hospital da Luz (CES/13/2018/ME (approved on 12 128 April 2018)). Informed written consent was obtained from all the patients. During the study period, 97 PDAC patients had available fresh frozen tumor and plasma samples and were included in the present study. 50 out of 97

patients had two plasma samples available, one extracted at diagnosis before any treatment (P1), and another extracted months after (P2).

Tumor samples (resected patients and EUS-FNB) were collected into sterile 1ml Eppendorf tubes kept at 4°C, and immediately frozen in liquid nitrogen and stored at -80°C for later molecular analysis.

Blood samples were collected at diagnosis before any treatment. A small amount of blood (8mL) was collected into 2 EDTA-blood tubes and kept at 4°C; these were transported to the laboratory at 4°C within a maximum period of four, ideally 2 hours. Blood components were then separated by centrifugation (2000 xg, 10 min at 4°C) and placed in cryotubes and plasma samples were flash-frozen in liquid nitrogen and stored at -80°C for later analysis.

The controls groups used in the ARMS-HRMA reactions consisted of gDNA from 6 different cell lines, described in Table 2.1.

## 2.2. Control samples (cell lines)

In this work, we have used 6 different cell lines with different *KRAS* genotype to extract the genomic DNA (gDNA) to be used as controls in the ARMS-HRMA reactions. The characterization of the different cell lines is described in Table 2.1.

**Table 2.1:** Characterization of the different cell lines used in this study

Cell Line	Reference	Origin	Genotype ( <i>KRAS</i> ) (mutation in codon 12 or 13 of KRAS protein)
HT-29	ATCC HTB-38™	Isolated from a 44-year-old, white, female patient with colorectal adenocarcinoma.	wild type
LS174T	ATCC CL-188™	Isolated from the colon of a White, 58-year-old, female adenocarcinoma patient with colorectal cancer.	heterozygous (p.G12D)
SW480	ATCC CCL-228™	Isolated from the large intestine of a Dukes C colorectal cancer patient Leibovitz's L-15	homozygous (p.G12V)
HCT116	ATCC CCL-247™	Isolated from the colon of an adult male with colon cancer	heterozygous (p.G13D)
H358	ATCC CRL-5807™	Isolated from the bronchiole of a male patient with bronchioalveolar carcinoma.	heterozygous (p.G12C)
PSN-1	ATCC CRL-3211™	Isolated from the pancreas of a patient with adenocarcinoma	heterozygous (p.G12R)

#### Methods

### 2.3. Cell culture

HCT116 and HT-29 tumor cell lines were grown in Dulbecco's Modified Eagle Medium (DMEM; GibcoTM, ThermoFisher Scientific, Waltham, MA, USA), PSN-1 and H358 cell lines were grown in Roswell Park Memorial Institute Medium (RPMI; GibcoTM, ThermoFisher Scientific, Waltham, MA, USA), LS174T cell line was grown in Eagle's Minimum Essential Medium (EMEM; Merck, Darmstadt, Germany), SW480 cell line was grown in Leibovitz's L-15 Medium (GibcoTM, ThermoFisher Scientific, Waltham, MA, USA) all supplemented with 10% (v/v) Fetal Bovine Serum (FBS; GibcoTM, ThermoFisher Scientific, Waltham, MA, USA) and 1% (v/v) antibiotic/antimycotic (GibcoTM, ThermoFisher Scientific, Waltham, MA, USA) and maintained in 25 cm2 culture flasks (VWR, Pennsylvania, USA) at 37°C in a 99% humidified atmosphere of 5% (v/v) CO2 (CO2 Incubator Leec, United Kingdom).

#### 2.4. DNA extraction

DNA extraction from PDAC patient's tumor and plasma samples and from all control cell lines was performed using the High Pure PCR Template Preparation Kit. The extraction protocol was performed according to the protocol provided by the company with some modifications, described below for tumor and plasma samples.

For tumor samples, 25-50 mg of tumor sample were added to a 1.5 ml Eppendorf tube. To facilitate the tissue digestion process, the tumor piece was cut into smaller portions using a surgical blade and needle. 200  $\mu$ L of Lysis Buffer and 40  $\mu$ L of reconstituted Proteinase K were added to the Eppendorf tube and the content was mixed. The Eppendorf tube was then incubated at 55°C for 1 hour or until the tissue was digested completely i. e. no discernible clumps of tissue were present inside the tube. The tube was inverted and flicked multiple times during incubation to promote the physical disruption of the tissue. After incubation, 200  $\mu$ L of binding Buffer were added to the tube, the contents were mixed immediately, and the tube was incubated again at 70 °C for 10 minutes.

For plasma samples, 300  $\mu$ L of plasma were added to two different Eppendorf tubes. If there was not enough sample available, 200  $\mu$ L of plasma were added to two Eppendorf tubes or 300  $\mu$ L to a single tube instead. 300  $\mu$ L of Binding Buffer and 60  $\mu$ L of proteinase K were

added to each tube, scaled down to 200  $\mu$ L and 40  $\mu$ L respectively for tubes with 200  $\mu$ L of plasma sample. The tubes were then incubated at 70°C for 10 minutes.

For tumor samples, 100  $\mu$ L of isopropanol were added to the Eppendorf tube after the incubation step. For plasma samples, 150  $\mu$ L of isopropanol were added, scaled down to 100  $\mu$ L for tubes with 200  $\mu$ L of plasma sample. With the help of a pipette tip, the insoluble fragments of tissue were discarded to avoid clogging the filter. The content in the Eppendorf tube was pipetted into the High Pure filter's reservoir in a collecting tube and centrifuged at 8000xg for 1 minute and 30 seconds (1 minute for plasma samples). After replacing the collection tube, 500  $\mu$ L of Inhibition Buffer was added and the assembly was centrifuged at 8000xg for 1 minute and 30 seconds (1 minute for plasma samples). After replacing the collection tube, 500  $\mu$ L of Wash Buffer was added and the assembly was centrifuged at 8000xg for 1 minute and 30 seconds (1 minute for plasma samples). After the last step was repeated once, the tube was centrifuged at 13000xg for 30 seconds (10 seconds for plasma). This time the collection tube was replaced by an Eppendorf tube. Then, 50  $\mu$ L (30  $\mu$ L for plasma samples) of Elution Buffer preheated to 70°C was added to the filter reservoir assembled in the Eppendorf tube and centrifuged a final time at 8000 xg for 1 minute and 30 seconds.

Tumor sample DNA concentration was measured using the Microvolume Spectrophotometer NanoDrop (Thermo Fisher, Waltham, Massachusetts, EUA).

## 2.5. Amplification of KRAS exon 2

A PCR was performed on all tumor samples to analyze the exon 2 of the *KRAS* gene. The primers used are presented in Table 2.2. The PCR reaction mixture composition (for a total of 20  $\mu$ L) is presented in Table 2.3. The reaction mixture for tumor samples used 100 ng of gDNA, while the reaction mixture for plasma samples used 2  $\mu$ L of DNA regardless of the concentration. The reactions were performed in a DNA Engine® Thermal Cycler (Bio-Rad, Hercules, California, USA) following the PCR program described in Table 2.4.

**Table 2.2:** Primers used for the amplification of the exon 2 of KRAS. These primers were designed by PhD student Beatriz Oliveira.

Primer Forward	5'-GGTGGAGTATTTGATAGTGTA-3'
Primer Reverse	5'-TGGACCCTGACATACTCCCAAG-3'

Table 2.3: PCR Reaction Mixture used to amplify exon 2 of KRAS

Reagent	Final Concentration	Volume (μL)
H2O DEPC	-	13.52 μL
Buffer Dream 10x	1x	2 μL
dNTPs (10 mM)	0.8 mM	1.6 μL
Primer Fwr (10 μM)	0.12 μΜ	0.24 μL
Primer Rev (10μ)	0.12 μΜ	0.24 μL
Dream Taq	0.15 units	0.4 μL
DNA template	5 ng/μL (tumor)	2 μL

**Table 2.4:** PCR Program used for the amplification of exon 2 of the *KRAS* gene

Initial Denaturation	95 °C	5 min	1 cycle
Denaturation	95 °C	30 sec	
Primer annealing	61°C (Tumor) / 53°C (Plasma)	30 sec	30 cycles
Extension	72 °C	20 sec	_

# 2.7. Gel Electrophoresis

Gel Electrophoresis was used to analyze the amplification products of both PCR and ARMS-HRMA. For the visualization of PCR products, a 1% (m/v) agarose gel was prepared with 100 ml of TAE, while ARMS-HRMA products were visualized in a 2% (m/v) agarose gel, both prepared with 15  $\mu$ L of GelRed. GeneRuler 1k bp DNA Ladder was used as a molecular marker. A negative control (with no template DNA) was used do discard contamination. Electrophoresis was performed in an electrophoresis tank at 80 V for 90 minutes. The gel was then visualized in the GelDocTM EZ Imager.

# 2.8. Direct sequencing

KRAS exon 2 amplification products of tumor samples were sequenced in STABVIDA (Setubal, Portugal). The chromatograms were analyzed using the FinchTV software (Geospiza, Inc).

#### 2.9. ARMS-HRMA

ARMS-HRMA technique was used to search for 5 different mutations in DNA extracted from control cell lines and PDAC patient's tumor and plasma samples. The first ARMS step is the amplification of the 96 bp region using the ARMS technique. This step favors the amplification of DNA sequences harboring the mutation corresponding to the forward primer used (see Table 2.5). The last nucleotide matches the mutated nucleotide, while the one before does not match the sequence, which will result in two mismatched nucleotides in a wild-type sequence, while only 1 mismatched nucleotide in the presence of the respective mutation. The HRMA step allows the analysis of the ARMS products to disclose positive (mutant KRAS) and negative cases (no mutation found). The reaction mixture is described in Table 2.6 and was performed in a total of 10  $\mu$ L. The ARMS step is followed immediately by the HRMA step, both performed in the QIAGEN Rotor-Gene Q Real-time PCR cycler 5plex (Qiagen, Hilden, Germany). The ARMS-HRMA program used is described in Table 2.7. The resulting derivative plot of the melting profile was generated using Rotor-Gene Q Series Software 2.3.5 (Qiagen, Hilden, Germany).

Each ARMS-HRMA assay was performed with a wild-type control using gDNA from the HT-29 cell line, and a positive control using gDNA from the cell lines described in Table 2.1 depending on the mutation. When analyzing tumor samples, 50 ng of sample and control gDNA were used in a total volume of 10  $\mu$ L, while in plasma samples the controls used lower amounts of gDNA (0.25 ng for G12D, G12V, G13D and G12C; 2.5 ng for G12R) and 1  $\mu$ L of sample was used regardless of concentration.

Mutation scoring was done based on at least 2 separate assays. The fluorescence values of the samples were normalized using a wild-type and mutation controls. Using the resulting normalized fluorescence values of the melting peaks, samples were scored as positive or negative for a specific mutation based on a defined threshold and a qualitative evaluation.

Table 2.5: Primers used in ARMS-HRMA

Common reverse primer	5' CTCTATTGTTGGATCATATTCG 3'
Forward G12D primer	5' CTTGTGGTAGTTGGAGCTTA 3'
Forward G12V primer	5' CTTGTGGTAGTTGGAGCTTT 3'
Forward G12R primer	5' CTTGTGGTAGTTGGAGCGC 3'
Forward G12C primer	5' CTTGTGGTAGTTGGAGCGT 3'
Forward G13D primer	5' CTTGTGGTAGTTGGAGCTGGTTA 3'

Table 2.6: Reaction mixture used in ARMS-HRMA

Reagent	Final concentration	Volume used (μL)
H2O DEPC	-	2.1 μL
NZYTaq II 2xGreen Master Mix	1x	5 μL
DMSO 15%	2% (v/v)	1.33 μL
Primer Forward (10 μM)	0.3 μΜ	0.3 μL
Primer Reverse (10 μM)	0.3 μΜ	0.3 μL
Template	5 ng/μL (tumor)	1 μL

Table 2.7: ARMS-HRMA program used

Initial Denaturation	95°C	3 min	1 cycle
Denaturation	95 °C	30 sec	
Primer annealing	G12D - 54°C G12V - 52°C G12R - 56°C G12C - 57°C G13D - 53°C	15 sec	10 cycles
Extension	72 °C	10 sec	
Denaturation	95 ℃	30 sec	
Primer annealing	60°C	45 sec	25 cycles
Extension	72 °C	10 sec	
Melting	Melting  Temperature increase: from 45°C to 90°C.  1°C incrementation every step / wait 5 s each step		

# 2.9.1. Statistical analysis of ARMS-HRMA results

One-way ANOVA with Dunnett's multiple comparisons test and unpaired parametric ttests were used to evaluate differences between the normalized melting intensities of samples and of positive controls.

# 2.9.2. Data presentation

Melting curve derivative plots and pie charts were created using the Microsoft Excel software, version 2411. Sankey charts were also created in the Microsoft Excel software but with the Power-user add-on, version 1.7.13.0. Bar plots were created using the GraphPad Prism 8 software.

# 3. RESULTS AND DISCUSSION

#### 3.1. Cohort characterization

The cohort analyzed in this work was composed of 97 PC patients. At the end of the experimental work, it turns out that 9 out of the 97 patients, were not PDAC patients (different tumor subtypes) while 88 were true PDAC cases. Although this work focused on PDAC, the samples of these 9 patients are still useful for the validation of the ARMS-HRMA methodology and so they were kept in our analysis.

All the 97 patients had an associated tumor sample. Tumor samples nomenclature was based on the patient number, a number between 1 and 159, and an added "T" (e.g. a tumor sample from patient 7 would be named "7T"). In 7 out of the 97 patients, plasma samples were not able to be successfully extracted. Plasma samples nomenclature was based on the patient number, with an added "P1" or "P2". P1 and P2 refer to the timing of plasma sample collection, where samples with "P1" were collected first and samples with "P2" were collected a few months after.

## 3.2. DNA Extraction of tumor and plasma samples

DNA concentrations, and purity ratios (260/230 and 260/280) from tumor and plasma samples can be found in Table A1 (Appendix). DNA extraction was generally successful for every tumor sample, with an average DNA concentration of 131.8 ng/µl. The few cases where tumor extraction yielded concentrations below 50 ng/µl were associated with tumor pieces of large sizes. These samples still presented large chunks of undigested tissue after 3h of digestion periods, which had to be removed before the first centrifugations to prevent clogging the High Pure Filter membrane. The removed chunks carry a lot of genetic material and therefore their removal was probably responsible for the low yields of the DNA extraction at the end of the procedure. One way to prevent this, is to divide these large tumor pieces into two tubes before the digestion step to facilitate the tissue digestion, or by using a longer digestion period. Samples 132T, 139T, and 141T\* show a lower 260/230 and 260/280 ratios, due to an experimental error where the samples were accidentally eluted to the tubes used in the wash steps, which contaminated the samples.

DNA extraction from plasma samples was not as successful as from tumor samples due to the lower amount of cfDNA in plasma samples. When trying to measure the DNA concentrations of the first batches of extractions from plasma samples, using a microvolume spectro-photometer NanoDrop (Thermo Fisher, Waltham, Massachusetts, EUA), no peaks were observed, and concentration values were very low and inconsistent (below the limit of the detection). For this reason, instead of measuring the concentration of DNA extracted from plasma samples, we decided to use a fixed volume in all ARMS-HRMA reactions, regardless of its concentration.

After the extractions, a PCR amplification was performed using the extracted DNAs from all samples to confirm the amplification of exon 2 of *KRAS* gene and PCR products were visualized through gel electrophoresis.

# 3.3. KRAS amplification by PCR and Gel electrophoresis

The assessment of mutations in the exon 2 of the *KRAS* gene by SS requires a high amount of template DNA, so a PCR was performed on all tumor samples. After the completion of the PCR reaction, an agarose gel electrophoresis was performed using 1  $\mu$ L of the amplification product. An example of gel electrophoresis performed with the amplification products of samples 125T, 126T, 127T, 128T, 129T, 131T and HT-29 control can be seen in Figure 3.1. The presence of a defined band of about 400 bp was indicative of a successful amplification and the amplification product was ready to be sequenced.

To have a qualitative assessment of the DNA extracted from plasma samples, a PCR reaction was performed with every plasma sample. For most of the plasma samples, the PCR amplification products had lower intensities compared to the bands of the amplification products of HT-29 control (at 2.5 ng/ $\mu$ L). An example of gel electrophoresis performed with the amplification products of samples 8P1, 9P1, 9P2, 30P1, 38P1, 78P2, 84P2, 153P1 and HCT116-29 control can be seen in Figure 3.2. We can then estimate that the concentration of DNA should be lower than 2.5 ng/ $\mu$ L. Band intensity was sometimes inconsistent between two extractions from the same plasma sample, indicating that the 2 DNA extractions were not equally successful in every sample.

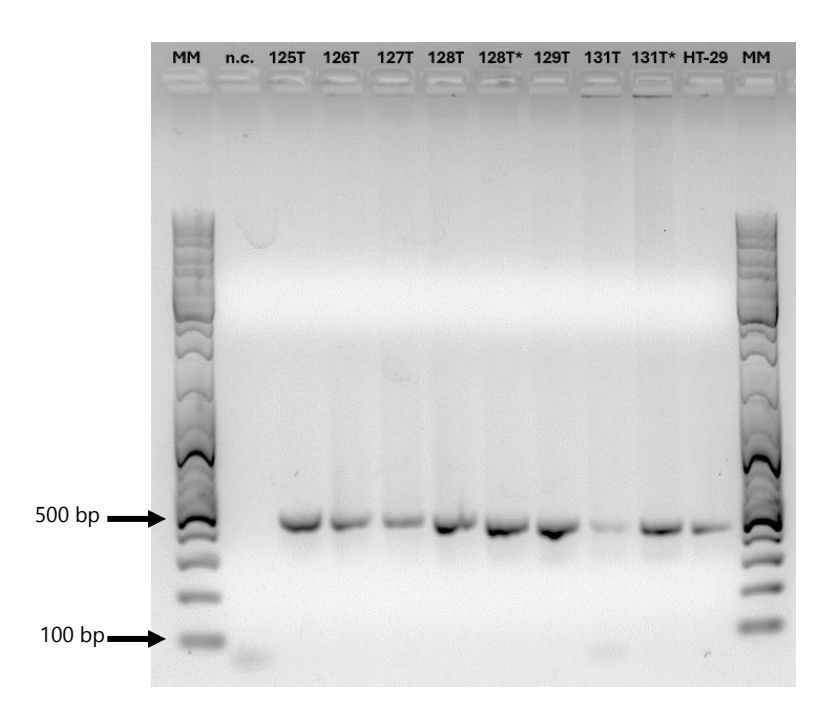


**Figure 3.1: Gel Electrophoresis of PCR products.** MM - GeneRuler DNA Ladder Mix SM0331 Molecular Marker; n.c. - negative control (no template); 125T, 126T, 128T, 129T, 131T - tumor samples; HT-29 - cell line. 1% (m/v) agarose gel in TAE 1x was used; Gel Red was added to the agarose gel to ensure visualization, and the gel was run at 80V for 90 min. Samples with \* are a second DNA extraction of the same tumor sample.

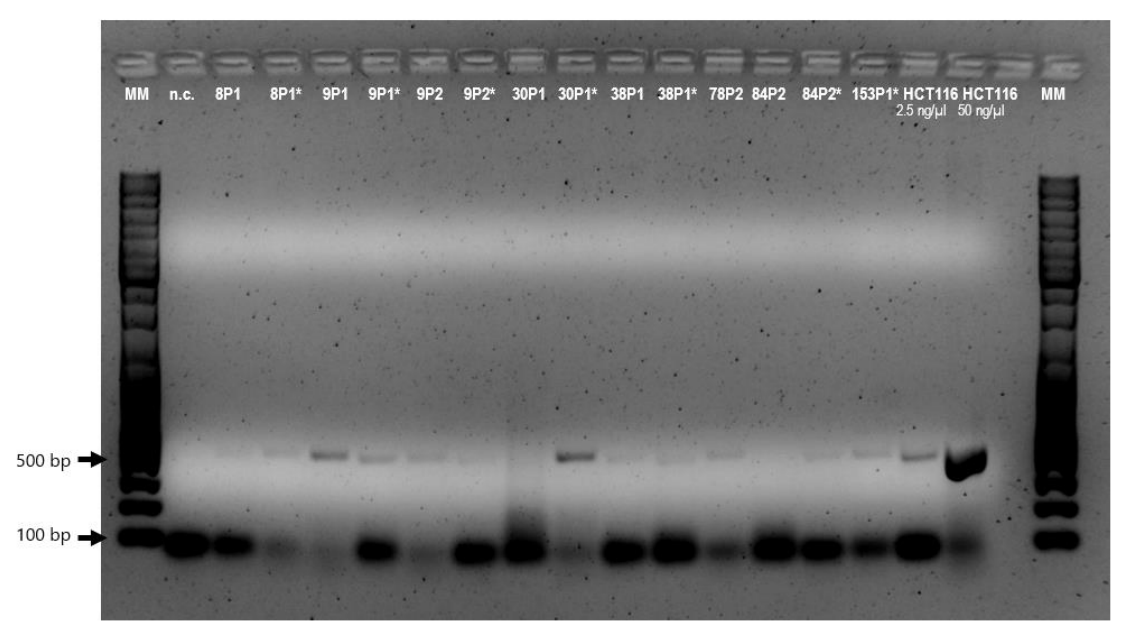


Figure 3.2: Gel Electrophoresis of plasma samples amplification products. MM - Molecular Marker; n.c. - negative control (no template); 8P1, 9P1, 30P1, 38P1, 78P2, 84P2, 153P1 - plasma samples; HCT116 - cell line. 1% (m/v) agarose gel in TAE 1x; Gel Red was added to the agarose gel to ensure visualization, and the gel was run at 80V for 90 min. Samples with \* are a second DNA extraction of the same plasma sample.

### 3.4. SS results

All tumor samples had a successful amplification by PCR and were sent for SS. The resulting two chromatograms (one sequenced using the Primer Forward and one sequenced with the Primer Reverse) for each sample were analyzed to assess the presence of mutations in codons 12 and 13, based on the analysis of the fluorescence peaks. Examples of chromatograms from tumor samples where it is possible to detect G12D, G12V, G12R, and G13D mutations are depicted in Figure 3.3. A summary of the SS results for all tumor samples can be found in Table 3.1.

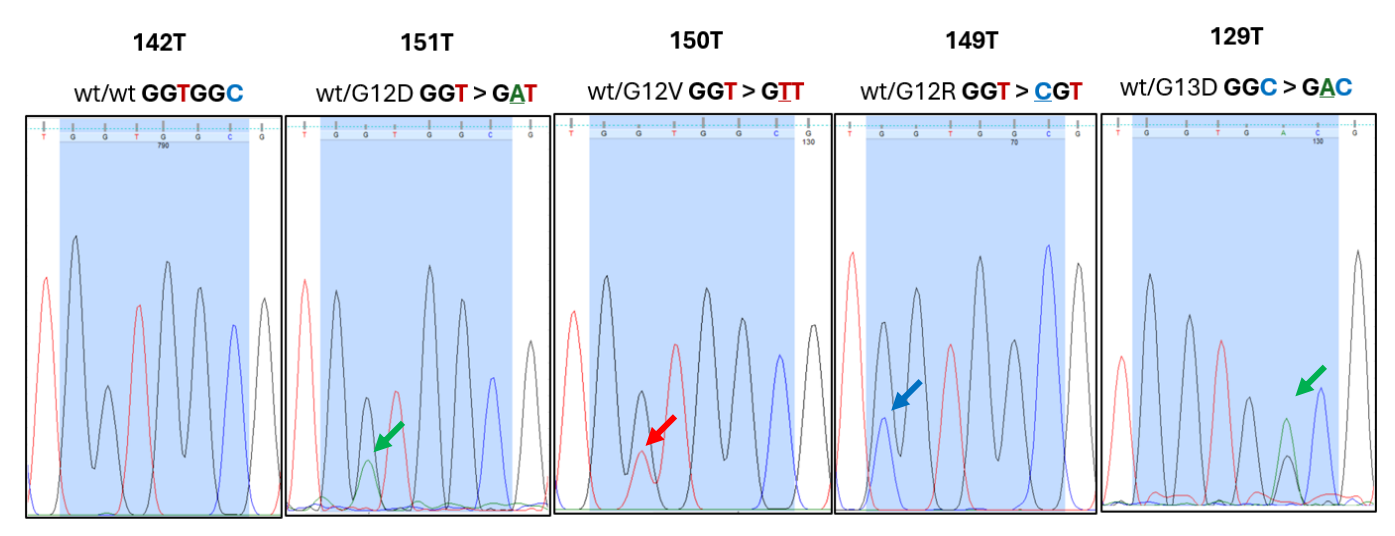


Figure 3.3: Representative images of the region under study extracted from chromatograms of 5 different tumor samples. Each genotype is represented at the top of each image (allowing the identification wild type and mutated samples). Samples 151T, 150T, 149T and 129T present a noticeable second fluorescence peak, indicated by an arrow.

**Table 3.1:** SS results of all tumor samples used in this study. Samples with \* were analyzed by me. The SS results for the remaining tumor samples were analyzed by PhD students Beatriz Oliveira and André Luz, and MSc student Beatriz Costa.

KRAS Genotype (allele)	Samples
Homozygous (wt/wt)	1T, 3T, 9T, 11T, 21T, 22T, 24T, 25T, 34T, 36T, 39T, 40T, 42T, 43T, 44T, 46T, 47T, 66T,69T, 74T, 75T, 79T, 81T, 89T, 107T*, 109T, 111T*, 112T, 115T*, 120T, 125T*, 126T*, 128T, 129T*, 130T, 131T*, 132T*, 139T*, 141T*, 142T*, 143T*, 146T, 155T, 156T, 158T
heterozygous (wt/G12D)	7T, 8T, 13T, 17T, 23T, 30T, 31T, 37T, 38T, 48T, 58T, 59T, 88T, 93T, 100T, 105T*, 116T, 119T*, 123T, 136T, 145T, 147T, 148T, 149T, 151T*
heterozygous (wt/G12V)	4T, 6T, 10T, 12T, 18T, 35T, 78T, 83T, 84T, 98T, 140T, 150T*, 153T, 154T
heterozygous (wt/G12R)	5T, 20T, 28T, 73T, 121T, 124T*, 134T, 149T*
heterozygous (wt/G12C)	65T, 90T
heterozygous (wt/G13D)	1 127T*
heterozygous (wt/G12A)	1 110T (G12A)

## 3.5. Mutation scoring using ARMS-HRMA

The mutation-specific primers used were designed to allow a higher amplification efficiency of DNA sequences that contain the target mutation over the wild-type sequences or sequences with other mutations. When a sample is scored as "positive" for a given mutation by ARMS-HRMA, that specific mutation was detected in that sample. Following the same logic, a "negative" result only means that the tested mutation is not present and does not exclude the possibility of the presence of other mutations. As such, throughout this work, we have used the nomenclature for a "negative" result as "not detected" (ND for short abbreviation).

In theory, the differentiation between positive and negative cases could be done through a gel electrophoresis, like in a standard ARMS procedure, but our previous results<sup>85</sup> revealed that the system was not binary. Mismatched primers still allowed some amplification,

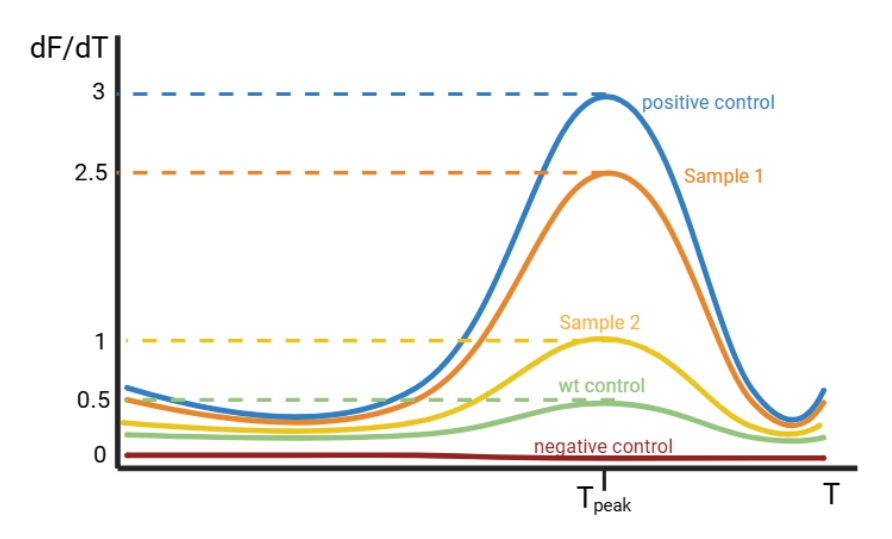
although to a lesser extent, reducing the ability to differentiate a positive from negative case from a band in a gel electrophoresis. The combination of the ARMS with the HRMA (ARMS-HRMA) allows the distinction between positive and negative cases by the analysis of the melting profile of each sample after the ARMS step. More specifically, the HRMA allows the visualization of melting peaks. During HRMA, melting curves present a steep decrease in fluorescence around the melting Temperature (Tm) which generates a peak which can be seen in a plot of the derivative of fluorescence (dF/dT) as a function of temperature (T), represented in Figure 3.4. Melting peak intensity of mutated samples are generally higher than non-mutated ones, due to the higher efficiency of amplification of mutated sequences.

Mutation scoring is performed based on whether the intensity of the melting peaks, normalized using wild-type and mutated positive controls, which are lower or higher respectively, than a defined threshold. Even though the values used for mutation scoring are from the 1<sup>st</sup> derivative of the fluorescence values, I will refer to them as just fluorescence values or fluorescence intensity for simplicity.

Fluorescence values normalization is done according to the formula shown in the bottom of Figure 3.4, where the fluorescence values of the negative control are subtracted from the controls' and samples' fluorescence values. Then, wild-type fluorescence values are subtracted from both the positive control's and the sample's fluorescence values. The final normalized fluorescence of a sample was obtained by calculating the ratio between the sample's fluorescence value and the positive control's fluorescence value at the melting peak temperature. This means that the normalized fluorescence intensity of the positive control is always 1 and the normalized fluorescence intensity of the wild-type control is always 0. Melting peak temperatures were around 78 °C for G12D, G12V, G12C and G13D mutations and 79 °C for G12R mutations. The ARMS-HRMA exported data presented the recorded fluorescence values in intervals of 1 °C starting at 45.5 °C. Since the melting peaks were not always located at exactly 78 °C or 79°C, the fluorescence values were retrieved from the closest temperature (77.5, 78.5 or 79.5 °C).

gDNA from LS174T, SW480, PSN-1, H358 and HCT116 cell lines was used as positive controls when testing for G12D, G12V, G12R, G12C and G13D mutations respectively, while gDNA from the HT-29 cell line was used in the wild-type controls. The mean of normalized fluorescence values of multiple assays was used for the mutation scoring of PDAC patients. I used 0.5 as the threshold, as it was used in Oliveira et al.<sup>85</sup>, where samples with a normalized fluorescence above 0.5 were scored as positive and samples with a normalized fluorescence below 0.5 were scored as negative. The general mutation scoring process is exemplified in

Figure 3.4. Some adjustments to this process were made depending on the mutation or type of sample that was being analyzed and will be described on their respective sections.



Normalized Fluorescence intensity = (Intensity sample-Intensity negative control)-(Intensity wt- Intensity negative control)

(Intensity positive control-Intensity negative control)-(Intensity wt-Intensity negative control)

Figure 3.4: Schematization of a typical ARMS-HRMA derivative plot and formula used to normalize fluorescence. The normalization of the fluorescence values of a sample was done using the fluorescence values at the melting peak temperature (T<sub>peak</sub>) which was around 78 °C for G12D, G12V, G12C and G13D mutations and 79 °C for G12R mutations. Using the formula to normalize the fluorescence values of hypothetical samples 1 and 2 we obtain the values of 0.8 and 0.2 respectively. Using a threshold of 0.5<sup>85</sup>, Sample 1 would be scored as a "positive" result for the mutation tested while Sample 2 would be scored as a "negative" result.

To validate the use of ARMS-HRMA for *KRAS* mutations, it is important to note that, although the mutation scoring was done based on normalized fluorescence values, a critical look at the melting curves when testing any of the 5 mutations was essential. A sample with a low-intensity peak may have a normalized fluorescence intensity above 0.5. This could occur if a positive control presented an abnormally low melting peak, due to an experimental error (meaning that more than one ARMS-HRMA detection should be performed for each sample - 3 replicates) or due to low quality of gDNA (a different extraction should be performed), which would inflate every sample's normalized fluorescence intensity as it is calculated with a ratio using the positive control. A sample might also have a normalized fluorescence intensity below 0.5, when 2 out of 3 replicates present a high-intensity melting peak but a third does not. Since the mutation scoring would be based on the mean of these 3 replicates, one replicate where

the sample did not amplify can alter the value of the normalized fluorescence intensity to be below 0.5, which would result in a false negative call. This can happen due to an experimental error but also due to tumor heterogeneity, where between replicates different proportions of mutated to wild-type DNA could be present, leading to variability in the results. This process of analyzing both the direct endpoint of the results (the normalized fluorescence intensity) and the various melting profiles of a sample across multiple assays is extremely important. Not only is it relevant for the validation of the ARMS-HRMA methodology but also for future integration in a clinical setting, as it can give us some clues of how robust the methodology is and how involved a human operator should be during the mutation scoring process.

#### 3.5.1. ARMS-HRMA on tumor samples

In the analysis of tumor samples, equal amounts of tumor sample DNA and control DNA were used. Both the DNA extracted from the cell lines and the DNA extracted from the tumor samples were diluted to a 50 ng/µl concentration prior to their use in the analysis, to ensure that a 50 ng of DNA was present in each ARMS-HRMA reaction. Examples of ARMS-HRMA derivative plots of all tumor samples analyzed can be found in Figures A1, A2, A3 and A4 (Appendix).

### 3.5.1.1. G12D mutation analysis in tumor samples

G12D mutation scoring was based on the same process described in section 3.5 but has some deviations from the example shown in Figure 3.4. It is common for samples scored as negative for the G12D mutation to present a melting peak at around 74 °C, while sequences scored as positive present a peak at around 78 °C as the other mutations. Due to this fact, G12D positive cases are more easily identified when compared to the other mutations, since positive and negative cases of other mutations only differ in melting peak intensity and not in the Tm. Some samples occasionally presented 2 peaks when tested for G12D however, one at 74 °C and the other at 78 °C, so the analysis of the normalized fluorescence intensity was still necessary in many cases and used alongside the analysis of the temperature associated with the peaks. The values used to normalize the fluorescence of samples are the ones at 78 °C, where the positive control's melting peak is located, regardless of the presence of a peak at 74 °C. An example of a typical G12D ARMS-HRMA result can be seen in Figure 3.5.

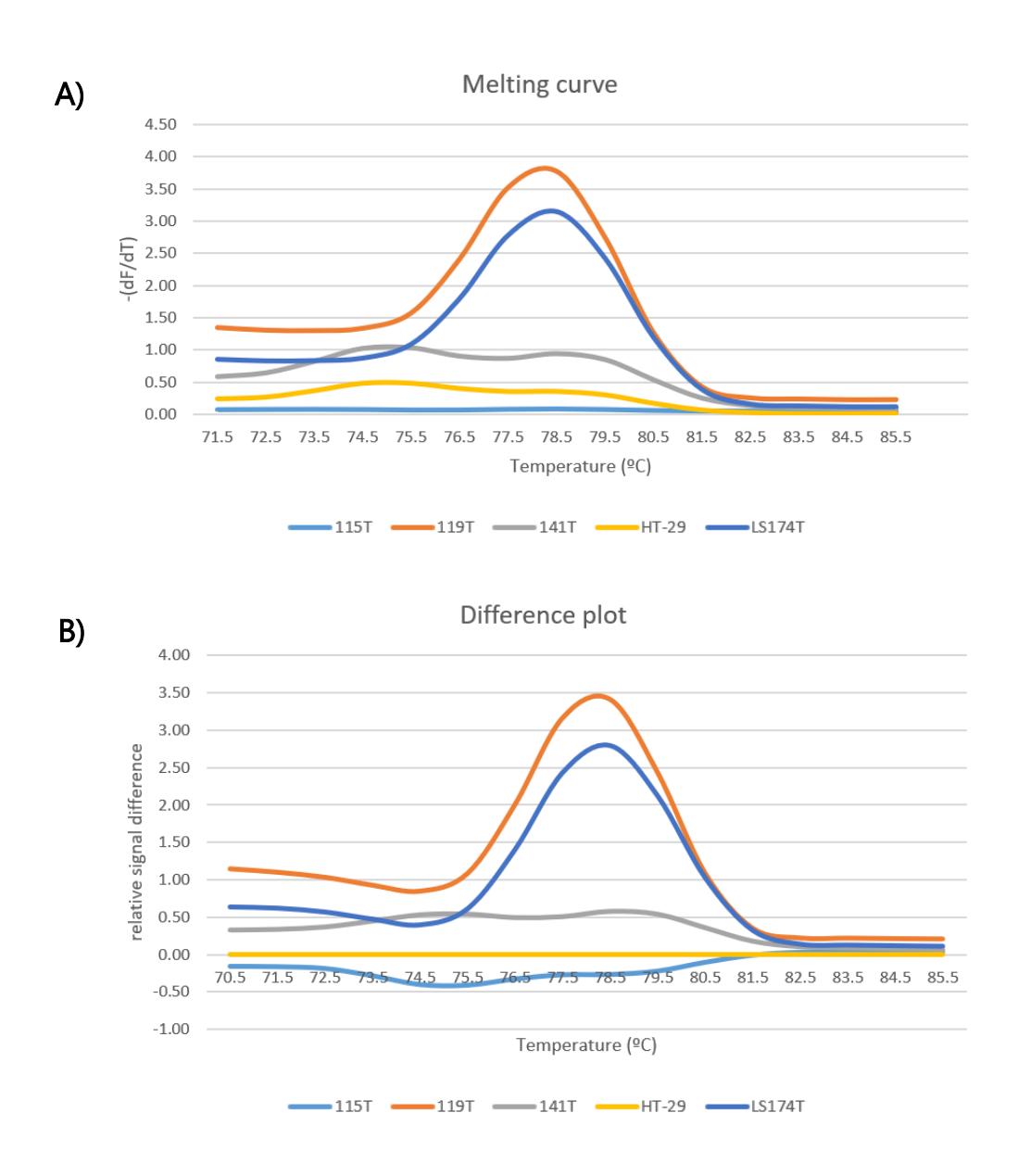


Figure 3.5: ARMS-HRMA results used in G12D mutation scoring of tumor samples 115T, 119T and 141T. A) Derivative plot of the melting curve of tumor samples 115T, 119T, 141T, wild-type control (HT-29) and G12D positive control (LS174T). B) Difference plot obtained by subtracting the wild-type control's fluorescence values from every curve.

In Figure 3.5 it is possible to see that sample 119T is a positive case, as it presents a high-intensity melting peak at the same temperature as the positive control. Two examples of negative cases are sample 115T, which does not present a peak, and sample 141T which presents two low-intensity peaks near 74 and 78 °C, a fact that was already described to occur when testing the G12D mutation. The analysis of samples with a melting peak of medium intensity at 78 °C relied on the normalized melting intensity.

G12D scoring of tumor samples analyzed exclusively by me using ARMS-HRMA results are summarized in Table 3.2, where 4 out of 21 samples scored positive for the G12D mutation. Sample scoring was based on the normalized fluorescence intensity. In Figure 3.6 the tumor samples are represented with their respective normalized fluorescence intensity. Samples 119T, 131T, 142T are clearly above the 0.5 threshold and therefore were considered positive. The normalized fluorescence intensities of samples 129T and 151T were 0.480 and 0.463 respectively, both very close to the chosen threshold. In these cases, the analysis of the melting curves served as the distinction between the two during mutation scoring. In one of the assays, the intensity of the positive control's melting peak is abnormally low and therefore very close to the melting peak of the 129T sample, which wrongly inflates the resulting normalization to a value close to 0.5. The 151T sample, presented a defined, high-intensity peak at 78 °C in two of the three assays used, while the third replicate did not present a peak, lowering the mean of the normalized fluorescence intensity. Based on this distinction, we considered the third replicate as an outlier and scored 151T as a positive case, while scoring 129T as a negative case.

**Table 3.2:** Summary of G12D mutations found in tumor samples analyzed by ARMS-HRMA ND: not detected

KRAS mutation	Samples
G12D	119T, 131T, 142T, 151T
ND	107T, 111T, 112T, 115T, 124T, 125T, 126T, 127T, 129T, 131T, 132T, 139T, 141T, 143T, 149T, 150T

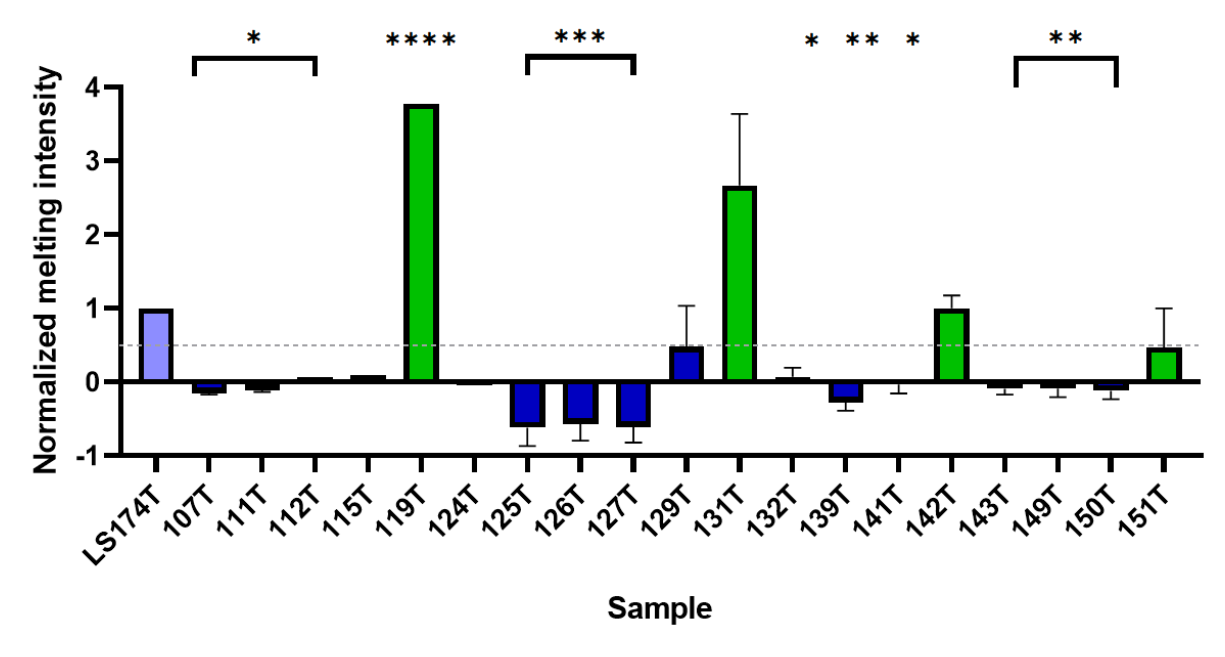
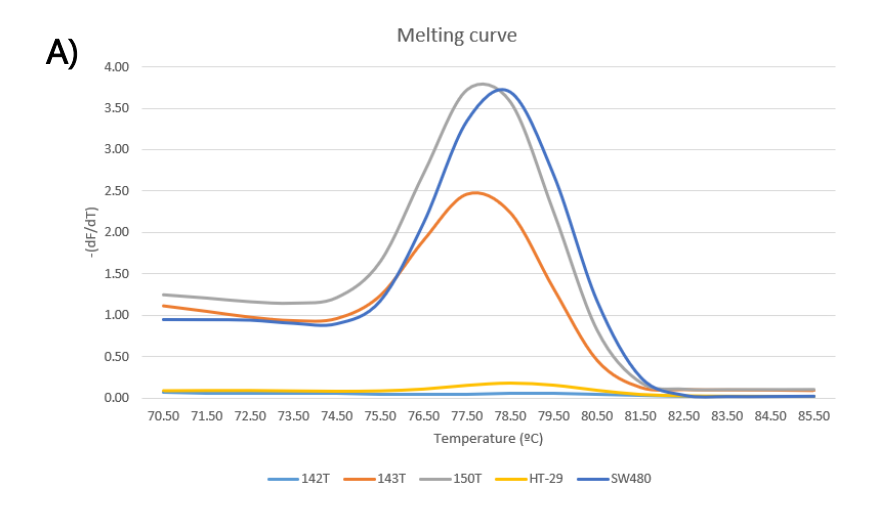


Figure 3.6: G12D scoring based on the normalized melting peak intensity of ARMS-HRMA. All samples are the average of the normalized melting peak intensity. Standard error of the mean (SEM) is represented in the error bars. Green bars represent samples that were scored as positive, while blue bars represent samples that were scored as negative. The 0.5 threshold is represented as a dotted line. Black asterisks indicate statistical difference between the normalized fluorescence intensity of the sample and the positive control (light blue) using One-way ANOVA with Dunnett's multiple comparisons test and unpaired parametric t-tests, (\*p < 0.05; \*\*p < 0.01; \*\*\*p < 0.001; \*\*\*\*p < 0.001; \*\*\*\*p < 0.0001).

## 3.5.1.2. G12V mutation analysis in tumor samples

G12V scoring mutation was a straightforward application of the standard scoring methodology described in section 3.5, where fluorescence levels at 78 °C are used to obtain the normalized fluorescence intensity of the samples. An example of a typical G12V ARMS-HRMA derivative plot can be seen in Figure 3.7.



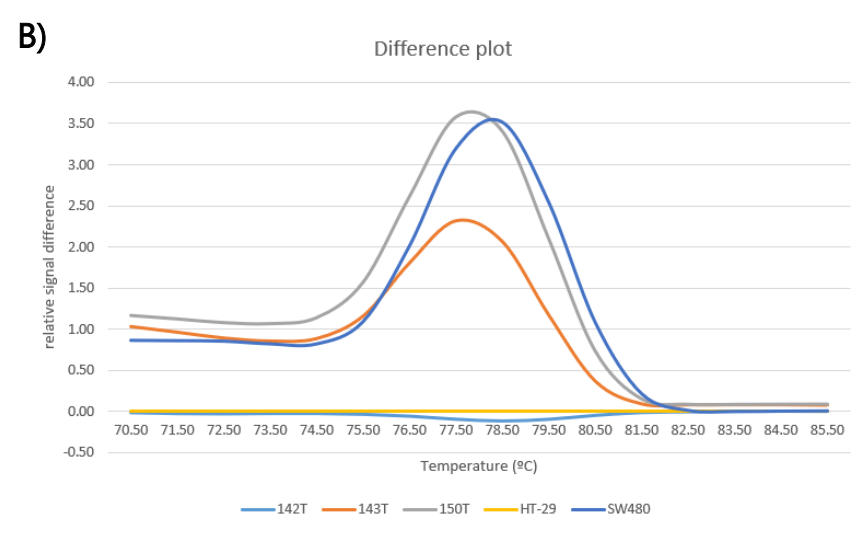


Figure 3.7: ARMS-HRMA results used in G12V mutation scoring of tumor samples 142T, 143T and 150T. A) Derivative plot of the melting curve of tumor samples 142T, 143T, 150T, wild-type control HT-29 and G12V positive control SW480. B) Difference plot obtained by subtracting the wild-type control's fluorescence values from every curve.

Figure 3.7 shows 2 samples with high-intensity melting peaks. The 150T melting peak shows a positive case, while the peak associated with the 143T sample has a lower intensity. The scoring is done based on the normalized fluorescence intensity.

G12V scoring of tumor samples analyzed exclusively by me using ARMS-HRMA are summarized in Table 3.3, where 5 out of 20 samples scored positive for the G12V mutation. In Figure 3.8 the tumor samples are represented with their respective normalized fluorescence intensity. Samples 111T, 141T and 150T are clearly above the 0.5 threshold and therefore scored as positive. Sample 132T has a melting peak with the same intensity as the positive control on the first replicates but does not present a melting peak on the other replicate. This

could be attributed to a mistake during the preparation of the reaction mixture, or to the possibility that this sample had a low % of mutated DNA when compared to the wild-type background, resulting in a lower amplification efficiency. Sample 143T presented two melting peaks with medium fluorescence intensity. The mean of the normalized fluorescence intensity of this sample ended up being below the threshold of 0.5 but since these peaks were distinct from other samples scored as negative and from the wild-type control, it was scored as positive.

**Table 3.3:** Summary of G12V mutations found in tumor samples analyzed by ARMS-HRMA ND: not detected

KRAS mutation	Samples
G12V	111T, 132T, 141T, 143T, 150T
ND	105T, 107T, 112T, 115T, 119T, 124T, 125T, 126T, 127T, 129T, 131T, 139T, 142T, 149T, 151T,

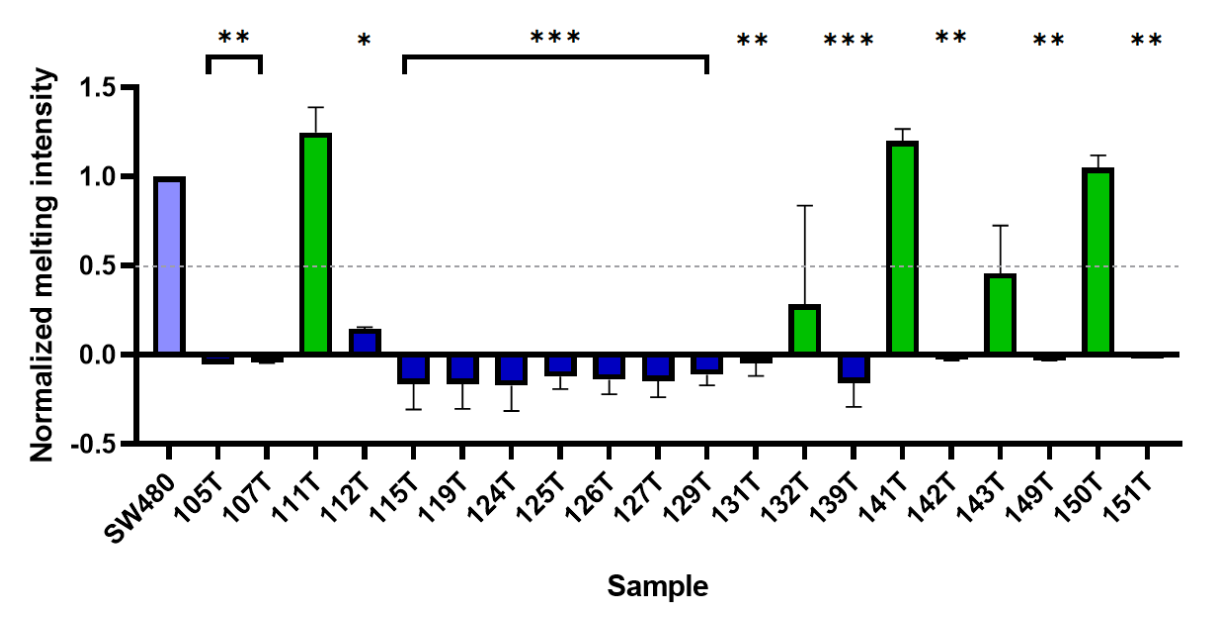


Figure 3.8: G12V scoring based on the normalized melting peak intensity of ARMS-HRMA. All samples are the average of the normalized melting peak intensity. Standard error of the mean (SEM) is represented in the error bars. Green bars represent samples that were scored as positive, while blue bars represent samples that were scored as negative. The 0.5 threshold is represented as a dotted line. Black asterisks indicate statistical difference between the normalized fluorescence intensity of the sample and the positive control (light blue) using One-way ANOVA with Dunnett's multiple comparisons test and unpaired parametric t-tests, (\*p < 0.05; \*\*p < 0.01; \*\*\*p < 0.001).

### 3.5.1.3. G12R mutation analysis in tumor samples

G12R mutation scoring was performed based on the mean of the normalized fluorescence intensity at 79 °C. Importantly, G12R ARMS-HRMA melting peaks usually present low intensities; nevertheless, G12R positive controls still present high-intensity melting peaks. One possible explanation is that the amplification efficiency of G12R ARMS step might be lower than the ARMS steps for other KRAS mutations. The high amount of mutated DNA present in positive controls still manages to amplify and present a high-intensity melting peak while tumor samples with lower amounts of mutated DNA amplify much less and therefore present low-intensity melting peaks. However, the negative cases of G12R ARMS-HRM, usually do not present a peak.

The only mutation scored as positive, 149T, has a normalized fluorescence intensity of 0.2 which is considerably lower than the chosen threshold of 0.5 as seen in Figure 3.10. Still, it was scored as positive, because it consistently presented a melting peak, compared to the other samples tested that did not present any peak at all, as observed in Figure 3.9. The annealing temperature used in the ARMS reaction for the G12R mutation is 56 °C, which is higher than the annealing temperatures for G12D (54 °C) or G12V (52 °C), which could be contributing to a lower amplification efficiency.

G12R scoring of tumor samples exclusively analyzed during this dissertation work using ARMS-HRMA are summarized in Table 3.4, where 1 out of 13 samples scored positive for the G12R mutation. In Figure 3.10, the tumor samples are represented with their respective normalized fluorescence intensity.

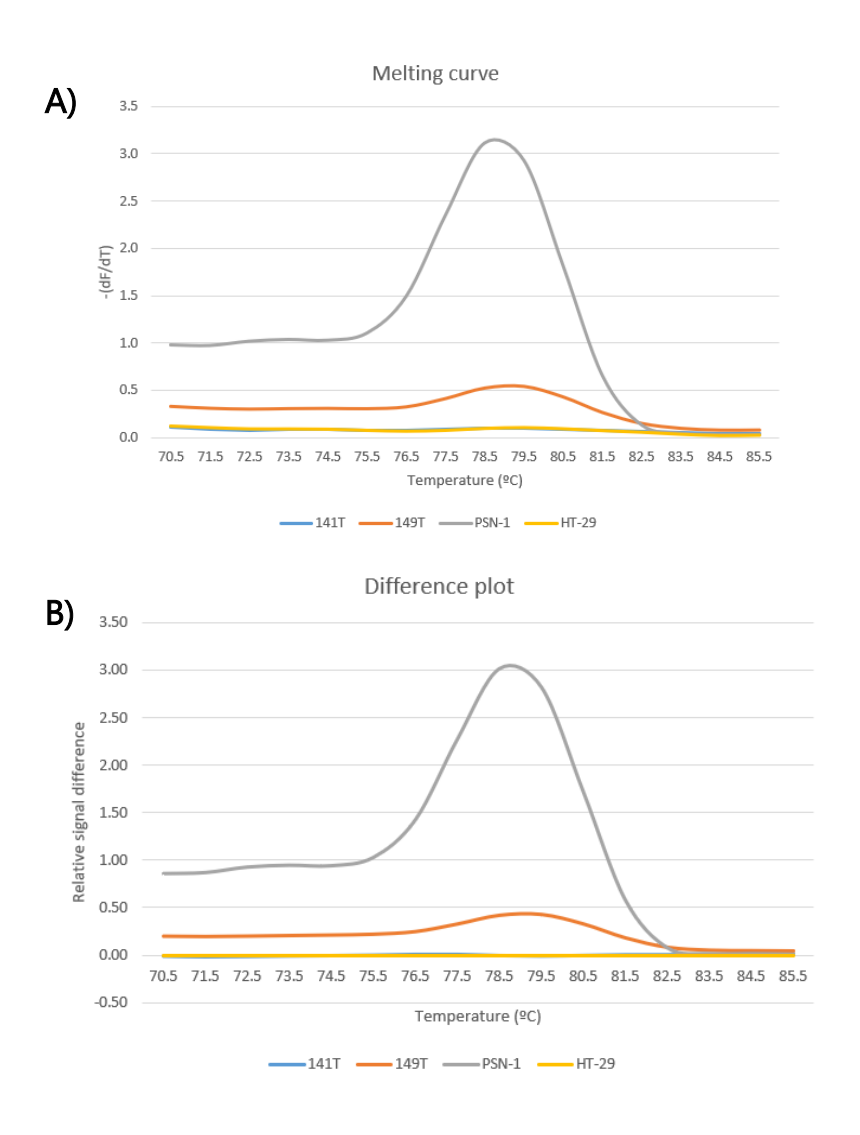


Figure 3.9: ARMS-HRMA results used in G12R mutation scoring of tumor samples 141T and 149T. A) Derivative plot of the melting curve of tumor samples 141T, 149T, wild-type control HT-29 and G12R positive control PSN-1. B) Difference plot obtained by subtracting the wild-type control's fluorescence values from every curve.

**Table 3.4:** Summary of G12R mutations found in tumor samples analyzed by ARMS-HRMA ND: not detected

KRAS mutation	Samples
G12R	149T
ND	107T, 111T, 125T, 126T, 131T, 132T, 139T, 141T, 142T, 143T, 150T, 151T

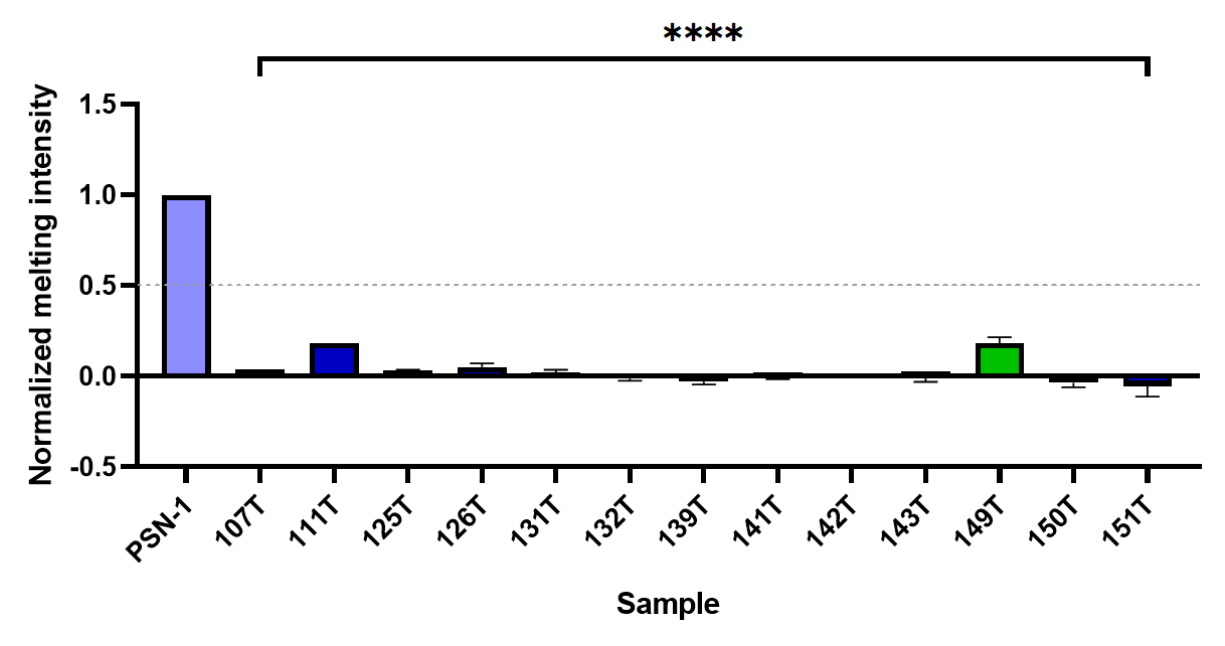


Figure 3.10: G12R scoring based on the normalized melting peak intensity of ARMS-HRMA. All samples are the average of the normalized melting peak intensity. Standard error of the mean (SEM) is represented in the error bars. Green bars represent samples that were scored as positive, while blue bars represent samples that were scored as negative. The 0.5 threshold is represented as a dotted line. Black asterisks indicate statistical difference between the normalized fluorescence intensity of the sample and the positive control (light blue) using One-way ANOVA with Dunnett's multiple comparisons test and unpaired parametric t-tests, (\*\*\*\*p < 0.0001).

## 3.5.1.4. G12C mutation analysis in tumor samples

G12C represents a very small fraction of *KRAS* mutations, and based on SS results, none of the tumor samples presented a G12C KRAS mutation. An example of a typical G12C ARM-HRMA derivative plot is presented in Figure 3.11 (performed by André Luz), where sample 65T was scored as positive. Although it does not present a very high-intensity and defined peak, its fluorescence intensity is still very high compared to other samples tested simultaneously (e.g. sample 109T).

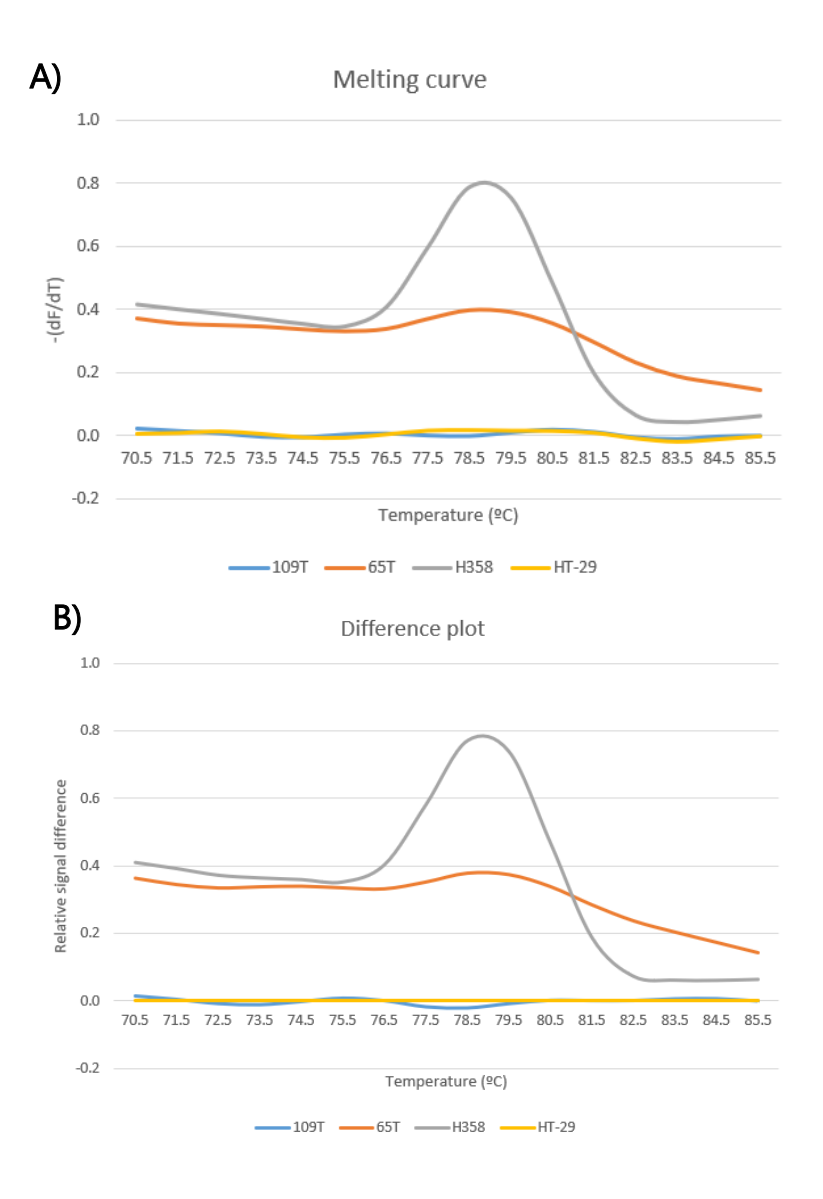


Figure 3.11: ARMS-HRMA results used in G12C mutation scoring of tumor samples 109T and 65T. A) Derivative plot of the melting curve of tumor samples 109T, 65T, wild-type control HT-29 and G12C positive control H358. B) Difference plot obtained by subtracting the wild-type control's fluorescence values from every curve.

## 3.5.1.5. G13D mutation analysis in tumor samples

G13D scoring was done according to the normalized fluorescence intensity at 78 °C. As G12C, G13D represents a very small fraction of *KRAS* mutations. An example of a G13D ARMS-HRMA derivative plot can be seen in Figure 3.12. In all replicates, sample 127T presented a very high-intensity peak, easily distinguishable from the wild-type control. Therefore, this sample was scored as positive. However, the positive control (DNA from HCT116) does not show the usual high-intensity melting peak associated with this positive control, as observed In Figure 3.13, which was correlated with the poor quality of this DNA sample. Considering this, we have discarded this positive control (from assay presented in Figure 3.12) and mutation scoring of these samples was not done based on normalized fluorescence intensity. G13D scoring of tumor samples exclusively analyzed by me using ARMS-HRMA are summarized in Table 3.5.

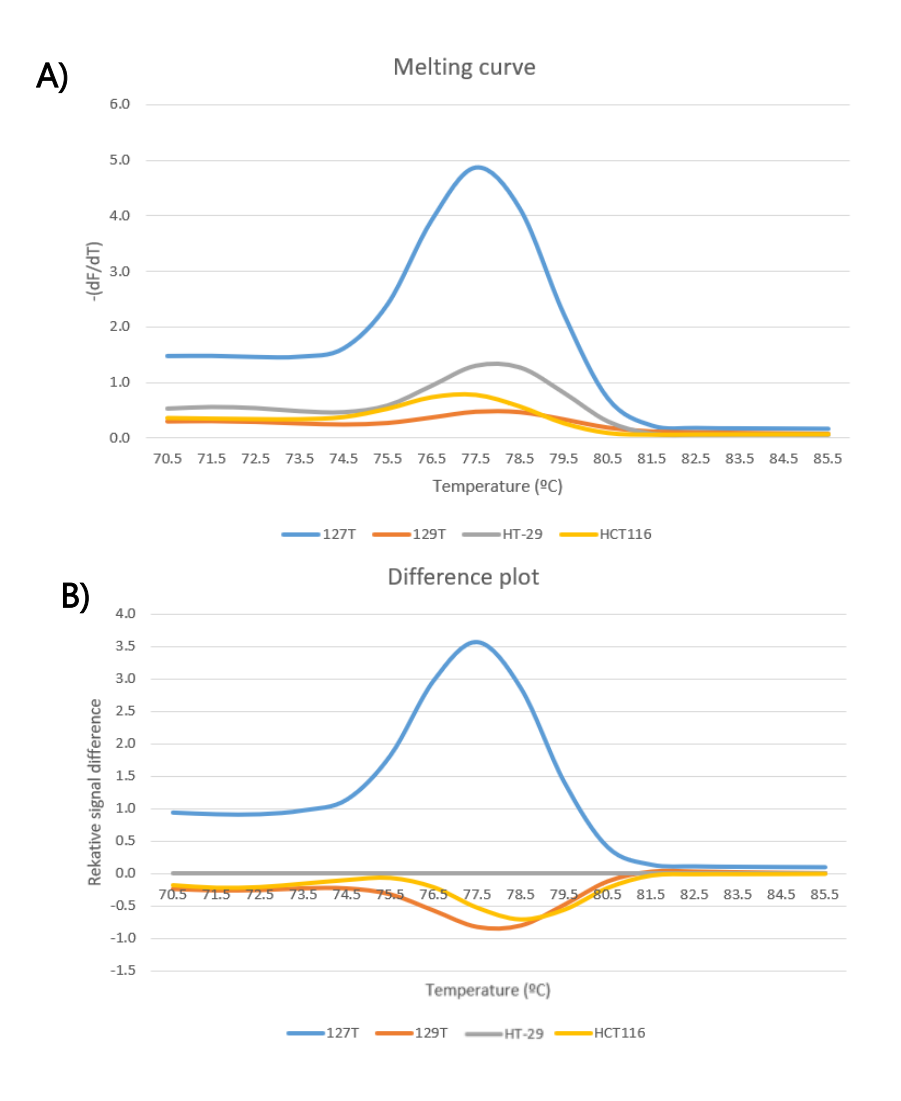


Figure 3.12: ARMS-HRMA results used in G13D mutation scoring of tumor samples 127T and 129T. A) Derivative plot of the melting curve of tumor samples 127T and 129T, wild-type control HT-29 and G13D positive control HCT116. B) Difference plot obtained by subtracting the wild-type control's fluorescence values from every curve.

**Table 3.5:** Summary of G13D mutations found in tumor samples analyzed by ARMS-HRMA ND: not detected

KRAS mutation	Samples
G13D	127T
ND	112T, 128T, 129T

#### 3.5.1.6. ARMS-HRMA tumor samples - summary

A summary of the KRAS mutations found in all tumor samples is presented in Table 3.6. These results include not only the samples that were exclusively analyzed by me (previous sections), but also samples that were also analyzed by the PhD students Beatriz Oliveira and André Luz and MSc student Beatriz Costa. In a total of 97 pancreatic cancer patients, ARMS-HRMA detected the G12D mutation in 35 samples (36%), G12V in 22 samples (23%), G12R in 10 samples (10%), G12C in 1 sample (1%) and G13D in 1 sample (1%). Interestingly, tumor samples 47T and 83T tested positive for both G12D and G12V mutations (2%), while sample 90T tested positive for both G12D and G12C mutations (1%), totaling 72 positive samples.

When analyzing the tumor samples of only the 88 PDAC patients, *KRAS* mutations were detected in 66 (77%). The proportion of mutations were 48% for G12D, 33% for G12V, 15% for G12R, 2% for G12C, 2% for G12D/ G12C (2%) and 3% for G12D/G12V. According to the literature, *KRAS* mutations are present in around 90% of PDAC patients<sup>7,24,28</sup> which is higher than the 77% we observed in this cohort. That said, ARMS-HRMA only analyzed 5 *KRAS* mutations, which does not take into account Q61 mutations, which account for around 5-7% of mutations<sup>24,25</sup>, and other rarer mutations. A cohort of 88 patients might also not be big enough to accurately represent the mutational landscape of PDAC. The observed proportion of *KRAS* mutations is consistent with what is described in the literature<sup>24,25</sup>, with G12D being the most common mutation, followed by G12V and then G12R.

**Table 3.6:** ARMS-HRMA results of the 97 tumor samples. \*For samples 5T, 16T and 22T, there was not enough DNA for ARMS-HRMA analysis. SS results showed that the KRAS genotype of sample 110T was wt/G12A, a mutation that is not included in this work and therefore was not analyzed by ARMS-HRMA.

KRAS Mutation	Samples
G12D	1T, 7T, 8T, 13T, 17T, 23T, 30T,31T, 37T, 38T, 42T, 44T, 48T, 58T, 59T, 66T, 69T, 74T, 88T, 89T, 90T, 93T, 100T, 105T, 116T, 119T, 120T, 123T, 131T, 136T, 142T, 145T, 147T, 148T, 151T, 159T
G12V	4T, 6T, 9T, 10T, 12T, 18T, 21T, 35T, 36T, 39T, 75T, 78T, 84T, 98T, 111T, 132T, 140T, 141T, 143T, 150T, 153T, 154T
G12R	20T, 28T, 73T, 121T, 124T, 128T, 134T, 146T, 149T, 155T
G12C	65T
G13D	127T
G12D/G12V	47T, 83T
G12D/G12C	90T
No mutations detected	3T, 11T, 24T, 25T, 34T, 40T, 43T, 46T, 79T, 81T, 107T, 109T, 112T, 115T, 125T, 126T, 129T, 130T, 139T, 156T, 158T
Results not available*	5T, 16T, 22T, 110T

#### 3.5.2. ARMS-HRMA on plasma samples

The process of mutation scoring in plasma samples followed the same rational of the one used in tumor samples with slight modifications as explained below. The fluorescence intensity of samples was normalized using a positive and a wild-type control, and samples whose normalized fluorescence intensity is above the 0.5 threshold were scored as positive. As in the analysis of tumor samples, the visual/qualitative analysis of the melting curves had an important role in mutation scoring.

Based on the knowledge obtained during tumor samples analysis, the use of replicates and, of controls samples with good DNA quality, is very important in the mutation scoring process. As previously explained (section 3.5.1), in the analysis of tumor samples, equal amounts of tumor sample DNA and control DNA were used. Both the DNA extracted from the cell lines and the DNA extracted from the tumor samples were diluted to a 50 ng/µl concentration prior to their use in the analysis, to ensure that a 50 ng of DNA was present in each ARMS-HRMA reaction. However, considering that it was not possible to quantify the DNA extracted from plasma samples, some adjustments to the mutation scoring process had to be made to guarantee the detection of mutations by ARMS-HRMA in plasma samples.

Moreover, the degree of fragmentation can also vary between plasma samples with similar amounts of DNA and most importantly, the proportion of mutated to wild-type DNA in plasma samples is much lower than in tumor samples (as the ctDNA origin would be the primary tumor). This proportion also varies depending on tumor size and cancer stage<sup>88</sup>. Considering all these factors, it was not possible to use equal amounts of plasma sample DNA and control DNA. Instead of 50 ng of gDNA from positive and negative control samples, we used 0.25 ng of gDNA. This concentration was chosen since using 50 ng (the amount used in tumor sample analysis) or 2.5 ng resulted in almost no differences in the melting intensity (Figure 3.13). Indeed, when we used 0.25 ng it was still possible to detect a melting peak in the positive controls, although with a lower intensity, which were still consistently above wild-type levels with the same concentration. The observation that wild-type controls in tumor analysis often did not present melting peaks when using 50 ng of gDNA became more frequent when reducing the amount of DNA used to 5 ng. After reducing the amount of wild-type control DNA to 0.25 ng, the presence of a melting peak became a very rare occurrence (Figure 3.13).

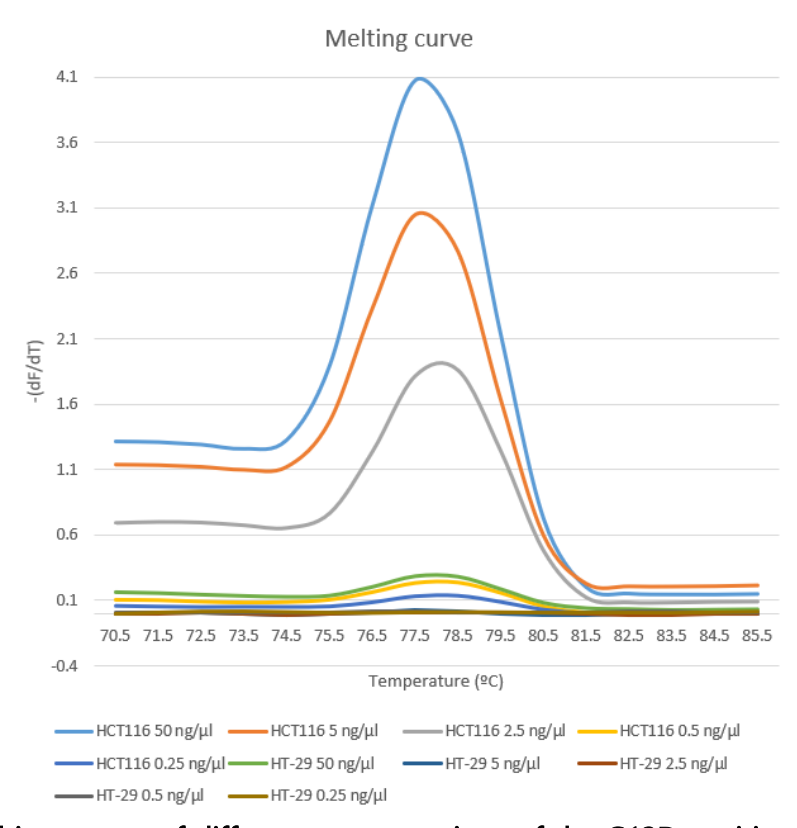


Figure 3.13: Melting curves of different concentrations of the G13D positive control HCT116 and wild-type control HT-29. It is possible to see that as the concentration of HCT116 gDNA is reduced, the intensity of the melting peaks is also reduced. It is also possible to see that only the 50 ng/ $\mu$ l concentration of the wild-type control presents a peak, but with a fluorescence intensity similar to that associated with the positive control at 0.5 ng/ $\mu$ l.

Another adaptation made to the mutation scoring method was the analysis of DNA from two different extractions of the same sample simultaneously. When using a portion of the plasma sample for DNA extraction, the already low proportion of mutated to wild-type DNA can be further reduced. The parallel analysis of the DNA from two extractions of the same sample facilitates the identification of positive cases. The calculation of the normalized fluorescence intensity was still done individually for each extraction of the same sample but when scoring a sample as positive or negative, both extractions were considered. We were more confident in scoring a sample as positive if it presented a melting peak in both extractions. In this case, we used the mean of the normalized fluorescence intensity of each extraction for mutation scoring. However, samples where only one of the extractions consistently presented a melting peak like the positive control were also scored as positive, and we used only one of the extractions to obtain the normalized fluorescence intensity values. Samples that did not present melting peaks in any of the extractions or that presented inconsistent low intensity

melting peaks were scored as negative. Examples of ARMS-HRMA derivative plots of all plasma samples analyzed can be found in Figures A5, A6, A7 and A8 (Appendix).

## 3.5.2.1. G12D mutation analysis in plasma samples

G12D mutation scoring of plasma samples was done as described in tumor samples in section 3.5.1.1. An example of a typical G12D ARMS-HRMA derivative plot with plasma samples can be seen in Figure 3.14. The melting curves of both the positive control and the positive sample are similar to the ones observed in tumor samples in Figure 3.5, but with a much lower fluorescence intensity. In the example provided both extractions of the 31P1 sample present a melting peak near the 78 °C, but the melting peak of the 31P1\* extraction is much closer to the melting peak of the positive control, while extraction 31P1 presents a melting curve with a pronounced peak near 74 °C, characteristic of negatives cases. A possible explanation for this difference is that the 31P1\* extraction might have a higher proportion of mutated DNA than the 31P1 extraction, resulting in the typical peak at 78 °C. Sample 31P2 on the other hand did not present a melting peak in both extractions, common on samples scored as negative.

G12D scoring of plasma samples exclusively analyzed by me using ARMS-HRMA results are summarized in Table 3.7. In Figure 3.15 plasma samples are represented with their respective normalized fluorescence intensity.

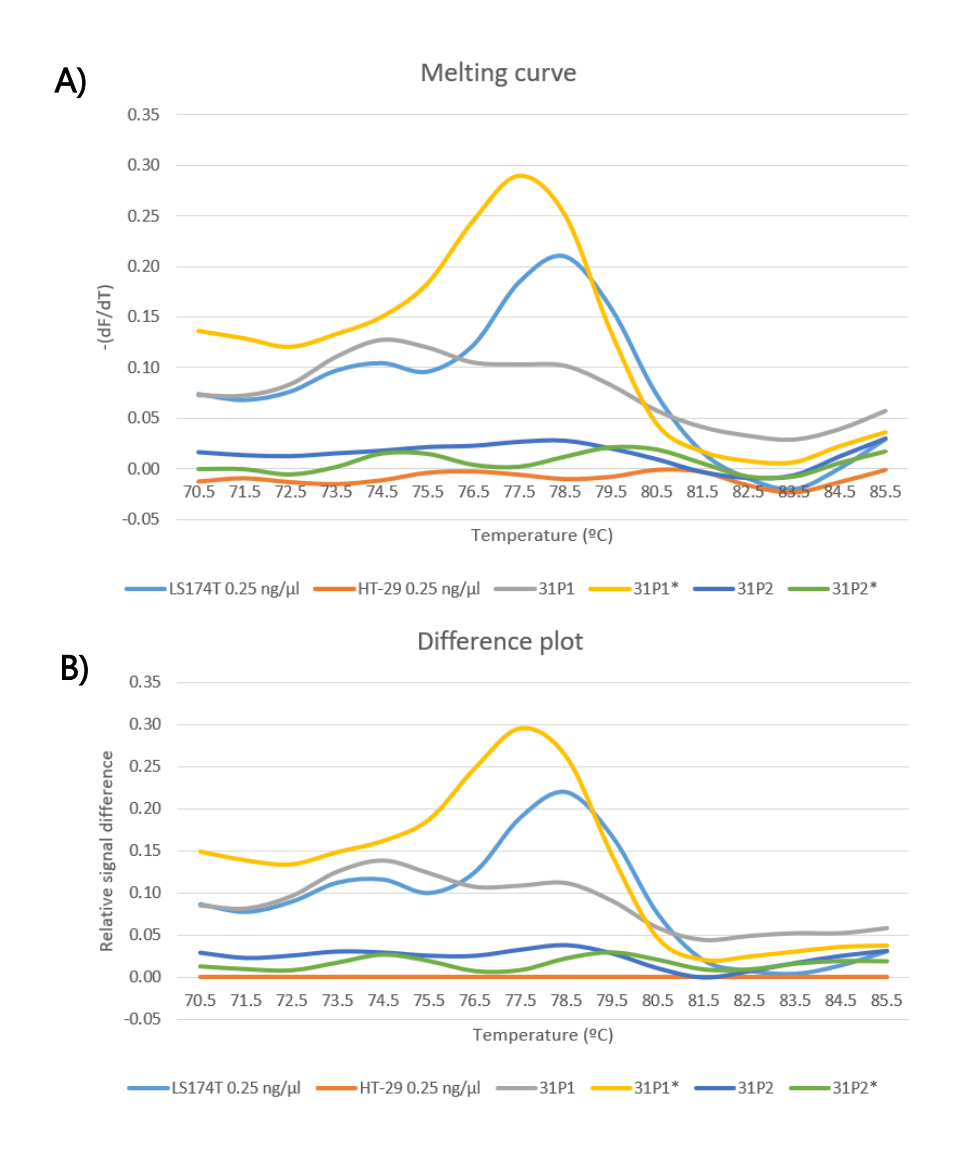


Figure 3.14: ARMS-HRMA results used in G12D mutation scoring of plasma samples 31P1 and 31P2. A) Derivative plot of the melting curve of plasma samples 31P1 and 31P2, wild-type control HT-29 and G12D positive control LS174T. B) Difference plot obtained by subtracting the wild-type control's fluorescence values from every curve. Samples with \* are a second extraction of the same sample.

**Table 3.7:** Summary of G12D mutations found in plasma samples analyzed by ARMS-HRMA.

ND: not detected

	KRAS Mutation	Samples
_	G12D	7P2, 8P2, 31P1, 38P1, 145P1
Г	ND	8P1, 9P1, 9P2, 22P1, 30P1, 31P2, 37P1, 42P1, 42P2, 44P1, 44P2, 116P1, 116P2, 120P1, 123P1, 123P2, 147P1, 147P2, 148P1

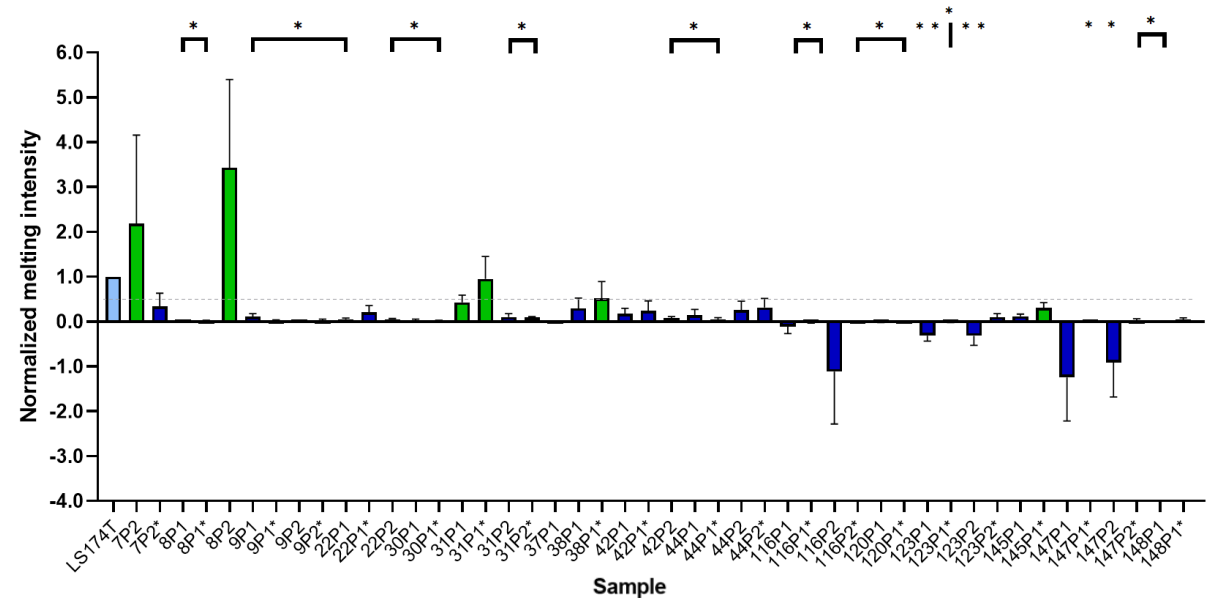


Figure 3.15: G12D scoring based on the normalized melting peak intensity of ARMS-HRMA. All samples are the average of the nor malized melting peak intensity. Standard error of the mean (SEM) is represented in the error bars. Green bars represent samples that were scored as positive, while blue bars represent samples that were scored as negative. The 0.5 threshold is represented as a dotted line. Black asterisks indicate statistical difference between the normalized fluorescence intensity of the sample and the positive control (light blue) using One-way ANOVA with Dunnett's multiple comparisons test and unpaired parametric t-tests, (\*p < 0.05; \*\*p < 0.01).

#### 3.5.2.2. G12V mutation analysis in plasma samples

G12V mutation scoring of plasma samples was done as described in tumor samples in section 3.5.1.2. An example of a typical G12V ARMS-HRMA derivative plot with plasma samples can be seen in Figure 3.16. In the example provided, we can clearly see the melting peaks of two extractions of the same sample, 143P1 and 143P1\*, while the two extractions of the sample 140P1 do not present any melting peaks. G12V scoring of plasma samples exclusively analyzed by me using ARMS-HRMA are summarized in Table 3.8. In Figure 3.17 values for plasma samples are represented with their respective normalized fluorescence intensity.

Many of the samples shown in Figure 3.17 do not have an associated SEM value because in some of the assays the positive controls failed to show a melting peak, likely due to loss in DNA quality. When using fresh DNA controls, melting peaks reappeared and samples were reanalyzed. Those assays were still used for the qualitative analysis of the samples even if they could not be used in the normalization of the fluorescence intensity.

When testing for the G12D mutation, samples sometimes showed melting peaks around 74°C, associated with a negative scoring. When testing for G12V however, samples tended to either present consistent peaks across different assays and between extractions, or not present peaks at all. This means that we could confidently still use these assays that had no positive control since it was still possible to observe the consistent melting peaks of these samples that were scored as positive.

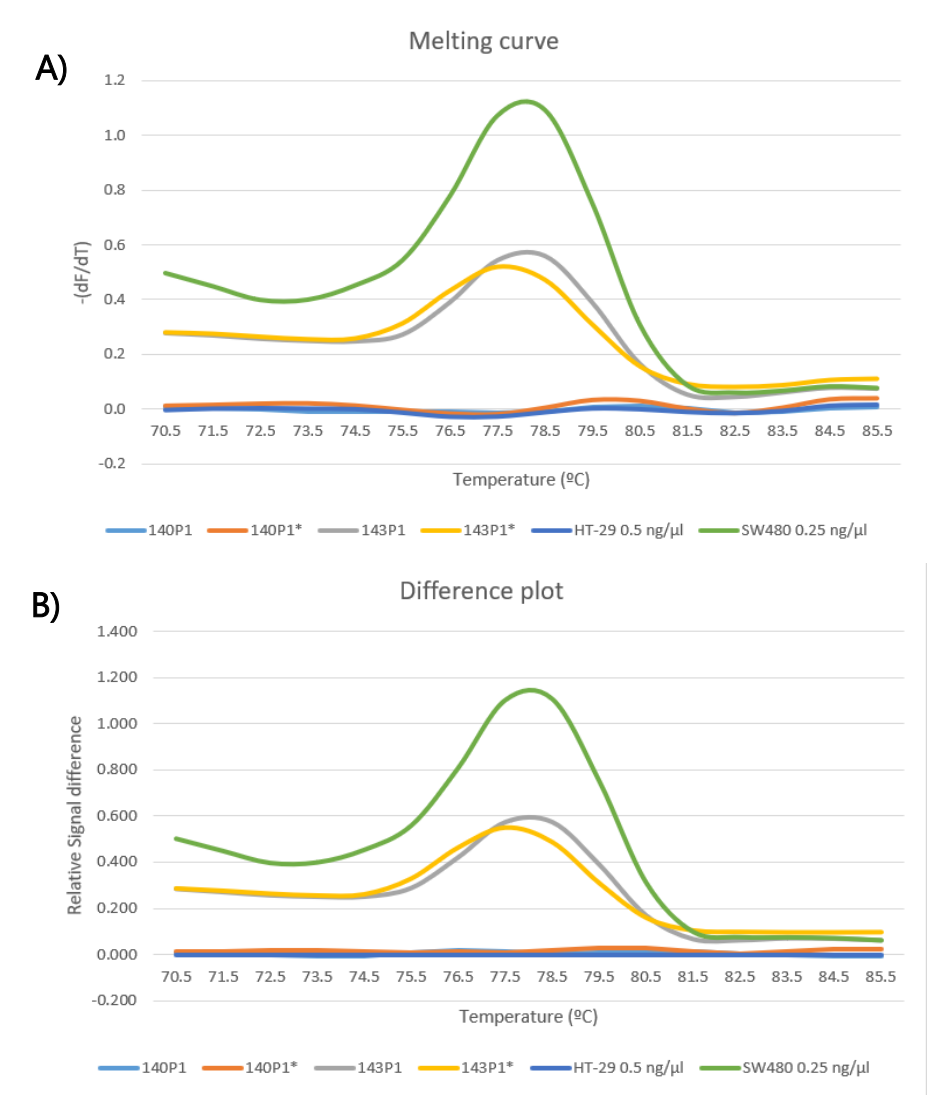


Figure 3.16: ARMS-HRMA results used in G12V mutation scoring of plasma samples 140P1 and 143P1. A) Derivative plot of the melting curve of plasma samples 140P1 and 143P1, wild-type control HT-29 and G12V positive control SW480. B) Difference plot obtained by subtracting the wild-type control's fluorescence values from every curve. Samples with \* are a second extraction of the same sample.

**Table 3.8:** Summary of G12V mutations found in plasma samples analyzed by ARMS-HRMA.

ND: not detected

KRAS mutation	Samples
G12V	4P2, 12P2, 21P2, 36P1, 36P2, 143P1, 153P1
ND	4P1, 9P1, 9P2, 12P1, 18P1, 18P2, 22P1, 22P2, 35P1, 35P2, 36P1, 75P2, 78P2, 84P2, 98P2, 111P1, 140P1, 140P2, 143P2, 154P1

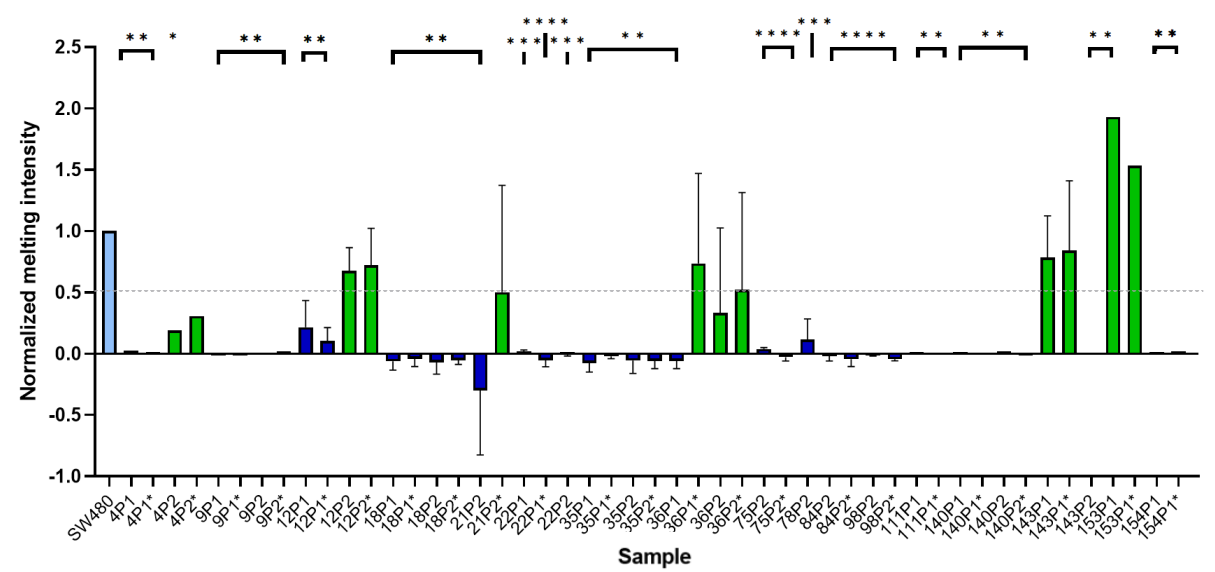


Figure 3.17: G12V scoring based on the normalized melting peak intensity of ARMS-HRMA. All samples are the average of the normalized melting peak intensity. Standard error of the mean (SEM) is represented in the error bars. Green bars represent samples that were scored as positive, while blue bars represent samples that were scored as negative. The 0.5 threshold is represented as a dotted line. Black asterisks indicate statistical difference between the normalized fluorescence intensity of the sample and the positive control (light blue) using One-way ANOVA with Dunnett's multiple comparisons test and unpaired parametric t-tests, (\*p < 0.05; \*\*p < 0.01; \*\*\*p < 0.001; \*\*\*\*p < 0.001; \*\*\*\*p < 0.0001).

#### 3.5.2.3. G12R mutation analysis in plasma samples

G12R mutation scoring of plasma samples was done as described in tumor samples (section 3.5.1.3). An example of a typical G12R ARMS-HRMA derivative plot with plasma samples can be seen in Figure 3.18. In the example provided, two samples from the same patient, 28P1 and 28P2, were scored as positive, with the two extractions of the 28P2 sample presenting melting peaks. Neither of the extractions of the 110P1 sample presented a melting peak, common in G12R negative cases. G12R scoring of plasma samples exclusively analyzed by me using ARMS-HRMA are summarized in Table 3.9. In Figure 3.19 values for plasma samples are represented with their respective normalized fluorescence intensity. In section 3.5.1.3, it was already mentioned that in the case of G12R mutation, a higher proportion of mutated DNA might be necessary for tumor samples to present a melting peak with the same intensity of the positive control. However, when analyzing the G12R mutation in plasma samples, it was not possible to use the established 0.25 ng of PSN-1 gDNA for the positive control since no melting peaks

appeared. To obtain a melting peak for the positive control, the amount of DNA used had to be increased to 2.5 ng. The intensity of these melting peaks was comparable to the positive controls of mutations G12V and G12D, where 1/10 of the DNA amount was used. Once again, this might indicate that the G12R ARMS reaction might not be as efficient as other mutations, needing a higher amount of template DNA to amplify. No differences were observed when using 0.25 or 2.5 ng of HT-29 gDNA, so it was decided to use 2.5 ng to match the positive control.

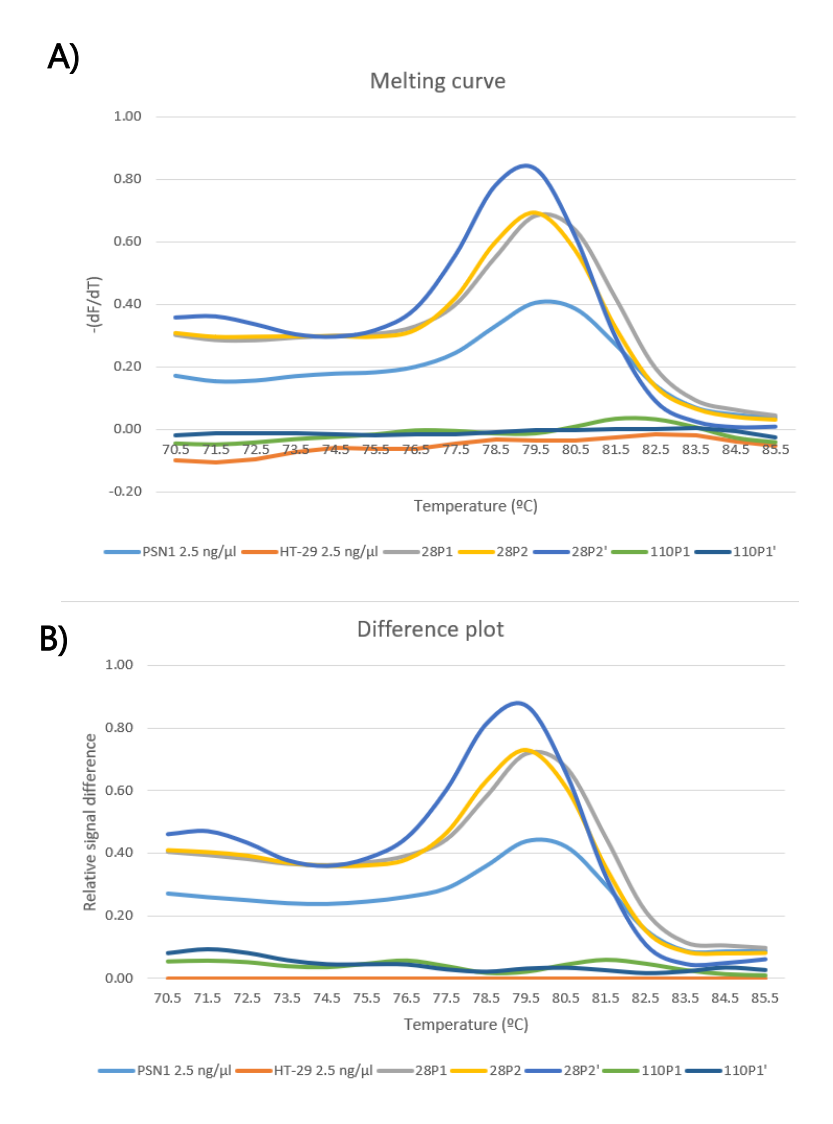


Figure 3.18: ARMS-HRMA results used in G12R mutation scoring of plasma samples 28P1, 28P2 and 110P1. A) Derivative plot of the melting curve of plasma samples 28P1, 28P2 and 110P1, wild-type control HT-29 and G12R positive control PSN-1. B) Difference plot obtained by subtracting the wild-type control's fluorescence values from every curve. Samples with \* are a second extraction of the same sample. This assay was performed by PhD student André Luz.

**Table 3.9:** Summary of G12R mutations found in plasma samples analyzed by ARMS-HRMA ND: not detected

KRAS mutation	Samples
G12R	73P2
ND	20P2, 73P1, 121P1, 124P1, 128P1, 128P2, 134P1, 146P1, 146P2, 149P1, 155P1

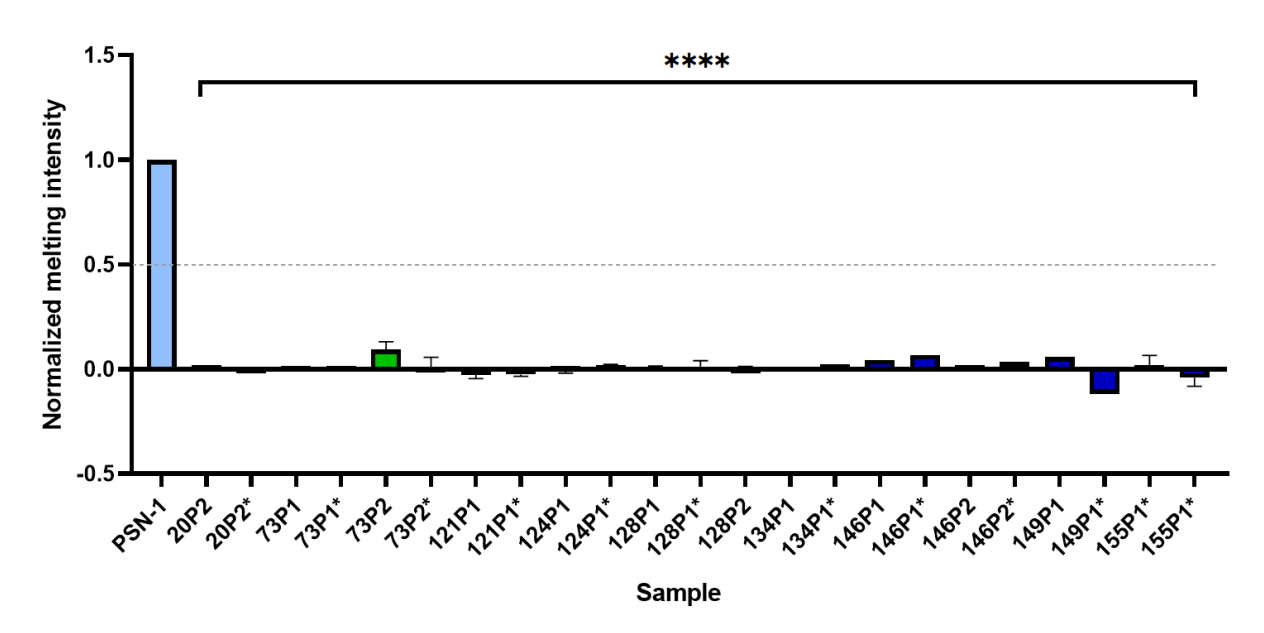


Figure 3.19: G12R scoring based on the normalized melting peak intensity of ARMS-HRMA. All samples are the average of the normalized melting peak intensity. Standard error of the mean (SEM) is represented in the error bars. Green bars represent samples that were scored as positive, while blue bars represent samples that were scored as negative. The 0.5 threshold is represented as a dotted line. Black asterisks indicate statistical difference between the normalized fluorescence intensity of the sample and the positive control (light blue) using One-way ANOVA with Dunnett's multiple comparisons test and unpaired parametric t-tests, (\*\*\*\*p < 0.0001).

#### 3.5.2.4. G12C mutation analysis in plasma samples

G12C mutation scoring of plasma samples was done as described in tumor samples (section 3.5.1.4). An example of a typical G12C ARMS-HRMA derivative plot of plasma samples can be seen in Figure 3.20. ARMS-HRMA only detected G12C mutations in 2 tumor samples, 65T and 90T as this is a rare *KRAS* mutation. Both 65P1 and 90P1 were tested by PhD student André Luz.

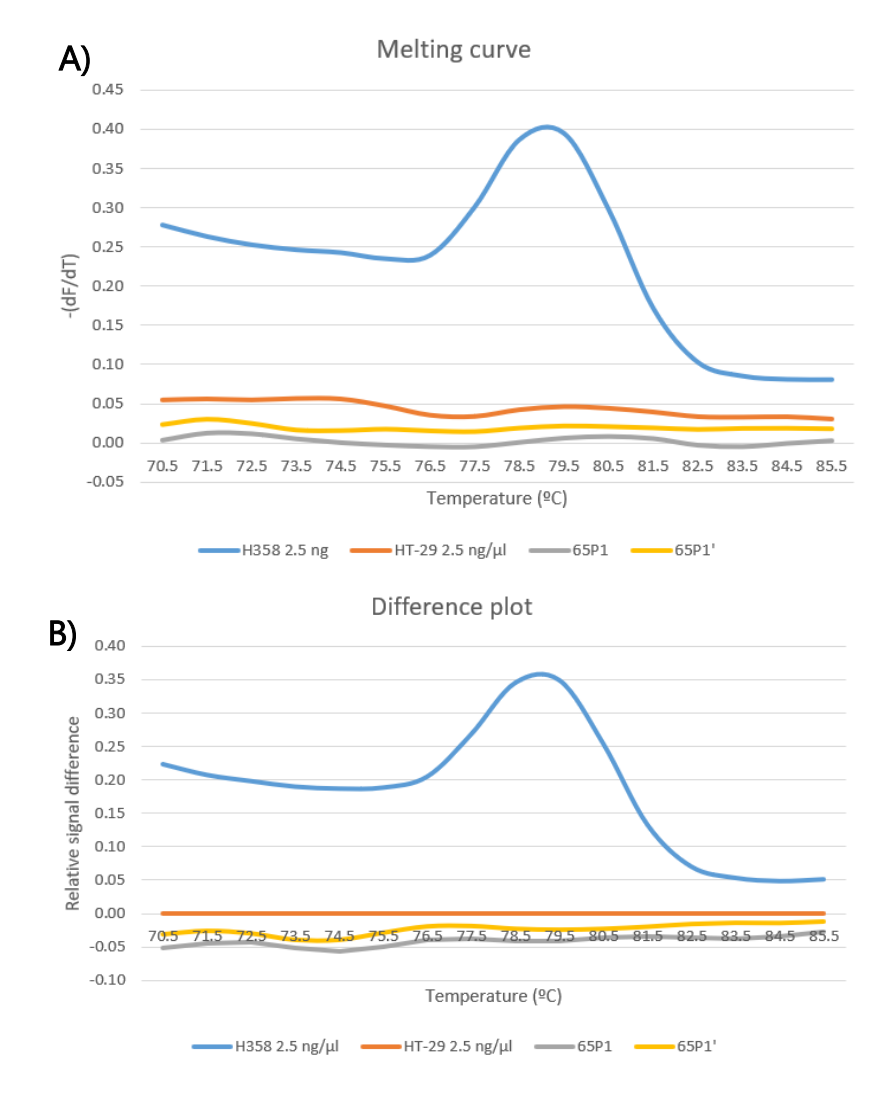


Figure 3.20: ARMS-HRMA results used in G12C mutation scoring of plasma sample 65P1. A) Derivative plot of the melting curve of plasma sample 65P1, wild-type control HT-29 and G12C positive control H358. B) Difference plot obtained by subtracting the wild-type control's fluorescence values from every curve. Samples with \* are a second extraction of the same sample. This assay was performed by PhD student André Luz.

## 3.5.2.5. G13D mutation analysis in plasma samples

G13D mutation scoring of plasma samples was done as described in tumor samples (section 3.5.1.5). An example of a typical G13D ARMS-HRMA derivative plot of plasma samples can be seen in Figure 3.21. ARMS-HRMA only detected a G13D mutation in sample 127T, 127P2 did not present a peak and therefore was scored as negative.

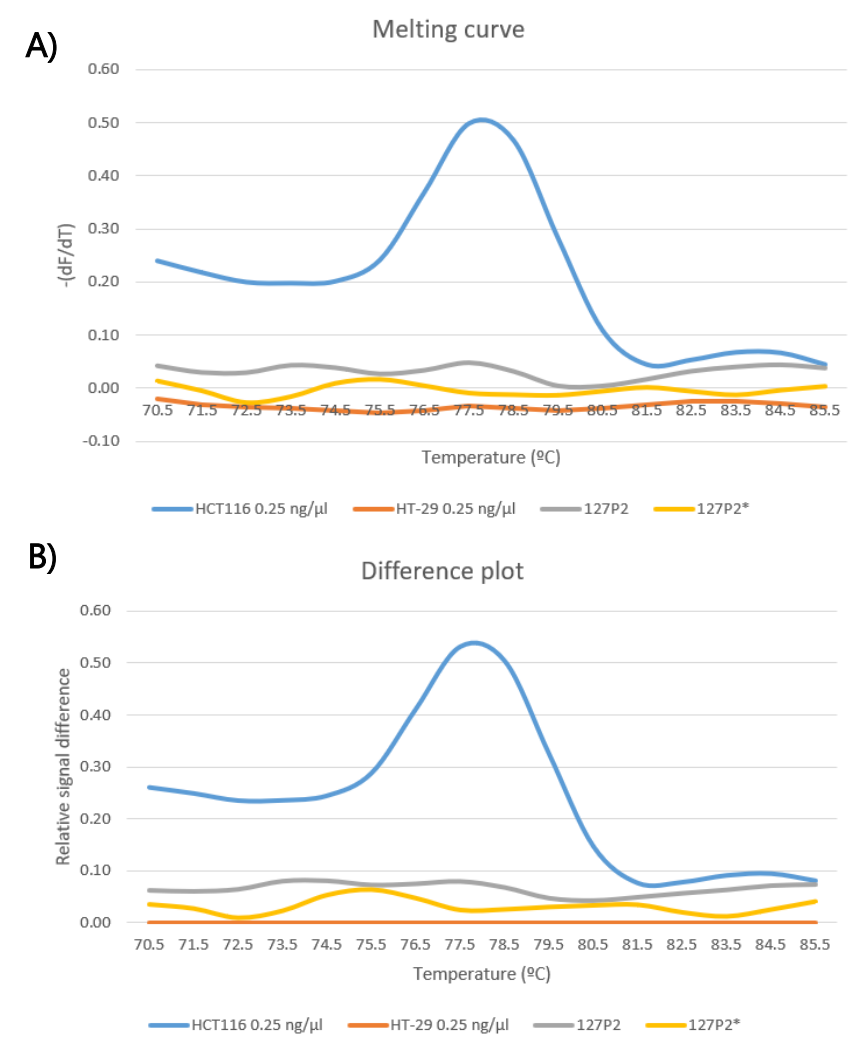


Figure 3.21: ARMS-HRMA results used in G13D mutation scoring of plasma sample 127P2. A) Derivative plot of the melting curve of plasma sample 127P1, wild-type control HT-29 and G13D positive control HCT116. B) Difference plot obtained by subtracting the wild-type control's fluorescence values from every curve. Samples with \* are a second extraction of the same sample.

#### 3.5.2.6. ARMS-HRMA on plasma samples - summary

The point of using liquid biopsies is to obtain information about the presence of mutations originated from the primary tumor in circulation in a more easily accessible biological fluid, like blood. For this reason, we focused on testing plasma samples of patients whose tumor samples scored positive for *KRAS* mutations. A summary of the mutations found in plasma samples of 65 patients with positive tumors can be found in Table 3.10. Mutations were found in plasma samples (either on P1 or P2) in 20 out of the 65 patients (31%). 9 out those 20 mutations were G12D (45%), 8 were G12V (40%), 2 were G12R (10%) and 1 plasma sample tested positive for both G12D and G12V (5%). A Sankey chart showing the interaction between the ARMS-HRMA results of both tumor and plasma samples of these 65 patients can be found in Figure 3.22.

**Table 3.10**: ARMS-HRMA results of plasma samples from patients with positive tumor samples. \*Patients where neither of the plasma samples, P1 and P2, tested positive for a *KRAS* mutation.

KRAS mutation	Samples		
G12D	7(P2), 8(P2), 31(P1), 38(P1), 66(P1), 69(P1), 89(P2), 90(P2), 145(P1)		
G12V 4(P2), 11(P2), 21(P2), 36(P1 and P2), 74(P1), 74(P1), 143(P1 and P2), 153(P1)			
G12R	28(P1 and P2), 73(P2)		
G12D/G12V	83(P1 and P2)		
Not detected*	1, 4, 6, 9, 10, 13, 17, 18, 20, 23, 30, 35, 37, 39, 42, 44, 47, 48, 58, 59, 65, 74, 84, 88, 98, 100, 105, 111, 116, 119, 120, 121, 123, 124, 127, 128, 134, 142, 146, 147, 148, 149, 154, 155, 159		

One of the biggest limitations of the application of liquid biopsies in performing mutational analysis of tumors is the low amount of ctDNA present in these samples<sup>89</sup>. The amount of ctDNA released in the bloodstream is increased as the tumor size<sup>90</sup> increases, but still extremely low in early phases of the disease<sup>89</sup>, which can hinder their utility in defining an early treatment strategy. ctDNA has limited stability with a short half-life<sup>91</sup>, which when combined with its highly fragmented nature can limit the amplification of the target sequence. The choice of DNA extraction method used should also consider the characteristics of ctDNA to mitigate the loss of the already low amounts of mutated DNA sequences. Commonly used DNA extraction kits based on columns with silica membranes, such as the one used in this work, might not be adequate for the isolation of small DNA fragments. In fact, Qiagen columns that use the

same basic principle show a lower yield and partial loss of DNA fragments with a size of below  $150 \text{ bp}^{92,93}$ .

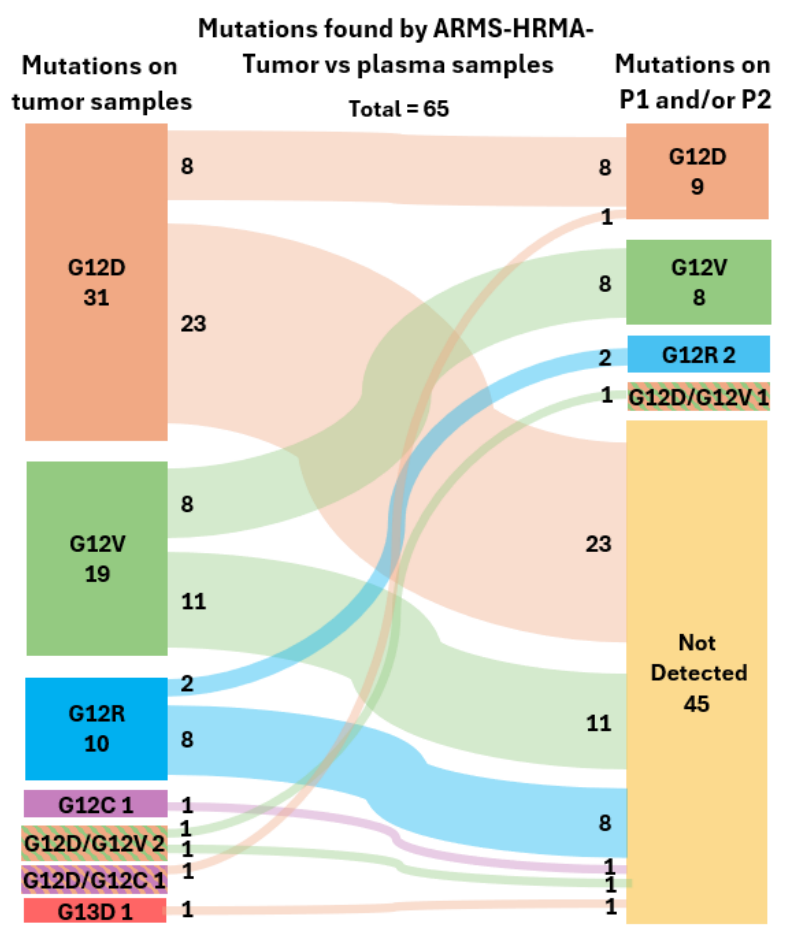


Figure 3.22: Sankey chart diagram of the ARMS-HRMA results of tumor and plasma samples.

The 65 patients included are patients that had both tumor and plasma samples available, and whose tumor samples tested positive for a KRAS mutation. ARMS-HRMA results are represented on the left and plasma sample ARMS-HRMA results are represented on the right. Correspondence between the tumor and plasma samples is represented by the flows in the middle. Using G12D as an example, it is possible to see that out of 31 patients with G12D-positive tumors, only 8 tested positive for that same mutation in their plasma samples.

## 3.6. Comparison between ARMS-HRMA and other molecular techniques

In Beatriz et al.<sup>85</sup> the robustness of the ARMS-HRMA technique was already established using tumor and plasma samples from 30 of the patients from this cohort. Regarding the G12V mutation, ARMS-HRMA results had a 100% concordance with ddPCR in tumor samples. Regarding the G12D mutation, 1 tumor sample was scored as positive by ARMS-HRMA but negative by ddPCR, which could be considered either a false positive or an argument in favor of the high sensitivity of ARMS-HRMA<sup>85</sup>. Sanger Sequencing however failed to detect one G12V mutation and two G12D mutations.

Even though no additional samples were analyzed by ddPCR in this work, all tumor samples in the cohort were sequenced using SS and therefore can be compared to the results obtained by ARMS-HRMA. This comparison can be seen in Table 3.11 and the Sankey chart diagram in Figure 3.23.

**Table 3.11:** Comparison between tumor sample SS and ARMS-HRMA results.

Tumor Cample	SS result	ARMS-HRMA	Tumor Comple	SS result	ARMS-HRMA	Tumor Comple	CC rosult	ARMS-HRMA
Tumor Sample	SS result	result	Tumor Sample	SS result	result	Tumor Sample	SS result	result
1	wt	G12D	44	wt	G12D	121	wt/G12R	G12R
3	wt	ND	46	wt	ND	123	wt/G12D	G12D
4	wt/G12V	G12V	47	wt	G12V/G12D	124	wt/G12R	G12R
5	wt/G12R	-	48	wt/G12D	G12D	125	wt	ND
6	wt/G12V	G12V	58	wt/G12D	G12D	126	wt	ND
7	wt/G12D	G12D	59	wt/G12D	G12D	127	wt/G13D	G13D
8	wt/G12D	G12D	65	wt/G12C	G12C	128	wt	G12R
9	wt	G12V	66	wt	G12D	129	wt	ND
10	wt/G12V	G12V	69	wt	G12D	130	wt	ND
11	wt	ND	73	wt/G12R	G12R	131	wt	G12D
12	wt/G12V	G12V	74	wt	G12D	132	wt	G12V
13	wt/G12D	G12D	75	wt	G12V	134	wt/G12R	G12R
16	wt/G12V	-	78	wt/G12V	G12V	136	wt/G12D	G12D
17	wt/G12D	G12D	79	wt	ND	139	wt	ND
18	wt/G12V	G12V	81	wt	ND	140	wt/G12V	G12V
20	wt/G12R	G12R	83	wt/G12V	G12V/G12D	141	wt	G12V
21	wt	G12V	84	wt/G12V	G12V	142	wt	G12D
22	wt	-	88	wt/G12D	G12D	143	wt	G12V
23	wt/G12D	G12D	89	wt	G12D	145	wt/G12D	G12D
24	wt	ND	90	wt/G12C	G12C	146	wt	G12R
25	wt	ND	93	wt/G12D	G12D	147	wt/G12D	G12D
28	wt/G12R	G12R	98	wt/G12V	G12V	148	wt/G12D	G12D
30	wt/G12D	G12D	100	wt/G12D	G12D	149	wt/G12R	G12R
31	wt/G12D	G12D	105	wt/G12D	G12D	150	wt/G12V	G12V
34	wt	ND	107	wt	ND	151	wt/G12D	G12D
35	wt/G12V	G12V	109	wt	ND	153	wt/G12V	G12V
36	wt	G12V	110	wt/G12A	-	154	wt/G12V	G12V
37	wt/G12D	G12D	111	wt	G12V	155	wt	G12R
38	wt/G12D	G12D	112	wt	ND	156	wt	ND
39	wt	G12V	115	wt	ND	158	wt	ND
40	wt	ND	116	wt/G12D	G12D	159	wt/G12D	G12D
42	wt	G12D	119	wt/G12D	G12D			<u> </u>
43	wt	ND	120	wt	G12D	1		

green - concordant with ARMS-HRMA red - not concordant with ARMS-HRMA yellow - comparison not possible

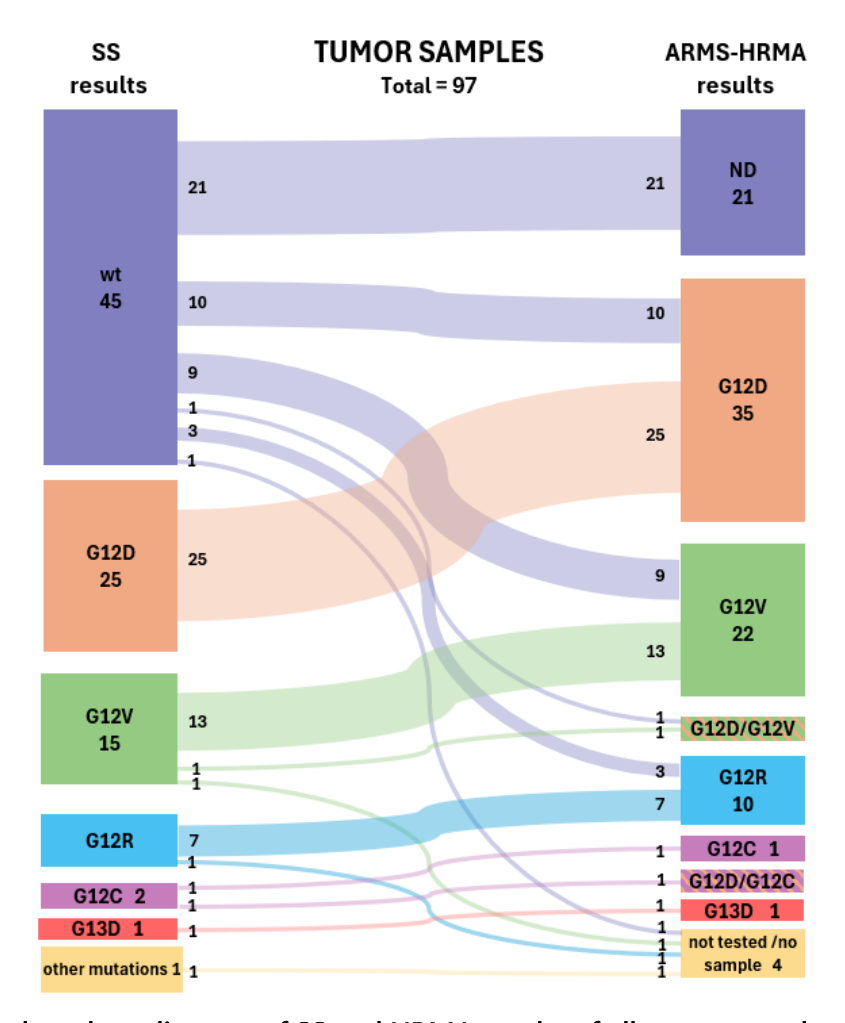


Figure 3.23: Sankey chart diagram of SS and HRMA results of all tumor samples. The SS results of tumor samples are represented on the left and respective ARMS-HRMA results are represented on the right. Correspondence between the two techniques is represented by the flows in the middle.

Out of 45 tumor samples scored as wild-type by SS, only 21 did not score positive for any mutations when analyzed by ARMS-HRMA, as seen in Figure 3.23. When compared to SS, ARMS-HRMA detected 10 additional G12D mutations, 9 additional G12V mutations, 3 additional G12R mutations. It also scored 1 tumor sample (47T) as G12V and G12D positive when SS did not. It also detected an additional G12D mutation in tumor samples 83T and 90T. Every mutation found through SS was also detected by ARMS-HRMA. These findings show the high sensitivity and specificity of ARMS-HRMA. It is also important to note that the reaction mixture used to obtain these results had a relatively low DNA concentration of just 5 ng/ $\mu$ L (50ng in a total volume of 10  $\mu$ L) once again highlighting the high sensitivity of the ARMS-HRMA methodology, which does not rely in very high amounts of template DNA.

During this work, no new tumor or plasma samples were analyzed by ddPCR. With the available data, the ddPCR results for 32 of the original tumor samples analyzed by PhD student Beatriz Oliveira were compared with SS and ARMS-HRMA (Figure 3.24). Positive cases found in both SS and ddPCR have a 100% concordance with ARMS-HRMA. However, 2 tumor samples were scored as G12V-positive (21T and 75T) and another 2 were scored as G12D-positive (44T and 69T) by ARMS-HRMA which were not detected by either SS or ddPCR. It is common for mutations scored as wild-type by SS to have mutations detected by ARMS-HRMA due to the higher limit of detection of SS, as seen in Figure 3.23. ddPCR, however, is a highly sensitive molecular technique with a very low limit of detection (Table 1.1). This disparity could be attributed to i) ARMS-HRMA results are false positives, ii) the sensitivity of the ARMS-HRMA is comparable or even slightly higher than that of ddPCR, or iii) tumor heterogeneity/representativity in samples might have affected the results consistency.

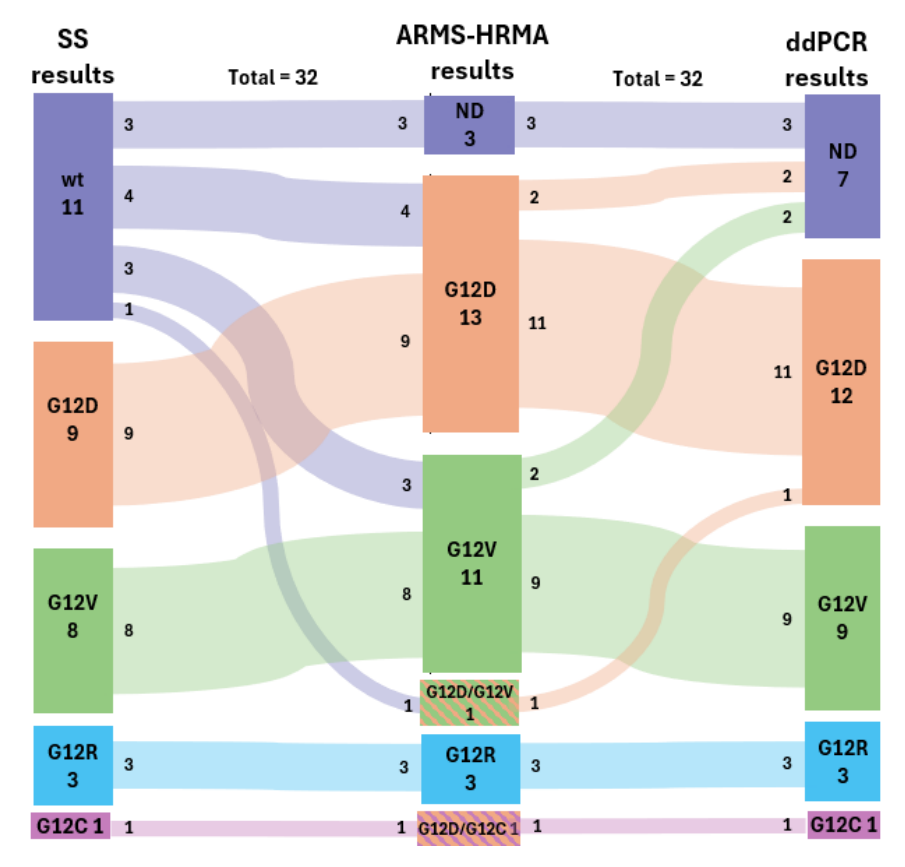


Figure 3.24: Sankey chart diagram of SS, ARMS-HRMA and ddPCR results for tumor samples. Since the number of tumor samples that were analyzed by ddPCR is reduced, the number of tumor samples used in this comparison is limited to 32. Tumor samples SS results are represented on the left, tumor ARMS-HRMA results are represented on the middle and tumor ddPCR results are represented on the right. Correspondence between techniques is represented by the flows in the middle.

Out of 32 patients included in the analysis of Figure 3.24, 21 had mutated tumor samples with concordant results between the 3 techniques (SS, ARMS-HRMA, ddPCR) and available plasma samples. The comparison between the mutated tumor samples (with concordant results between the 3 techniques) and plasma samples ARMS-HRMA results of these 21 patients can be seen in Figure 3.25. Out of the 21 plasma samples, 11 (53%) were positive for *KRAS* mutations. This is a higher % of positive plasma samples over the 31% observed in Figure 3.22 (discussed in section 3.5.2.6) which included 65 patients with mutated tumor samples (scored by ARMS-HRMA alone). Given the high limit of detection of SS, tumor samples with concordant results between the 3 techniques is likely associated with an increased mutated allele frequency or less heterogenous tumors, which would result in a higher proportion of mutated DNA and possibly in a higher proportion of mutations detected in ctDNA.

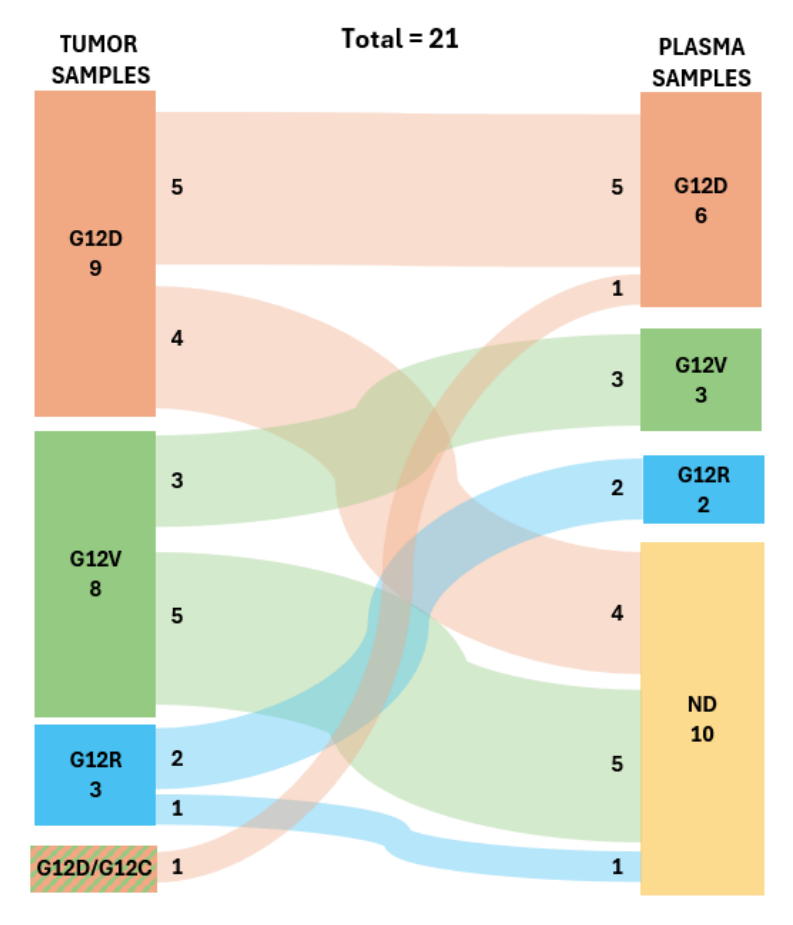


Figure 3.25: Sankey chart diagram comparing only the mutated tumor samples with concordant results by SS, ARMS-HRMA and ddPCR and plasma samples ARMS-HRMA results. Tumor samples results are represented on the left and plasma samples ARMS-HRMA results are represented on the right. Correspondence between the two techniques is represented by the flows in the middle.

## 3.7. Influence of experimental replicates on mutation scoring

The translation of ARMS-HRMA into a clinical setting requires a streamlined process, from sample preparation to mutation scoring, to support *KRAS* mutational testing for large volumes of samples. The validation of ARMS-HRMA required the analysis of multiple assays for each sample. Basing the mutation scoring process on multiple assays should result in more reliable results with a lower probability of false positives or negatives. However, performing a test multiple times in clinical setting might not be monetarily viable. The effect of using only the first assay in the tumor scoring process is represented in Figure 3.26.

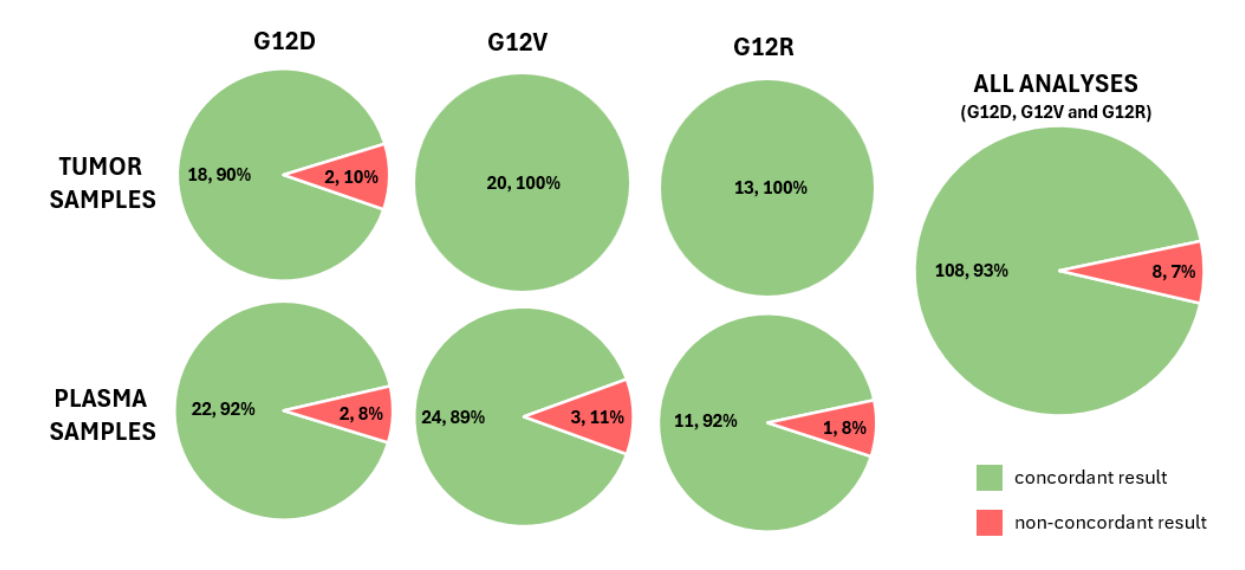


Figure 3.26: Effect of using only the first assay in the tumor scoring process. Samples with a concordant mutation scoring when using only the first assay and when using multiple assays to calculate the normalized fluorescence intensity are represent in green. Samples with different mutations scoring between the two methods are represented in red. Values inside the pie charts represent the number of samples tested for the corresponding mutation.

As an example, during G12D testing in tumor samples, sample 151T would be scored as negative if only the first assay was considered, since it did not present a melting peak. After analyzing all 3 assays however, 151T was scored as G12D positive. 129T would be considered G12D positive if only the first assay was considered, due to having a positive control with an abnormally low melting peak. Overall, only 7% of mutation analyses performed for the G12D, G12V and G12R mutations would be affected when not performing additional replicates. Out of the 8 cases described in Figure 3.26 as non-concordant results, 2 are samples wrongly considered positive when analyzing only the first assay and the other 6 are samples wrongly scored as positive.

When translating ARMS-HRMA into a clinical setting, the use of good-quality DNA in the positive controls is essential. Throughout this work, the gDNA used as a positive control sometimes did not present the usual high-intensity melting peak, which prevented an accurate normalization of the melting intensity. This issue was usually solved when switching the gDNA to a freshly extracted one, highlight the need for a good maintenance of experimental controls. To ensure accuracy of results the same should be done to the wild-type control as well, as to reduce the chance of false positives.

The qualitative analysis of the melting curves also proved to be an essential part of the mutation scoring method to assess the quality of the controls and reagents, but also to do a critical observation of samples' melting curves. As mentioned in section 3.5.1.3, mutation scoring of 129T was done based on the observation that this sample consistently presented a melting peak when other samples and wild-type controls did not, and not by using the 0.5 threshold.

## 4. CONCLUSIONS AND FUTURE PROSPECTS

The primary objective of this work was the validation of ARMS-HRMA for 5 KRAS mutations, G12D, G12V, G12R, G12C and G13D, in tumor and plasma samples using a cohort of 97 pancreatic cancer patients. This project is a continuation of the work performed by Beatriz et al.<sup>85</sup> that validated ARMS-HRMA for the detection of G12D and G12V mutations in tumor samples and plasma samples from a cohort of 30 pancreatic cancer patients.

The analysis of tumor samples by ARMS-HRMA was successful for all 5 mutations. Out of 97 tumor samples, 93 were analyzed by ARMS-HRMA. There was not enough DNA for the ARMS-HRMA analysis of 3 tumor samples (5T, 16T and 22T) and SS results showed that the genotype of tumor sample 110T was wt/G12A, a mutation not included in this work. Out of 93 tumor samples analyzed by ARMS-HRMA, 72 tested positive for *KRAS* mutations while the remaining 21 tested negative for all 5 mutations. Out of the 72 positive cases, 35 were G12D (49%), 22 were G12V (29%), 10 were G12R (14%), 1 were G12C (1%), 1 were G13D (1%), 2 tested positive for both G12D and G12V (3%) and 1 tested positive for both G12C and G12D (1%).

SS, the current gold standard for mutation analysis, detected KRAS mutations in 52 out of 97 tumor samples (54%), and all of them (besides G12A) were also detected by ARMS-HRMA. However, SS failed to detect KRAS mutations in 23 tumor samples scored as positive by ARMS-HRMA, meaning that KRAS mutation detection improved significantly when using ARMS-HRMA over SS, by increasing sensitivity without losing specificity. The high limit of detection of SS (10%-20% according to Table 1.1) hinders the mutation analysis of tumors with lower proportions of mutated DNA since up to 85% of a PDAC tumor can be constituted by stroma cells<sup>83</sup>. Tumor heterogeneity can drive this proportion to be even lower, hindering mutation detection by SS even further. ddPCR is a much more sensitive technique with a much lower limit of detection (0.001%-0.1% according to Table 1.1). Out of 32 tumor samples that were analyzed by ddPCR, 25 were scored as positive for KRAS mutations. Every mutation detected by ddPCR in these 25 samples was also detected by ARMS-HRMA which highlights the high sensitivity of ARMS-HRMA even further. Furthermore, ARMS-HRMA detected mutations in 4 additional samples that were scored as wild-type by ddPCR and scored sample 47T as G12D and G12C positive when ddPCR only detected the G12C mutation. These cases could either be ARMS-HRMA false positives or an additional testimony to the high sensitivity of ARMS-HRMA. Based on these findings, ARMS-HRMA surpasses SS as a high sensitivity methodology for the

detection of *KRAS* mutations in tumor samples, with the added benefit of also being the cheaper and faster option.

The analysis of ctDNA from plasma samples by ARMS-HRMA allowed the detection of KRAS mutations in 20 out of 65 (31%) patients with mutated tumor samples and available plasma samples. Out of the 20 positive cases, 9 were G12D (45%), 8 were G12V (40%), 2 were G12R (10%), and 1 tested positive for G12D and G12V (5%). The limit of detection of SS does not allow the reliable detection of mutations in ctDNA as their proportion in cancer patients can be as low as 0.1% of total cfDNA. Beatriz et al.85 had already referred the inadequacy of SS for the detection of KRAS mutations in ctDNA, so these results are still a significant upgrade over SS and can provide valuable information for PDAC monitoring. The % of plasma samples that presents KRAS mutations depends on multiple factors. Cancer patients with less advanced diseases generally present lower amounts of ctDNA in their bloodstream, since ctDNA concentration is correlated with tumor size<sup>89,90</sup>, which can limit the detection of mutations. Another limiting factor of ctDNA analysis is its extraction efficiency. ctDNA extraction protocols are affected by its low half-life, high degree of fragmentation and low concentrations in early-stage diseases. It would be interesting to test ARMS-HRMA performance using DNA extraction kits optimized for plasma samples to hopefully obtain higher yields of ctDNA, and consequently obtain more accurate results. Another consideration regarding the extraction protocol used in this work is that ctDNA extraction was performed from a plasma volume of 200-300 µL. Extracting ctDNA from a higher volume of plasma sample would be desirable, as it should result in a higher yield of ctDNA.

With the current G12C KRAS targeted inhibitor and the ongoing investment in developing targeted therapies for other *KRAS* mutations, tumor molecular profiling becomes increasingly more valuable. The identification of patients who test negative for all mutations could also be relevant when defining a treatment strategy, as *KRAS* mutations are associated with resistance to some chemotherapy options such as EGFR inhibitors in other cancers<sup>94</sup>. If a tumor sample is available for molecular analysis, ARMS-HRMA profiling could provide relevant information when guiding treatment strategy, as it provides a more accurate look into the tumor's molecular profile. However, this approach would benefit from the inclusion of more *KRAS* mutations beyond the 5 tested in this work. KRAS codon 61, for example, harbors mutations that are also associated with PDAC such as Q61H, which is found in around 4-5% of patients<sup>95,96</sup>. The cost-effectiveness of the inclusion of other rarer mutations needs to be assessed for the mutational analysis to remain economically viable. Regarding plasma sample analysis, even though ARMS-HRMA only allowed the detection of *KRAS* mutations in plasma

samples in around a third of patients with mutated tumors, this information could still be very useful in monitoring disease progression during treatment, since repeatedly detecting *KRAS* mutations in ctDNA is a good indicator of progressive disease<sup>97</sup>. The analysis of *KRAS* mutations in plasma samples by ARMS-HRMA could then be a valuable tool, by helping medical doctors assess the patient's response to the treatment, as repeated detection of *KRAS* mutations in ctDNA could be an indicator to change chemotherapy regiment.

ARMS-HRMA was shown to be a rapid, cost-effective, reliable, and simple methodology for the analysis of KRAS mutation in tumor samples. That said, it could benefit from additional validation and adjustments. A cohort of 97 patients already provided a good insight into the performance of ARMS-HRMA, but a bigger sample size would be needed to confidently translate this methodology to a clinical setting. Even with its advantages, ARMS-HRMA still suffers from only being able to test one mutation at a time. A multiplex approach was considered, where a conjugation of mutation specific primers would be used to test for multiple mutations at a time. The melting curves of the 5 tested mutations are very similar, with G12V, G12D, G12C and G13D mutations presenting a melting peak at around 78°C and G12R presenting a peak around 79 °C, making the identification of mutation on a positive case very difficult. Additionally, the different annealing temperatures, obtained by the optimization of the ARMS reaction to the different mutations, would also hinder the optimization of a single reaction for the detection of multiple mutations. Most importantly, since the different KRAS mutations are associated with different prognoses and therapeutic options, losing the ability to discern mutations would not be ideal, as aiding PDAC treatment is the main objective of this work. Therefore ARMS-HRMA multiplexing was not pursued.

There is a growing investment in the development of technologies that can be integrated in Point-of care testing (POCT) as these tests provide faster results, without the need of specialized staff and with lower costs. Microfluidic systems are one example, where the engineering of fluid flow manipulation in micro-sized objects allows the development of small, more automated analytical systems<sup>98</sup>. Microfluidic tools can work with volumes from the micro to picolitre scales, manipulating them at the submillimeter scale, which has the advantages of high sensitivity, low consumption of reagents, laminar flow, cost effectiveness, and high spatiotemporal resolution<sup>98</sup>. Biosensors integrated in microfluidic devices allow the detection of different types of biomarkers such as mRNA expression profiles, circulating DNA and tumor cells, proteins, proteomic pattern, lipids and metabolites<sup>99</sup>, which is useful for the diagnosis of autoimmune, infectious, neurodegenerative and cardiovascular diseases<sup>100</sup>. Cancer is no exception, with significant progress being made in the use of microfluidic devices in both cancer

diagnosis and research<sup>98</sup>. Since molecular techniques have been successfully integrated in microfluidic devices, the successful integration of the ARMS-HRMA could streamline the mutation scoring process even further. Melting curve analysis (MCA) is already possible in microfluidic platforms. Li et al.<sup>101</sup> developed a microfluidics platform for the discrimination of *KRAS* point mutations through MCA, which uses the same basic principles of HRMA of analyzing the differences in the melting profile of mutated DNA sequences. In this device, the micro/nanostructure renders the establishment of superhydrophilic patterns within a superhydrophobic substrate, which allow the formation of droplets that contain the DNA sequences and fluorescence probes. A temperature gradient is created throughout the device, and the melting curve is obtained by the measurement of the fluorescence levels by a microscope across the different temperatures, allowing MCA. That said, this implementation is still quite complex and needs specialized equipment (as the detection of fluorescence is done with a fluorescence microscope). It would still be interesting to see if the coupling of a preemptive ARMS step to a similar MCA system could make POCT ARMS-HRMA a step closer to reality.

## 5. BIBLIOGRAPHY

- 1. Bray F, Laversanne M, Sung H, et al. Global cancer statistics 2022: GLOBOCAN estimates of incidence and mortality worldwide for 36 cancers in 185 countries. *CA Cancer J Clin.* 2024;74(3):229-263. doi:10.3322/caac.21834
- 2. Pulumati A, Pulumati A, Dwarakanath BS, Verma A, Papineni RVL. Technological advancements in cancer diagnostics: Improvements and limitations. *Cancer Rep.* 2023;6(2):e1764. doi:10.1002/cnr2.1764
- 3. Masucci M, Karlsson C, Blomqvist L, Ernberg I. Bridging the Divide: A Review on the Implementation of Personalized Cancer Medicine. *J Pers Med.* 2024;14(6):561. doi:10.3390/jpm14060561
- 4. Khalaf N, El-Serag HB, Abrams HR, Thrift AP. Burden of Pancreatic Cancer: From Epidemiology to Practice. *Clin Gastroenterol Hepatol.* 2021;19(5):876-884. doi:10.1016/j.cgh.2020.02.054
- 5. Zhang Z, Zhang H, Liao X, Tsai H i. KRAS mutation: The booster of pancreatic ductal adenocarcinoma transformation and progression. *Front Cell Dev Biol.* 2023;11. Accessed September 19, 2023. https://www.frontiersin.org/articles/10.3389/fcell.2023.1147676
- 6. Ferlay J, Ervik M, Lam F, Laversanne M, Colombet M, Mery L, Piñeros M, Znaor A, Soerjomataram I, Bray F (2024). Global Cancer Observatory: Cancer Today. Lyon, France: International Agency for Research on Cancer. Available from: https://gco.iarc.who.int/to-day, accessed 23/9/2024
- 7. Mizrahi JD, Surana R, Valle JW, Shroff RT. Pancreatic cancer. *The Lancet*. 2020;395(10242):2008-2020. doi:10.1016/S0140-6736(20)30974-0
- 8. Bengtsson A, Andersson R, Ansari D. The actual 5-year survivors of pancreatic ductal adenocarcinoma based on real-world data. *Sci Rep.* 2020;10(1):16425. doi:10.1038/s41598-020-73525-y
- 9. Springfeld C, Jäger D, Büchler MW, et al. Chemotherapy for pancreatic cancer. *Presse Médicale*. 2019;48(3, Part 2):e159-e174. doi:10.1016/j.lpm.2019.02.025
- 10. Zhang S, Xiao X, Yi Y, et al. Tumor initiation and early tumorigenesis: molecular mechanisms and interventional targets. *Signal Transduct Target Ther*. 2024;9(1):1-36. doi:10.1038/s41392-024-01848-7

- 11. Weston A, Harris CC. Multistage Carcinogenesis. In: *Holland-Frei Cancer Medicine. 6th Edition.* BC Decker; 2003. Accessed August 12, 2024. https://www.ncbi.nlm.nih.gov/books/NBK13982/
- 12. Basu AK. DNA Damage, Mutagenesis and Cancer. *Int J Mol Sci.* 2018;19(4):970. doi:10.3390/ijms19040970
- 13. Chen J, Potlapalli R, Quan H, et al. Exploring DNA Damage and Repair Mechanisms: A Review with Computational Insights. *BioTech*. 2024;13(1):3. doi:10.3390/biotech13010003
- 14. Manders F, van Boxtel R, Middelkamp S. The Dynamics of Somatic Mutagenesis During Life in Humans. *Front Aging*. 2021;2:802407. doi:10.3389/fragi.2021.802407
- 15. Sherr CJ. Principles of Tumor Suppression. *Cell.* 2004;116(2):235-246. doi:10.1016/S0092-8674(03)01075-4
- 16. Visser KE de, Joyce JA. The evolving tumor microenvironment: From cancer initiation to metastatic outgrowth. *Cancer Cell.* 2023;41(3):374-403. doi:10.1016/j.ccell.2023.02.016
- 17. Basturk O, Hong SM, Wood LD, et al. A REVISED CLASSIFICATION SYSTEM AND RECOM-MENDATIONS FROM THE BALTIMORE CONSENSUS MEETING FOR NEOPLASTIC PRECUR-SOR LESIONS IN THE PANCREAS. *Am J Surg Pathol.* 2015;39(12):1730-1741. doi:10.1097/PAS.0000000000000533
- 18. Marstrand-Daucé L, Lorenzo D, Chassac A, Nicole P, Couvelard A, Haumaitre C. Acinar-to-Ductal Metaplasia (ADM): On the Road to Pancreatic Intraepithelial Neoplasia (PanIN) and Pancreatic Cancer. *Int J Mol Sci.* 2023;24(12):9946. doi:10.3390/ijms24129946
- 19. Storz P, Crawford HC. Carcinogenesis of Pancreatic Ductal Adenocarcinoma. *Gastroenter-ology*. 2020;158(8):2072-2081. doi:10.1053/j.gastro.2020.02.059
- 20. Wang S, Huang S, Sun YL. Epithelial-Mesenchymal Transition in Pancreatic Cancer: A Review. *BioMed Res Int.* 2017;2017:2646148. doi:10.1155/2017/2646148
- 21. Joshi VB, Gutierrez Ruiz OL, Razidlo GL. The Cell Biology of Metastatic Invasion in Pancreatic Cancer: Updates and Mechanistic Insights. *Cancers*. 2023;15(7):2169. doi:10.3390/cancers15072169
- 22. Le Large TYS, Bijlsma MF, Kazemier G, van Laarhoven HWM, Giovannetti E, Jimenez CR. Key biological processes driving metastatic spread of pancreatic cancer as identified by multi-omics studies. *Semin Cancer Biol.* 2017;44:153-169. doi:10.1016/j.sem-cancer.2017.03.008
- 23. Poorebrahim M, Abazari MF, Moradi L, et al. Multi-targeting of K-Ras domains and mutations by peptide and small molecule inhibitors. *PLoS Comput Biol.* 2022;18(4):e1009962. doi:10.1371/journal.pcbi.1009962

- 24. Parikh K, Banna G, Liu SV, et al. Drugging KRAS: current perspectives and state-of-art review. *J Hematol Oncol Hematol Oncol*. 2022;15(1):152. doi:10.1186/s13045-022-01375-4
- 25. Huang L, Guo Z, Wang F, Fu L. KRAS mutation: from undruggable to druggable in cancer. Signal Transduct Target Ther. 2021;6(1):1-20. doi:10.1038/s41392-021-00780-4
- 26. Wang H, Chi L, Yu F, et al. Annual review of KRAS inhibitors in 2022. *Eur J Med Chem.* 2023;249:115124. doi:10.1016/j.ejmech.2023.115124
- 27. Hunter JC, Manandhar A, Carrasco MA, Gurbani D, Gondi S, Westover KD. Biochemical and Structural Analysis of Common Cancer-Associated KRAS Mutations. *Mol Cancer Res.* 2015;13(9):1325-1335. doi:10.1158/1541-7786.MCR-15-0203
- 28. Nusrat F, Khanna A, Jain A, et al. The Clinical Implications of KRAS Mutations and Variant Allele Frequencies in Pancreatic Ductal Adenocarcinoma. *J Clin Med.* 2024;13(7):2103. doi:10.3390/jcm13072103
- 29. Zhu C, Guan X, Zhang X, et al. Targeting KRAS mutant cancers: from druggable therapy to drug resistance. *Mol Cancer*. 2022;21(1):159. doi:10.1186/s12943-022-01629-2
- 30. Bannoura SF, Khan HY, Azmi AS. KRAS G12D targeted therapies for pancreatic cancer: Has the fortress been conquered? *Front Oncol.* 2022;12. doi:10.3389/fonc.2022.1013902
- 31. Zafra MP, Parsons MJ, Kim J, et al. An In Vivo Kras Allelic Series Reveals Distinct Phenotypes of Common Oncogenic Variants. *Cancer Discov.* 2020;10(11):1654-1671. doi:10.1158/2159-8290.CD-20-0442
- 32. Pantsar T. The current understanding of KRAS protein structure and dynamics. *Comput Struct Biotechnol J.* 2020;18:189-198. doi:10.1016/j.csbj.2019.12.004
- 33. Gebregiworgis T, Kano Y, St-Germain J, et al. The Q61H mutation decouples KRAS from upstream regulation and renders cancer cells resistant to SHP2 inhibitors. *Nat Commun.* 2021;12(1):6274. doi:10.1038/s41467-021-26526-y
- 34. Stefanicka-Wojtas D, Kurpas D. Personalised Medicine—Implementation to the Healthcare System in Europe (Focus Group Discussions). *J Pers Med.* 2023;13(3):380. doi:10.3390/jpm13030380
- 35. Gilazieva Z, Ponomarev A, Rutland C, Rizvanov A, Solovyeva V. Promising Applications of Tumor Spheroids and Organoids for Personalized Medicine. *Cancers*. 2020;12(10):2727. doi:10.3390/cancers12102727
- 36. Gambardella V, Tarazona N, Cejalvo JM, et al. Personalized Medicine: Recent Progress in Cancer Therapy. *Cancers*. 2020;12(4):1009. doi:10.3390/cancers12041009
- 37. Turashvili G, Brogi E. Tumor Heterogeneity in Breast Cancer. *Front Med.* 2017;4. doi:10.3389/fmed.2017.00227

- 38. Krasinskas AM, Moser AJ, Saka B, Adsay NV, Chiosea SI. *KRAS* mutant allele-specific imbalance is associated with worse prognosis in pancreatic cancer and progression to undifferentiated carcinoma of the pancreas. *Mod Pathol.* 2013;26(10):1346-1354. doi:10.1038/modpathol.2013.71
- 39. Barzi A, Weipert CM, Espenschied CR, et al. ERBB2 (HER2) amplifications and co-occurring KRAS alterations in the circulating cell-free DNA of pancreatic ductal adenocarcinoma patients and response to HER2 inhibition. *Front Oncol.* 2024;14. doi:10.3389/fonc.2024.1339302
- 40. Gambardella V, Lombardi P, Carbonell-Asins JA, et al. Molecular profiling of advanced solid tumours. The impact of experimental molecular-matched therapies on cancer patient outcomes in early-phase trials: the MAST study. *Br J Cancer*. 2021;125(9):1261-1269. doi:10.1038/s41416-021-01502-x
- 41. Espiau-Romera P, Courtois S, Parejo-Alonso B, Sancho P. Molecular and Metabolic Subtypes Correspondence for Pancreatic Ductal Adenocarcinoma Classification. *J Clin Med.* 2020;9(12):4128. doi:10.3390/jcm9124128
- 42. Bilreiro C, Andrade L, Santiago I, Marques RM, Matos C. Imaging of pancreatic ductal adenocarcinoma An update for all stages of patient management. *Eur J Radiol Open.* 2024;12:100553. doi:10.1016/j.ejro.2024.100553
- 43. Clarke DL, Clarke BA, Thomson SR, Garden OJ, Lazarus NG. The role of preoperative biopsy in pancreatic cancer. *HPB*. 2004;6(3):144-153. doi:10.1080/13651820410030862
- 44. Chien MS, Lin CC, Lai JH. Endoscopic Ultrasonography-Guided Fine-Needle Biopsy for Patients with Resectable Pancreatic Malignancies. *Gastroenterol Insights*. 2024;15(2):375-385. doi:10.3390/gastroent15020026
- 45. Taherian M, Wang H, Wang H. Pancreatic Ductal Adenocarcinoma: Molecular Pathology and Predictive Biomarkers. *Cells.* 2022;11(19):3068. doi:10.3390/cells11193068
- 46. Quirós-Caso C, Arias Fernández T, Fonseca-Mourelle A, et al. Routine flow cytometry approach for the evaluation of solid tumor neoplasms and immune cells in minimally invasive samples. *Cytometry B Clin Cytom.* 2022;102(4):272-282. doi:10.1002/cyto.b.22081
- 47. Masoumi-Moghaddam S, Lundy J, Gao H, et al. The EUS molecular evaluation of pancreatic cancer: A prospective multicenter cohort trial. *Endosc Ultrasound*. 2021;10(5):335-343. doi:10.4103/EUS-D-20-00230
- 48. Zhang L, Sanagapalli S, Stoita A. Challenges in diagnosis of pancreatic cancer. *World J Gastroenterol.* 2018;24(19):2047-2060. doi:10.3748/wjg.v24.i19.2047
- 49. Kitano M, Minaga K, Hatamaru K, Ashida R. Clinical dilemma of endoscopic ultrasound-guided fine needle aspiration for resectable pancreatic body and tail cancer. *Dig Endosc.* 2022;34(2):307-316. doi:10.1111/den.14120

- 50. Cherciu Harbiyeli IF, Constantin A, Cazacu IM, et al. Technical Performance, Overall Accuracy and Complications of EUS-Guided Interventional Procedures: A Dynamic Landscape. *Diagnostics*. 2022;12(7):1641. doi:10.3390/diagnostics12071641
- 51. Razzano D, Bouza SJ, Hernandez PV, et al. Comprehensive molecular profiling of pancreatic ductal adenocarcinoma in FNA, biopsy, and resection specimens. *Cancer Cytopathol.* 2022;130(9):726-734. doi:10.1002/cncy.22589
- 52. Reissig TM, Tzianopoulos I, Liffers ST, et al. Smaller panel, similar results: genomic profiling and molecularly informed therapy in pancreatic cancer. *ESMO Open.* 2023;8(3):101539. doi:10.1016/j.esmoop.2023.101539
- 53. Boukovala M, Westphalen CB, Probst V. Liquid biopsy into the clinics: Current evidence and future perspectives. *J Liq Biopsy.* 2024;4:100146. doi:10.1016/j.jlb.2024.100146
- 54. Luo G, Jin K, Deng S, et al. Roles of CA19-9 in pancreatic cancer: Biomarker, predictor and promoter. *Biochim Biophys Acta BBA Rev Cancer*. 2021;1875(2):188409. doi:10.1016/j.bbcan.2020.188409
- 55. Liu C, Deng S, Jin K, et al. Lewis antigen-negative pancreatic cancer: An aggressive subgroup. *Int J Oncol.* 2020;56(4):900-908. doi:10.3892/ijo.2020.4989
- 56. Connal S, Cameron JM, Sala A, et al. Liquid biopsies: the future of cancer early detection. *J Transl Med.* 2023;21:118. doi:10.1186/s12967-023-03960-8
- 57. Buscail E, Maulat C, Muscari F, et al. Liquid Biopsy Approach for Pancreatic Ductal Adenocarcinoma. *Cancers*. 2019;11(6):852. doi:10.3390/cancers11060852
- 58. Wang ZY, Ding XQ, Zhu H, Wang RX, Pan XR, Tong JH. KRAS Mutant Allele Fraction in Circulating Cell-Free DNA Correlates With Clinical Stage in Pancreatic Cancer Patients. *Front Oncol.* 2019;9. doi:10.3389/fonc.2019.01295
- 59. Zhou Z, Lin T, Chen S, et al. Omics-based molecular classifications empowering in precision oncology. *Cell Oncol.* 2024;47(3):759-777. doi:10.1007/s13402-023-00912-8
- 60. Mullis K, Faloona F, Scharf S, Saiki R, Horn G, Erlich H. Specific enzymatic amplification of DNA in vitro: the polymerase chain reaction. *Cold Spring Harb Symp Quant Biol.* 1986;51 Pt 1:263-273. doi:10.1101/sqb.1986.051.01.032
- 61. Artika IM, Dewi YP, Nainggolan IM, Siregar JE, Antonjaya U. Real-Time Polymerase Chain Reaction: Current Techniques, Applications, and Role in COVID-19 Diagnosis. *Genes.* 2022;13(12):2387. doi:10.3390/genes13122387
- 62. Sanger F, Nicklen S, Coulson AR. DNA sequencing with chain-terminating inhibitors. *Proc Natl Acad Sci U S A*. 1977;74(12):5463-5467.

- 63. Mansfield ES, Worley JM, McKenzie SE, Surrey S, Rappaport E, Fortina P. Nucleic acid detection using non-radioactive labelling methods. *Mol Cell Probes.* 1995;9(3):145-156. doi:10.1006/mcpr.1995.0023
- 64. Heather JM, Chain B. The sequence of sequencers: The history of sequencing DNA. *Genomics*. 2016;107(1):1-8. doi:10.1016/j.ygeno.2015.11.003
- 65. Newton CR, Graham A, Heptinstall LE, et al. Analysis of any point mutation in DNA. The amplification refractory mutation system (ARMS). *Nucleic Acids Res.* 1989;17(7):2503-2516.
- 66. Islam MT, Alam ARU, Sakib N, et al. A rapid and cost-effective multiplex ARMS-PCR method for the simultaneous genotyping of the circulating SARS-CoV-2 phylogenetic clades. *J Med Virol.* 2021;93(5):2962-2970. doi:10.1002/jmv.26818
- 67. Vogelstein B, Kinzler KW. Digital PCR. *Proc Natl Acad Sci.* 1999;96(16):9236-9241. doi:10.1073/pnas.96.16.9236
- 68. Nazir S. Medical diagnostic value of digital PCR (dPCR): A systematic review. *Biomed Eng Adv.* 2023;6:100092. doi:10.1016/j.bea.2023.100092
- 69. Mao X, Liu C, Tong H, Chen Y, Liu K. Principles of digital PCR and its applications in current obstetrical and gynecological diseases. *Am J Transl Res.* 2019;11(12):7209-7222.
- 70. Wittwer CT, Reed GH, Gundry CN, Vandersteen JG, Pryor RJ. High-Resolution Genotyping by Amplicon Melting Analysis Using LCGreen. *Clin Chem.* 2003;49(6):853-860. doi:10.1373/49.6.853
- 71. Gundry CN, Vandersteen JG, Reed GH, Pryor RJ, Chen J, Wittwer CT. Amplicon melting analysis with labeled primers: a closed-tube method for differentiating homozygotes and heterozygotes. *Clin Chem.* 2003;49(3):396-406. doi:10.1373/49.3.396
- 72. Vossen RHAM, Aten E, Roos A, den Dunnen JT. High-Resolution Melting Analysis (HRMA)—More than just sequence variant screening. *Hum Mutat.* 2009;30(6):860-866. doi:10.1002/humu.21019
- 73. Qin D. Next-generation sequencing and its clinical application. *Cancer Biol Med.* 2019;16(1):4-10. doi:10.20892/j.issn.2095-3941.2018.0055
- 74. Hu T, Chitnis N, Monos D, Dinh A. Next-generation sequencing technologies: An overview. *Hum Immunol.* 2021;82(11):801-811. doi:10.1016/j.humimm.2021.02.012
- 75. Liu L, Li Y, Li S, et al. Comparison of Next-Generation Sequencing Systems. *BioMed Res Int.* 2012;2012(1):251364. doi:10.1155/2012/251364
- 76. Malapelle U, Bellevicine C, Salatiello M, et al. Sanger sequencing in routine KRAS testing: a review of 1720 cases from a pathologist's perspective. *J Clin Pathol.* 2012;65(10):940-944. doi:10.1136/jclinpath-2012-200773

- 77. Franklin WA, Haney J, Sugita M, Bemis L, Jimeno A, Messersmith WA. *KRAS* Mutation. *J Mol Diagn*. 2010;12(1):43-50. doi:10.2353/jmoldx.2010.080131
- 78. Tsiatis AC, Norris-Kirby A, Rich RG, et al. Comparison of Sanger Sequencing, Pyrosequencing, and Melting Curve Analysis for the Detection of *KRAS* Mutations. *J Mol Diagn*. 2010;12(4):425-432. doi:10.2353/jmoldx.2010.090188
- 79. Shackelford RE, Whitling NA, McNab P, Japa S, Coppola D. KRAS Testing: A Tool for the Implementation of Personalized Medicine. *Genes Cancer*. 2012;3(7-8):459-466. doi:10.1177/1947601912460547
- 80. Olmedillas-López S, Olivera-Salazar R, García-Arranz M, García-Olmo D. Current and Emerging Applications of Droplet Digital PCR in Oncology: An Updated Review. *Mol Diagn Ther*. 2022;26(1):61-87. doi:10.1007/s40291-021-00562-2
- 81. Jennings LJ, Arcila ME, Corless C, et al. Guidelines for Validation of Next-Generation Sequencing–Based Oncology Panels. *J Mol Diagn JMD*. 2017;19(3):341-365. doi:10.1016/j.jmoldx.2017.01.011
- 82. Singh RR. Next-Generation Sequencing in High-Sensitive Detection of Mutations in Tumors: Challenges, Advances, and Applications. *J Mol Diagn.* 2020;22(8):994-1007. doi:10.1016/j.jmoldx.2020.04.213
- 83. Bulle A, Lim KH. Beyond just a tight fortress: contribution of stroma to epithelial-mesen-chymal transition in pancreatic cancer. *Signal Transduct Target Ther*. 2020;5(1):1-12. doi:10.1038/s41392-020-00341-1
- 84. Siravegna G, Mussolin B, Venesio T, et al. How liquid biopsies can change clinical practice in oncology. *Ann Oncol.* 2019;30(10):1580-1590. doi:10.1093/annonc/mdz227
- 85. Oliveira BB, Costa B, Morão B, et al. Combining the amplification refractory mutation system and high-resolution melting analysis for KRAS mutation detection in clinical samples. *Anal Bioanal Chem.* 2023;415(14):2849-2863. doi:10.1007/s00216-023-04696-6
- 86. Nacchio M, Sgariglia R, Gristina V, et al. KRAS mutations testing in non-small cell lung cancer: the role of Liquid biopsy in the basal setting. *J Thorac Dis.* 2020;12(7):3836-3843. doi:10.21037/jtd.2020.01.19
- 87. U.S. Food and Drug Administration. Available from: https://www.fda.gov/medical-de-vices/in-vitro-diagnostics/list-cleared-or-approved-companion-diagnostic-devices-in-vitro-and-imaging-tools, accessed 23/9/2024
- 88. Sánchez-Herrero E, Serna-Blasco R, Robado de Lope L, González-Rumayor V, Romero A, Provencio M. Circulating Tumor DNA as a Cancer Biomarker: An Overview of Biological Features and Factors That may Impact on ctDNA Analysis. *Front Oncol.* 2022;12:943253. doi:10.3389/fonc.2022.943253

- 89. Fiala C, Diamandis EP. Utility of circulating tumor DNA in cancer diagnostics with emphasis on early detection. *BMC Med.* 2018;16(1):166. doi:10.1186/s12916-018-1157-9
- 90. Bleckman RF, Haag CMSC, Rifaela N, et al. Levels of circulating tumor DNA correlate with tumor volume in gastro-intestinal stromal tumors: an exploratory long-term follow-up study. *Mol Oncol.* n/a(n/a). doi:10.1002/1878-0261.13644
- 91. Qin Z, Ljubimov VA, Zhou C, Tong Y, Liang J. Cell-free circulating tumor DNA in cancer. *Chin J Cancer.* 2016;35(1):36. doi:10.1186/s40880-016-0092-4
- 92. Fleischhacker M, Schmidt B, Weickmann S, et al. Methods for isolation of cell-free plasma DNA strongly affect DNA yield. *Clin Chim Acta*. 2011;412(23):2085-2088. doi:10.1016/j.cca.2011.07.011
- 93. Devonshire AS, Whale AS, Gutteridge A, et al. Towards standardisation of cell-free DNA measurement in plasma: controls for extraction efficiency, fragment size bias and quantification. *Anal Bioanal Chem.* 2014;406(26):6499-6512. doi:10.1007/s00216-014-7835-3
- 94. Siddiqui AD, Piperdi B. KRAS Mutation in Colon Cancer: A Marker of Resistance to EGFR-I Therapy. *Ann Surg Oncol.* 2010;17(4):1168-1176. doi:10.1245/s10434-009-0811-z
- 95. Waters AM, Der CJ. KRAS: The Critical Driver and Therapeutic Target for Pancreatic Cancer. *Cold Spring Harb Perspect Med.* 2018;8(9):a031435. doi:10.1101/cshperspect.a031435
- 96. Luo J. KRAS mutation in pancreatic cancer. *Semin Oncol.* 2021;48(1):10-18. doi:10.1053/j.seminoncol.2021.02.003
- 97. Kruger S, Heinemann V, Ross C, et al. Repeated mutKRAS ctDNA measurements represent a novel and promising tool for early response prediction and therapy monitoring in advanced pancreatic cancer. *Ann Oncol.* 2018;29(12):2348-2355. doi:10.1093/annonc/mdy417
- 98. Akgönüllü S, Bakhshpour M, Pişkin AK, Denizli A. Microfluidic Systems for Cancer Diagnosis and Applications. *Micromachines*. 2021;12(11):1349. doi:10.3390/mi12111349
- 99. Sanjay ST, Fu G, Dou M, et al. Biomarker detection for disease diagnosis using cost-effective microfluidic platforms. *The Analyst*. 2015;140(21):7062-7081. doi:10.1039/c5an00780a
- 100. Kumar AS, Venkatesalu S, Dilliyappan S, et al. Microfluidics as diagnostic tools. *Clin Chim Acta*. 2024;556:117841. doi:10.1016/j.cca.2024.117841
- 101. Li M, Wan L, Law MK, et al. One-shot high-resolution melting curve analysis for KRAS point-mutation discrimination on a digital microfluidics platform. *Lab Chip.* 2022;22(3):537-549. doi:10.1039/D1LC00564B

# 6. APPENDIX

**Table A1:** DNA Concentration and purity ratios of DNA extracted from tumor samples. Samples with \* and \*\* are a second and third extraction of the same samples, respectively.

Sample	Concentration (ng/ul)	Purity ratios			
Sample	Concentration (ng/µL)	260/280 ratio	260/230 ratio		
105T	76.6	1.94	1.84		
105T*	55	1.81	1.24		
105T	42.6	1.92	1.62		
107T	43.2	2.02	1.77		
107T*	54.9	1.98	1.63		
111T	193.4	1.92	2.24		
111T*	79.6	1.98	1.63		
112T	142.1	1.97	2.31		
112T*	16.5	2.24	1.78		
115T	23.8	1.47	0.52		
115T*	39.3	1.76	1.22		
119T	38.1	1.9	1.41		
124T	15.3	1.53	0.74		
125T	54.7	1.78	1.46		
126T	147.5	1.93	2.06		
127T	71.8	1.8	1.73		
128T	355.6	1.89	2.26		
128T*	74.8	1.78	1.14		
129T	130.8	1.88	2.01		
131T	15.7	1.79	1.21		
131T*	53.5	1.82	1.8		
132T	142	1.34	0.61		
139T	50.8	1.05	0.39		
141T	131.7	1.63	1.15		
141T*	237.9	1.78	2.04		
142T	995.9	1.92	2.36		
143T	481.5	1.86	2.31		
149T	57.3	1.76	1.3		
150T	85.6	1.82	1.96		
151T	47.6	1.8	1.53		

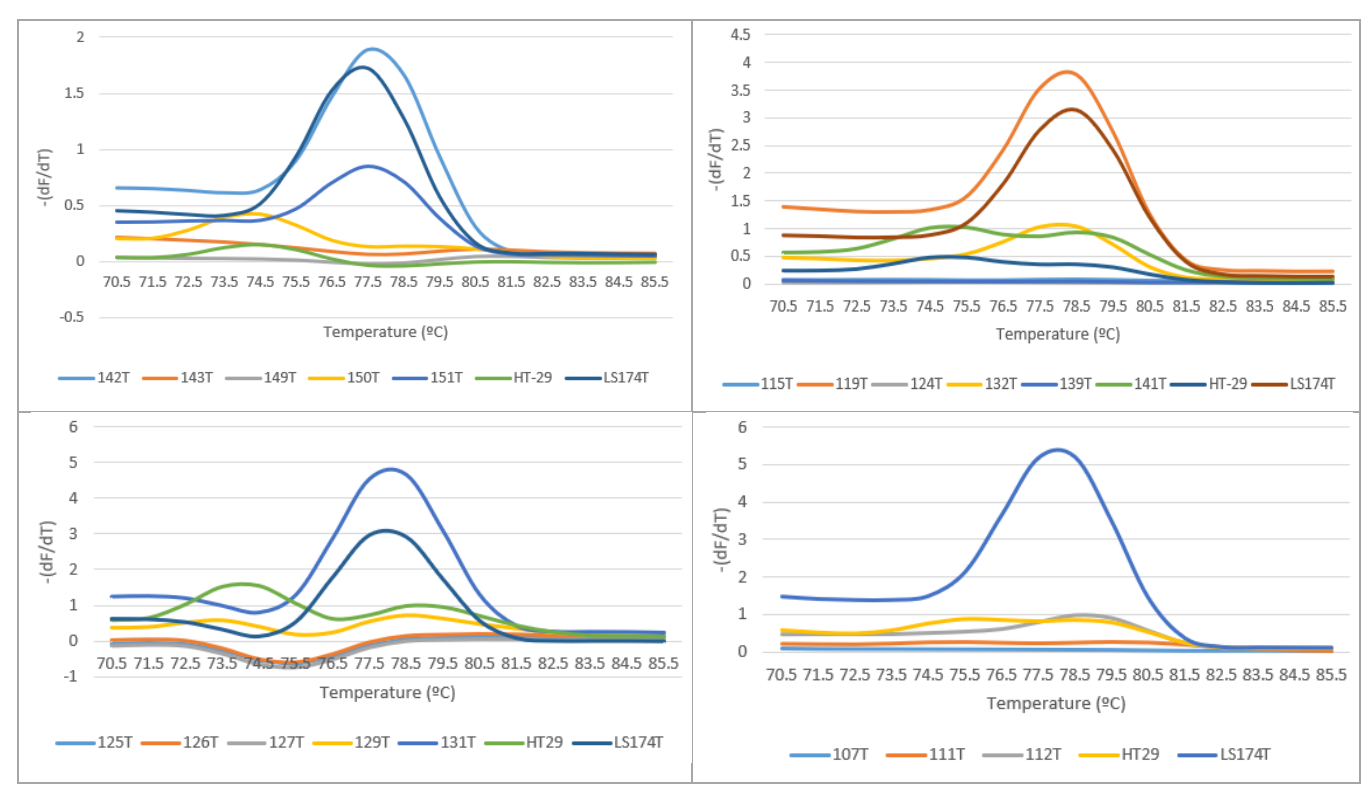


**Figure A1: ARMS-HRMA derivative plots used in G12D scoring of tumor samples.** Only one replicate is represented for each sample.

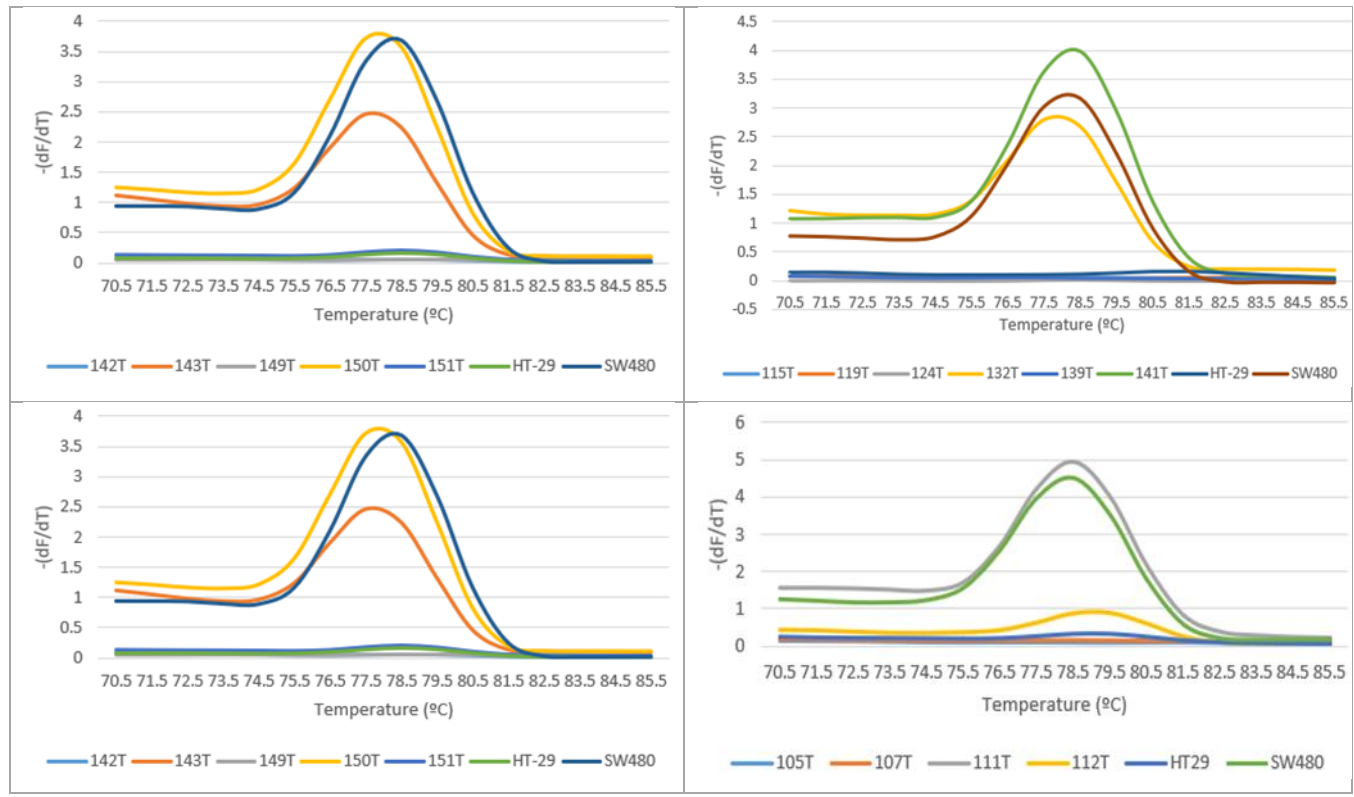


Figure A2: ARMS-HRMA derivative plots used in G12V scoring of tumor samples. Only one replicate is represented for each sample.

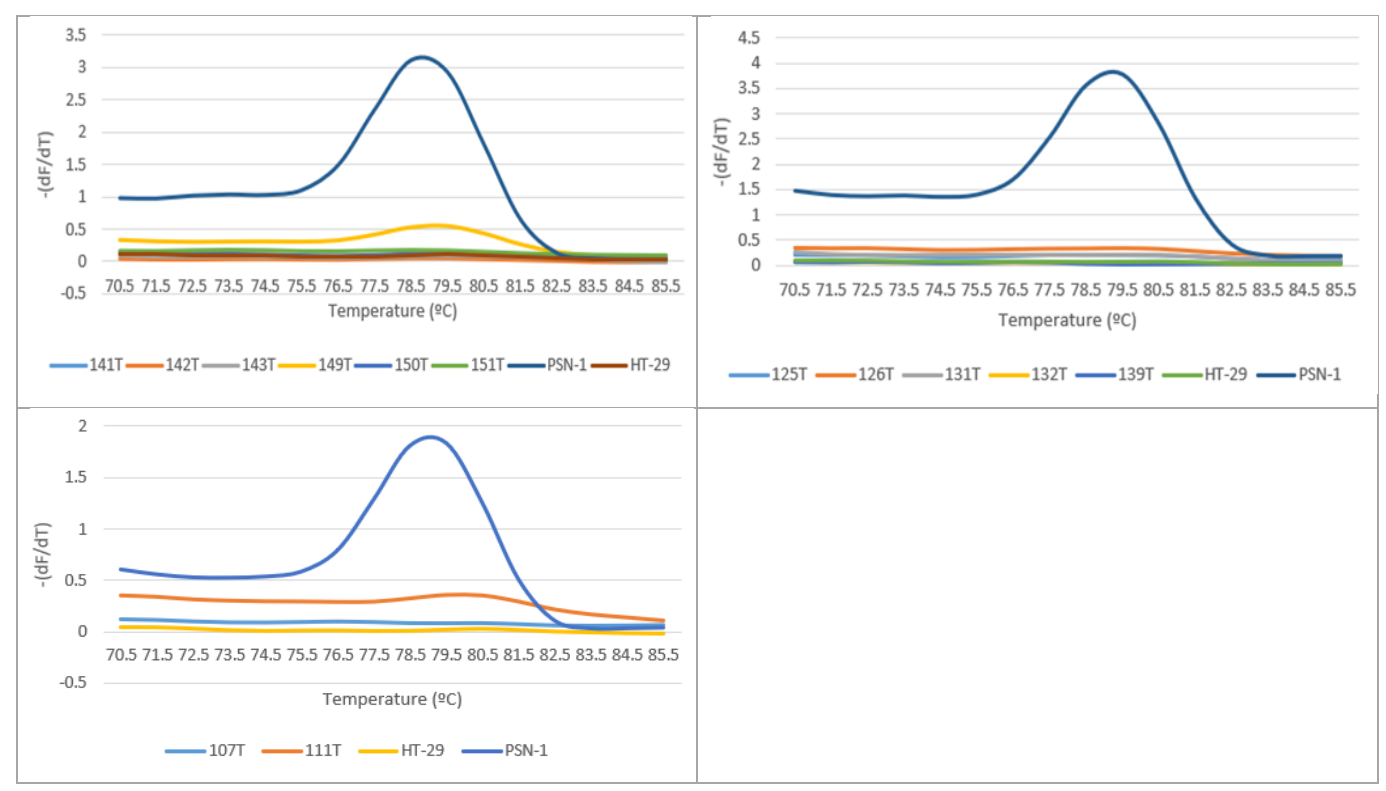


Figure A3: ARMS-HRMA derivative plots used in G12R scoring of tumor samples. Only one replicate is represented for each sample.

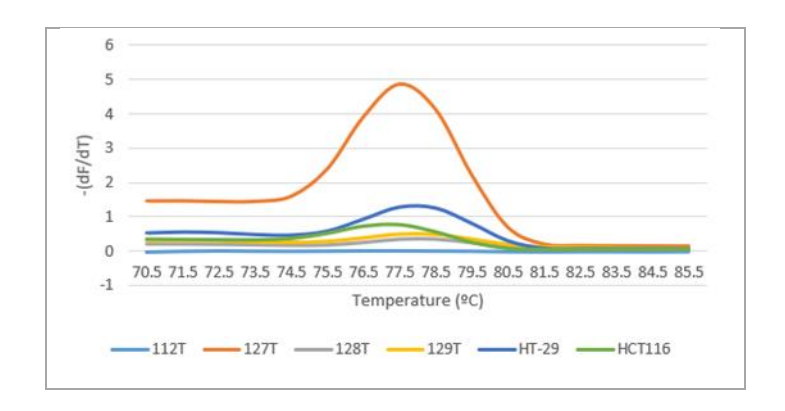


Figure A4: ARMS-HRMA derivative plots used in G13D scoring of tumor samples. Only one replicate is represented for each sample.

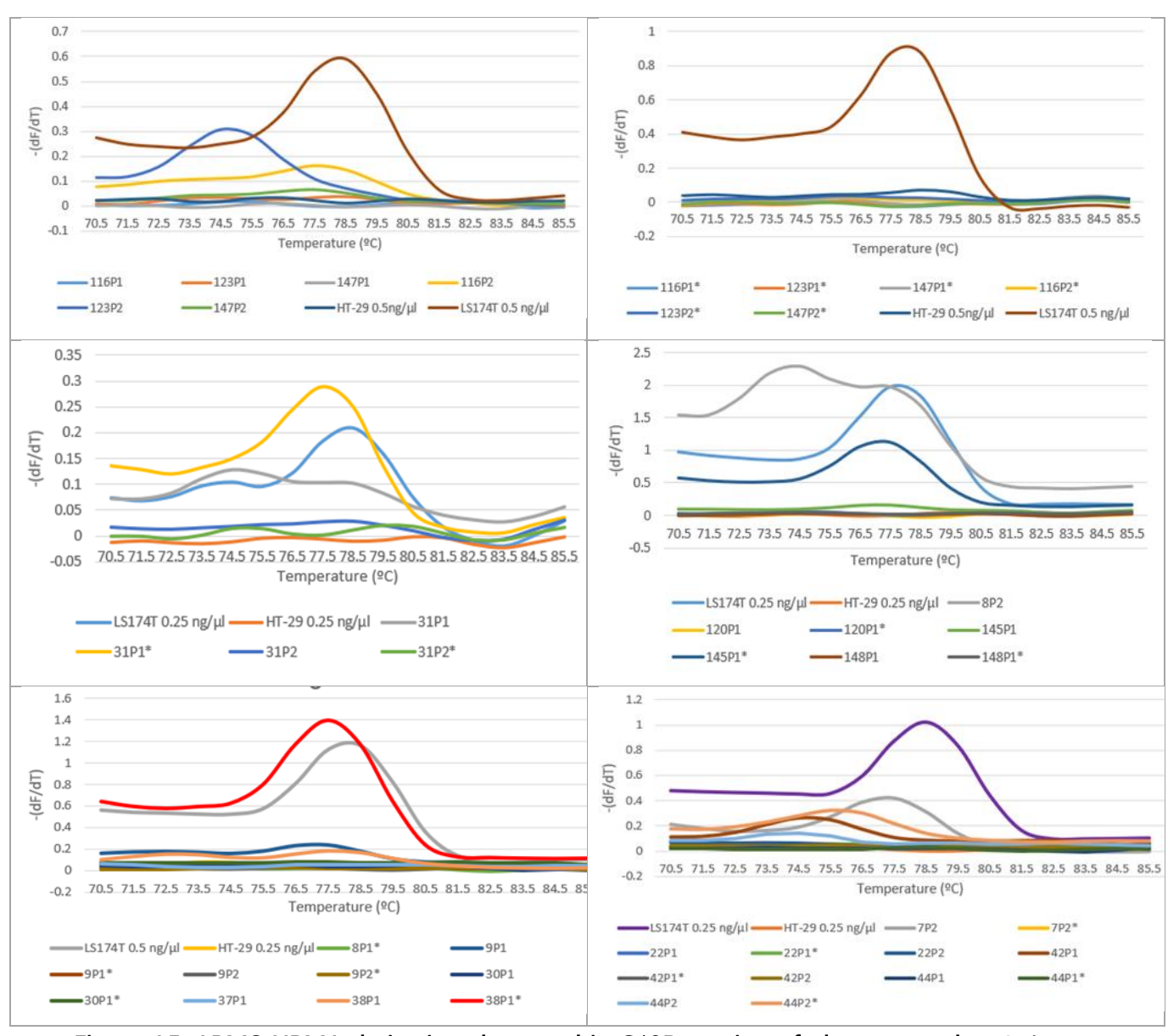


Figure A5: ARMS-HRMA derivative plots used in G12D scoring of plasma samples. Only one replicate is represented for each sample.

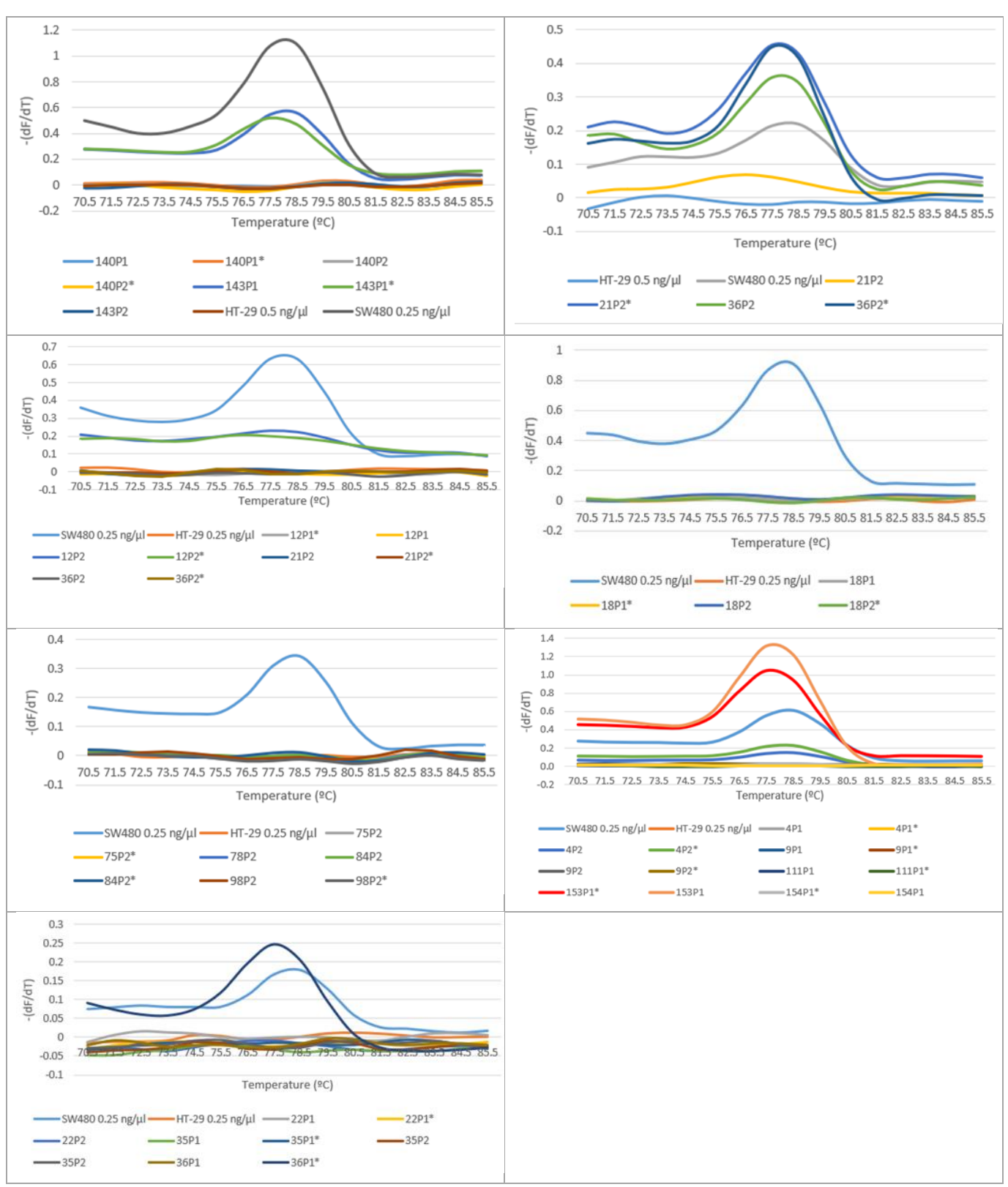


Figure A6: ARMS-HRMA derivative plots used in G12V scoring of plasma samples. Only one replicate is represented for each sample.

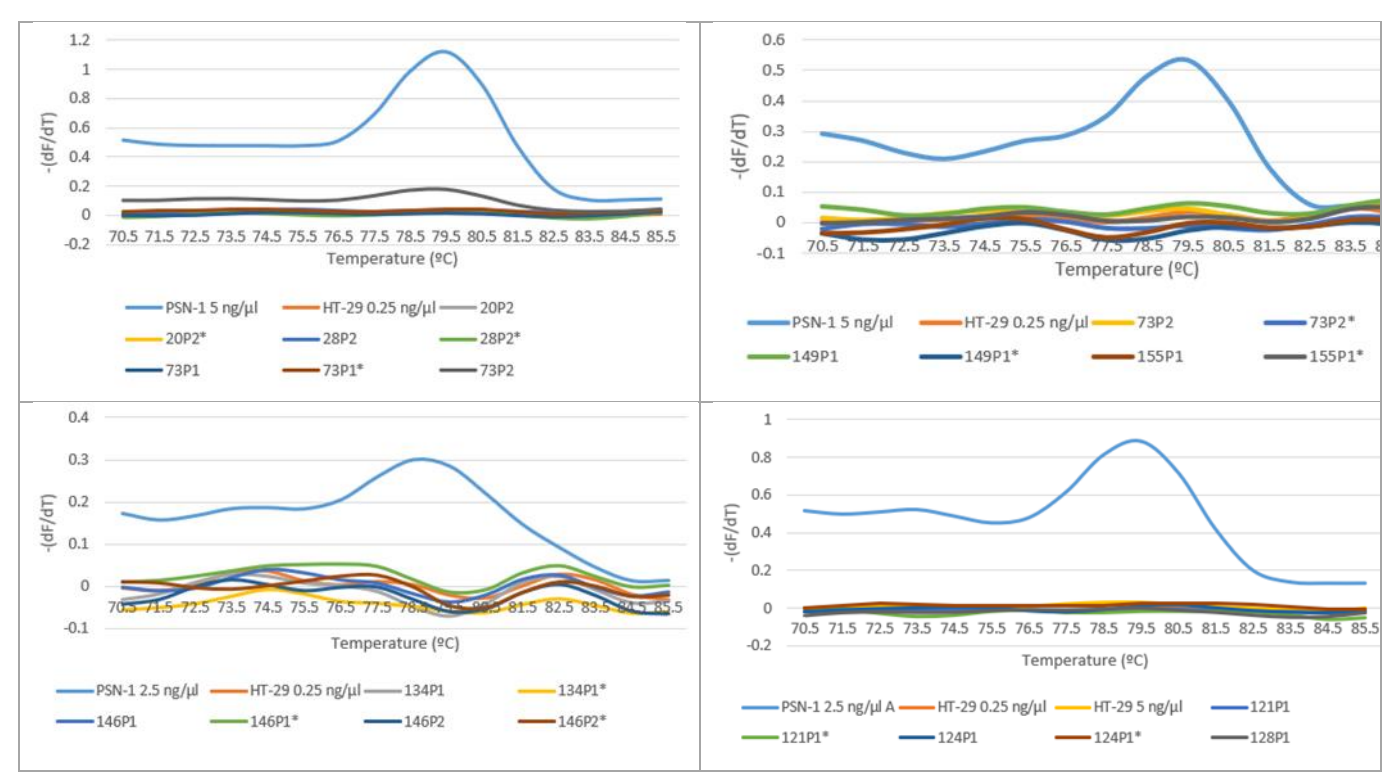


Figure A7: ARMS-HRMA derivative plots used in G12R scoring of plasma samples. Only one replicate is represented for each sample.

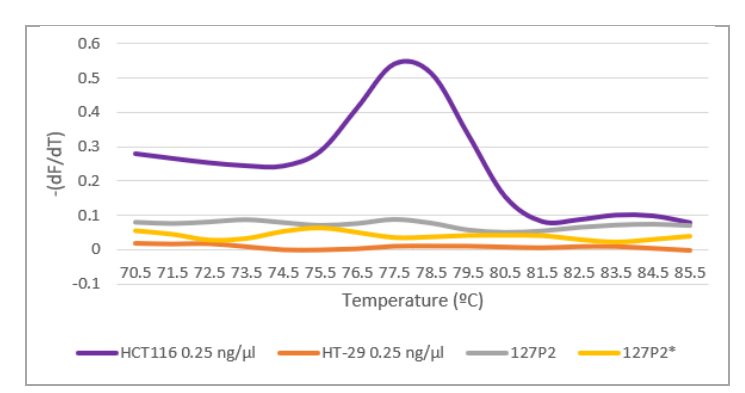


Figure A8: ARMS-HRMA derivative plots used in G13D scoring of plasma samples. Only one replicate is represented for each sample.





RÚBEN DOURADO VALIDATION OF ARMS-HRMA FOR KRAS MUTATIONS IN TUMOR AND PLASMA SAMPLES FROM PANCREATIC CANCER PATIENTS

2024